3.0 INTRODUCTION

During the U2C17 outage, SONGS Unit 3 was shut down due to a primary-to-secondary leak. Eddy current inspections of the Unit 3 steam generators revealed that the cause of the leak was tube-to-tube wear (TTW) in the U-bend region of a cluster of tubes located near the center of the tube bundle. Based on a root cause evaluation performed by SCE [11], the TTW in the SONGS steam generators was caused by in-plane tube movement due to in-plane fluid-elastic instability (FEI).

No indications of TTW were reported during the initial U2C17 inspections of the Unit 2 steam generators, which included full-length eddy current inspections of all tubes with bobbin coil probes. However, since 823 indications of TTW were detected in the SONGS-3 steam generators [12] and the design of the SONGS-3 steam generators is the same as the SONGS-2 steam generators, supplemental +Point™ inspections of the U-bends were performed in SONGS-2. These supplemental inspections included the full-length of the U-bend for a group of tubes in the same region as those with TTW in Unit 3. These supplemental inspections resulted in the finding of two adjacent tubes with shallow TTW in SG E-089 of Unit 2. According to Reference [12], the wear depth was reported to be 14% through-wall (TW) based on EPRI Examination Technique Specification Sheet (ETSS) 27902.2. ETSS 27902.2 was developed for freespan wear caused by loose parts; this technique overestimates the depth of TTW and therefore results in a conservative measurement for purposes of assessing tube integrity. However it is more appropriate to base the engineering assessments in this OA on the best estimate of the wear depth. For this reason the tubes were re-sized using a site-specific ECT calibration standard developed for TTW. The tubes were also re-inspected using an ultrasonic (UT) technique. Both of these techniques resulted in an indicated TTW depth of 7% TW. The assessments in this OA are appropriately based on the 7% TW depth measurement from UT which is considered a more accurate measure of the true depth.

Tube wear at support locations (AVB and TSP) detected in Unit 2 is within previous industry experience and can be evaluated using standard practices as described in the EPRI Tube Integrity Assessment Guidelines [2]. These degradation mechanisms are not threatening in Unit 2, as demonstrated by Reference [6], which justified a full cycle of operation at full reactor power. However, given identical designs, Unit 2 must be judged, a priori, as susceptible to the same TTW degradation mechanism as Unit 3 where 8 tubes failed structural integrity requirements after 11 months of operation [12]. Indeed, the location and orientation of the two shallow TTW indications in Unit 2 are consistent with the behavior observed in Unit 3 and indicates that in-plane fluid-elastic instability in Unit 2 began shortly before the end of cycle 16 operation after 22 months of operation. It should be noted that this statement is contested by a viewpoint that TTW in Unit 2 is simply a consequence of tubes being in very close proximity to one another with self-limiting wear produced by a combination of turbulence and out-of-plane fluid-elastic excitation. This viewpoint has been evaluated completely and is considered to be arguable but not definitive. The argument that incipient in-plane fluid-elastic has developed in Unit 2 is considered a more logical explanation for the observed TTW but again cannot be stated as definitive. It is ultimately a moot point since the observations in Unit 3 make TTW via in-plane fluid-elastic instability a potential degradation mechanism for Unit 2. The severity of potential degradation via this mechanism dictates that it must be evaluated in a thorough manner both as a matter of logic and by the requirements of NEI 97-06 [5] and the EPRI Tube Integrity Assessment Guidelines [2]. Based on the extremely comprehensive evaluation of both Units, supplemented by thermal hydraulic and FIV analysis, assuming, a priori, that TTW via in-plane fluid-elastic instability cannot develop in Unit 2 would be inappropriate.

4.0 OPERATIONAL ASSESSMENT STRATEGY

Understanding the TTW phenomena observed in Unit 3 is key to developing a rational operational assessment strategy for Unit 2. Extensive analysis has led to a good understanding of how and why TTW developed in both Unit 3 and Unit 2. This is summarized in Section 4.1. The operational assessment strategy is then presented in Section 4.2.

4.1 Development of TTW

Both steam generators in Unit 3 had more than 160 tubes with TTW indications in U-bends. The three most degraded tubes exhibited wear scars that were more than 28 inches long with central regions of essentially uniform wear depths that were greater than 80 %TW. These central regions of uniform wear depth were about 5 inches long. One of these regions contained a pinhole wall penetration that led to a small primary-to-secondary leak, resulting in the shutdown of Unit 3. Figure 4-1 shows the profile of wear depth versus axial length for the leaking tube, R106 C78, in Unit 3 SG E-088.

TTW scars are located on the extrados and intrados locations of U-bends. Wear scars on extrados locations of a given U-bend have matching wear scars on intrados locations of the neighboring row tube in the same column. The matching wear scars have very similar depths of wear [13]. The nominal distance between extrados and intrados locations of neighboring U-bends in the same plane ranges from 0.25 inches to 0.325 inches due to the tube indexing, as mentioned earlier. There are instances where the closest approach distance is less than this value based on field measurements using bobbin coil ECT. The bobbin probe on the 140 kHz absolute channel can detect neighboring U-bends if the separation distance is less than approximately 0.15 inches. Using a proximity signal calibration curve, the separation distance between U-bends was measured for all steam generators. The results of these measurements are reported in Reference [14]. The smallest detected U-bend separation distance is close to contact. There are 36 U-bends in Unit 2 SG E-088 and 34 in SG E-089 with a separation less than or equal to 0.050 inches. The separation of the U-bends in Unit 2 with TTW is 0.190 inches as measured by UT. The U-bends with the smaller separation distances are much better candidates for wear by rubbing yet do not exhibit TTW. In Unit 3, TTW via in-plane fluid-elastic instability is incontrovertible based on evidence presented in the following paragraphs.

An SCE root cause analysis [11] has identified in-plane fluid-elastic instability as the mechanistic cause of TTW in the SONGS steam generators. Out-of-plane fluid-elastic instability has been observed in nuclear steam generators in the past and has led to tube bursts at normal operating conditions. However, the observation of in-plane fluid-elastic instability in steam generators in a nuclear power plant is a true paradigm shift. It is not uncommon for designers of nuclear steam generators to calculate that large U-bends supported only by lateral AVB's are fluid elastically unstable in the in-plane direction under the assumption of no effective in-plane supports. This is textbook knowledge and part of the technical literature.

The caption of Figure 4-2, taken from a book by M. K. Au-Yang that was published in 2001 [15], reads, "In-plane modes that have never been observed to be unstable even though the computed fluid-elastic stability margins are well below 1". The fluid-elastic stability margin, FSM, is the inverse of the stability ratio, SR[1]. An FSM well below 1 means an SR well above 1 and well into the unstable range. As an example of the extensive laboratory

[1] Stability ratio is defined as the ratio of the effective flow velocity to which the tube is subjected to the critical velocity. Critical velocity is the velocity at which the tube, with specific geometry and support conditions, becomes unstable. Stability ratios less than 1.0 represent a stable condition where the actual velocity is less than the critical velocity; stability ratios greater than 1.0 represent an unstable condition where the actual velocity exceeds the critical velocity.

testing campaigns conducted to detect in-plane fluid-elastic instability, Weaver and Schneider [16], in 1983, examined the flow induced response of heat exchanger U-tubes with flat bar supports. It is worth quoting the first conclusion of their paper:

> "The effect of flat bar supports with small clearance is to act as apparent nodal points for flow-induced tube response. They not only prevented the out-of-plane mode as expected but also the in-plane modes. No in-plane instabilities were observed, even when the flow velocity was increased to three times that expected to cause instability in the apparently unsupported first in-plane mode."

Additionally, in an effort to encourage the development of in-plane instability, Weaver and Schneider [16] substantially increased the clearances between flat bar supports and U-tubes, but no in-plane instability was observed. Other investigators, notably Westinghouse, have deliberately searched for in-plane instability with only support from flat bars and have not detected the phenomena. However in 2005, Janzen, Hagburg, Pettigrew and Taylor [17] reported in-plane instability. The abstract to their paper states, "For the first time in a U-bend tube bundle with liquid or two-phase flow, instability was observed in both the out-of-plane and in-plane direction." The test setup included tubes with a U-bend radius of 0.646 m (25.4 in.) with flat bar U-bend restraints inserted between columns at the apex of the U-bend. The bundle was subjected to air-water cross-flow directed at the mid-span between the 0^0 and 90^0 location (apex) of the bundle. Tube vibration was measured over a range of void fractions and flow rates, and for three tube-to-support diametral clearances: no support, 1.5 mm (59 mil) and 0.75 mm (30 mil). It is noted that these test clearances are significantly larger than the SONGS steam generator design clearance of 2 mils diametral.

Prior to the observations at SONGS Unit 3, no in-plane instability had been observed in any U-bend nuclear steam generator. The service history of U-bends with flat bar supports had been successful up to this point. This includes depending on in-plane effectiveness of flat bar supports to demonstrate relatively low values of stability ratios. Stability depends on both thermal-hydraulic flow conditions and in-plane support effectiveness. Logically either or both of these factors are causing the observed instability in SONGS Unit 3. From an overall engineering perspective it is worth considering an operational envelope that is the set of past design and operational factors that have led to successful performance. One technique for doing so is a spider diagram where many factors for different plants and designs are considered by plotting of relative ranking on axes arranged in a star pattern. Connecting the dots from one axis to another for a given plant creates a periphery that defines the operational parameters for that plant. The outer boundary of all these peripheries of past successful performance is the successful operational envelope.

It should be recognized that the goal of efficient and optimized design leads to expansion of the operational envelope over time and this has occurred in the past. Using data from [18], a spider diagram is presented in Figure 4-3. More parameters are needed to completely define all parameters that have an influence on in-plane FEI, for example some measure of support effectiveness. This could be something as specific as design clearances or as general as the ratio of the total support structure weight to the weight of supported U-bends. The two axes of Figure 4-3 with plotted data are bulk velocity ratio and mean void fraction ratio, which are those parameters that are publically available. High velocities increase susceptibility to instability and a high void fraction indicates lower damping and thus less resistance to instability. At 100% power, the thermal-hydraulic conditions in the u-bend region of the SONGS replacement steam generators exceed the past successful operational envelope for U-bend nuclear steam generators based on presently available data. The operational envelope will be reconsidered in Section 7.0 in the context of a lower power level (see also Figure 5-1). The service performance of SONGS Unit 3 at 100% power shows that there is a boundary to the successful operational envelope.

The following paragraphs discuss inspection results and their consistency with in-plane fluid-elastic instability. This provides the background needed to develop an operational assessment strategy.

Figure 4-4 and Figure 4-5 are tubesheet maps illustrating the U-bends in Unit 3 SG E-088 and SG E-089 that have TTW. The more detailed view of the positions of TTW indications in Figure 4-6, Figure 4-7 and Figure 4-8 are instructive. Note that the positions are contiguous with only one tube not affected. This argues against a random spatial and temporal occurrence of instability. There just aren't enough unaffected tubes to indicate that instability independently initiated at different positions at different times. Three dimensional plots of TTW depth versus column and row in Figure 4-9 and Figure 4-10 reinforce the concept that the development of instability at different positions is a sequence of dependent events and not a sequence of independent events. The plot of wear depths resembles a mound with the largest depths at the top and then sloping to lower values in all directions. This is also illustrated by the color coded depths in Figure 4-4 and Figure 4-5. The two U-bends in Unit 2 SG E-089 with shallow TTW indications are plotted as red points in Figure 4-8 to illustrate their position in the bundle for comparison with Unit 3.

TTW due to in-plane fluid-elastic instability is a unique degradation mechanism because one unstable tube can drive its neighbor to instability through repeated impact events. Repeated impacts move the neighbor tube relative to its AVBs causing accelerated wear and elongated wear. The in-plane effectiveness of the AVBs is degraded and an initially stable neighbor tube eventually becomes unstable. This leads to a growing region of instability and TTW. Impact events lead to the propagation of instability from one tube to another in the same column. Propagation of instability from one column to another must involve fluid coupling since tube-to-tube impact does not occur across columns. Fluid coupling is discussed in Reference [19]. The two basic theories of fluid-elastic instability have been termed fluid stiffness and fluid damping. With fluid damping perturbations/hysteresis effects in flow fields can lead to negative damping and thus lead to instability. Given the large displacements involved with instability and TTW, the fluid coupling argument is undeniably reasonable.

The extent of movement of unstable tubes, as well as tubes being driven to instability by impact from unstable tubes, is revealed by elongated wear scars at some AVB locations. Typically, turbulence induced wear leads to wear scars with a length equal to or less than the width of an AVB.

Figure 4-11 and Figure 4-12 show that the Unit 3 elongated wear scars only occur within the region of unstable tubes with TTW. In these figures elongated wear scars are identified by comparing a bobbin probe evaluation of AVB width with a +Pt™ probe evaluation of wear scar length. More complete results, based only on a bobbin probe evaluation of wear scar lengths, are shown in Figure 4-13 and Figure 4-14. Outside of the region of TTW the length of wear scars at AVB locations returns to normally expected values. It should be noted that because of field spread effects the bobbin probe typically overestimates wear scar lengths. Even though no evidence of elongated wear scars is evident in Unit 2, it doesn't necessarily rule out undetected in-plane instability. Wear scars at AVB locations may be too shallow to evaluate properly and AVB wear scar lengths may be shortened by a contact length that is small because of the presence of AVB twist. The best evidence of in-plane instability is the detection of TTW, not the detection of elongated AVB wear scars. Extensive inspections of the regions of interest with the +Pt™ probe show that possible undetected TTW would be less than 5 %TW. It is unreasonable to expect detectable elongation of AVB wear scars without the detection of TTW. The significance of elongated AVB wear scars is that the amount of elongation reveals the extent of unstable tube motion in-plane.

MHI Proprietary

When the displacement of the unstable tube in a direction perpendicular to the U-bend exceeds the local tube-to-tube spacing, it will impact the neighboring tube. By plotting the radially outward displacement versus angle around the U-bend, the points of impact with a neighboring tube can be determined. For Mode 1 displacements in the tubes of interest, the centers of impact with a neighbor tube are at 48° and 132° as measured from the positive x axis. The numbering sequence used to identify AVBs corresponds to 132° being on the hot leg and 48° being on the cold leg of the U-bends. Depth versus length profiles were determined for 777 separate TTW indications in Unit 3 with almost all containing some central region with an essentially uniform maximum depth. The center of impact was considered to be at the midpoint of this central region of maximum depth. Figure 4-17 shows a plot of impact locations compared to locations consistent with Mode 1, Mode 2 and Mode 3 displacement patterns. The impact points are overwhelmingly consistent with Mode 1 displacements. Parenthetically, the two TTW scars in Unit 2 are at 48°, the Mode 1 impact point. Mode 1 is the lowest natural frequency of in-plane U-bend vibration and thus is the first mode to be excited to instability. Mode 2 and Mode 3 displacements are shown in Figure 4-18 and Figure 4-19, respectively. Note that only one half of the cycle is illustrated in all modal displacement plots. The other half of the cycle produces displacements that are exactly opposite of those shown.

A tube subject to FEI in the in-plane direction can move in different modes, as shown in Figure 4-15, Figure 4-18 and Figure 4-19. Note that some impact points shown in Figure 4-17 are consistent with Mode 2 and Mode 3 displacement patterns. There are three possibilities for the appearance of these locations: excitation of instability in Modes 2 and 3, excitation of other vibration patterns due to initial Mode 1 impact events, or excitation of Mode 2 and Mode 3 vibration due to a momentarily strong interaction of an unstable tube in Mode 1 with an AVB as it passes that AVB. It is likely that some combination of these conditions is operative, but this cannot be conclusively determined by analysis.

The mechanisms and forces involved in fluid-elastic instability in tube bundles are presented later in this section. For the present, it is sufficient to note that the forces at AVB locations needed to prevent the onset of fluid-elastic instability are low. In contrast, after instability develops, the amplitude of in-plane motion continuously increases and the forces needed to prevent in-plane motion at any given AVB location become relatively large. Hence shortly after instability occurs, U-bends begin to swing in Mode 1 and overcome hindrance at any AVB location.

4.2 Operational Assessment Strategy

From the behavior observed in Unit 3 and other non-nuclear heat exchangers, TTW rates driven by fluid-elastic instability are high. Therefore, the fundamental goal of the operational assessment strategy is to adjust the operating power level and inspection interval to reduce the development of in-plane fluid-elastic instability and the resulting occurrence of TTW to an acceptably low probability event. The goal of the power reduction is to place Unit 2 back inside of the successful operational envelope and restore stability.

The strategy of the operational assessment for TTW therefore consists of three elements. These are:

- Identify the plant operating condition and the length of the next operating interval necessary to prevent a loss of SG tube integrity.

- The operating power level and operating interval will be reduced to ensure an acceptably low probability of in-plane FEI. These operating conditions establish a high probability that structural and leakage integrity requirements [2] will be met (operating interval is defined as time at reduced power not calendar time).

- Identify and implement defense in depth (DID) measures relative to TTW that add assurance that structural and leakage integrity requirements will be maintained for the plant operating period.

To ensure U-bend stability, the two tubes in Unit 2 that are now argued to be unstable and exhibiting TTW will be shown to be stable at a lower power level. At sufficiently low flow conditions, no in-plane support is required to maintain stability. At higher flow conditions or, equivalently, to argue that the maximum stability ratio will remain at some low value, say 0.75 for the sake of conservatism, some degree of in-plane support effectiveness needs to be demonstrated. There are no universally established or accepted criteria for support effectiveness. Operating experience and laboratory testing has shown the small gaps between AVBs and U-bends, without any friction force, does provide an effective support condition. Conversely, arguments have been advanced that very small friction forces provide an effective support to preclude in-plane tube motion. For convenience in calculations, support effectiveness is expressed in terms of contact forces at AVB locations. This is a surrogate for more complex tube to support interactions. Lowering the power level is expected to increase support effectiveness by positioning SONGS Unit 2 within the operating window shown to be acceptable for other plants.

Contact forces, as deteriorated by tube wear at support locations over time, will be calculated using advanced computational techniques. This will be combined with calculations of stability ratios to develop the probability of the onset of in-plane fluid-elastic instability, both as a function of operating power level and operating time. The operating power and operating time will be adjusted to provide a probability of occurrence of instability ≤ 0.05. This probability is based on considerations and requirements described in the EPRI SG Integrity Assessment Guidelines [2]. Without the development of TTW, the Structural Integrity Performance Criteria, SIPC, is automatically satisfied to a probability greater than 0.95.

The defenses in depth measures are as follows:

- After the onset of FEI, TTW would have to progress over some time period to lead to an unacceptable level of wear depth. Estimates of TTW growth rates are provided in this report.

- Tubes with a high risk of developing FEI, based on AVB wear patterns similar to those of Unit 3 unstable tubes, have been plugged and stabilized with wire cables.

- The onset of FEI is most likely in the high risk region. Since the two tubes with TTW are surrounded by plugged and stabilized tubes, then FEI must progress through a buffer zone of plugged tubes to reach pressurized, in-service tubes.

- Cable stabilizers do not substantially improve U-bend in-plane stability, but will prevent possible generation of large loose parts. [

]

The three elements of the strategy for the operational assessment of TTW in Unit 2 will provide the needed assurance that structural and leakage integrity requirements will be maintained throughout the next inspection interval.

The parameter that characterizes the state of fluid-elastic stability is termed the stability ratio, SR. Mathematically it represents the ratio of the effective fluid velocity to the critical fluid velocity at instability. At the onset of instability, the SR value is 1.0. If the stability ratio is less than 1.0, the structure of interest is fluid elastically stable. The details of calculating stability ratios are presented in Reference [20]. In general, the factors in the calculation are the geometry of the structure, fluid conditions such as velocity and density, damping sources and the mode of vibration being excited. Calculated stability ratios are benchmarked against laboratory experiments.

The development of in-plane fluid-elastic instability of U-bends depends on four factors. These are:

- Location in the bundle
- Operating power level
- Number of consecutive ineffective supports
- Operating time

Tube location in the bundle determines the thermal-hydraulic environment of a given U-bend. Fluid-elastic excitation depends on the fluid velocity and density. For a U-bend, these factors vary with position around the U-bend from the hot leg to the cold leg. This variation is accounted for in calculations of stability ratio. The operating power level has a dramatic effect on thermal-hydraulic conditions. Reduced power levels substantially lower fluid-elastic excitation. For given thermal-hydraulic conditions and tube geometry, the stability ratio is a direct function of the number of consecutive ineffective AVB supports. If too many consecutive supports are ineffective, the stability ratio will exceed 1.0. The allowable number of consecutive ineffective supports depends on the U-bend location in the bundle and the power level. Tube wear at AVB support locations degrades their effectiveness in terms of providing in-plane support. Thus, tube wear at AVB locations can turn an effective support into an ineffective support. Operating time is important because wear can increase over time. Limiting operating time will in turn limit wear at AVB locations, which then limits degradation of support effectiveness, maximizing stability.

Calculation of the probability of the onset of in-plane fluid-elastic instability requires information in three areas: stability ratios, contact forces at AVB locations and a criteria for deciding whether AVB supports are effective or ineffective in terms of in-plane support. Stability ratios need to be known as a function of position in the bundle, number of consecutive ineffective supports and power level. Contact forces at AVB locations cannot be determined deterministically since the dispersion of gaps between tubes and AVB supports is random, and thus probabilistic in nature. Therefore, contact forces have to be described in a probabilistic manner. At any given

AVB location, the contact force is not known exactly, but it can be demonstrated to be a selection from some known distribution of forces. Whether or not an AVB support is effective or ineffective in terms of in-plane support can be expressed in terms of the contact forces at that location. The derivation of the support effectiveness criterion is explained in Section 7.0.

In principle, the calculation of the probability of instability is straightforward. Stability ratios are available for each U-bend in the bundle as a function of the number of consecutive ineffective supports and power level [20]. Similarly, the distributions of contact forces are available for each AVB location in the bundle. Tube wear at AVB locations decreases the contact force at those locations. The distributions of contact forces as affected by wear have been calculated [26]. The required contact force for any AVB support to be considered effective is defined for each AVB location. With this input, one Monte Carlo trial of a steam generator is constructed in the following manner:

A flow chart of the above process is shown in Figure 4-20.

In principle, the above procedure is followed; in practice, several independent programs use mathematically equivalent algorithms to compute the probability of instability. The goal of the operational assessment is to determine the operating power level and associated inspection interval that provides the needed margin relative to the onset of in-plane fluid-elastic instability and thus precluding TTW.

The following sections describe stability ratios, contact forces at AVB locations and criteria for defining effective versus ineffective supports. This is followed by a more detailed description of probability of instability calculations and results defining the acceptable operating power level and inspection interval.

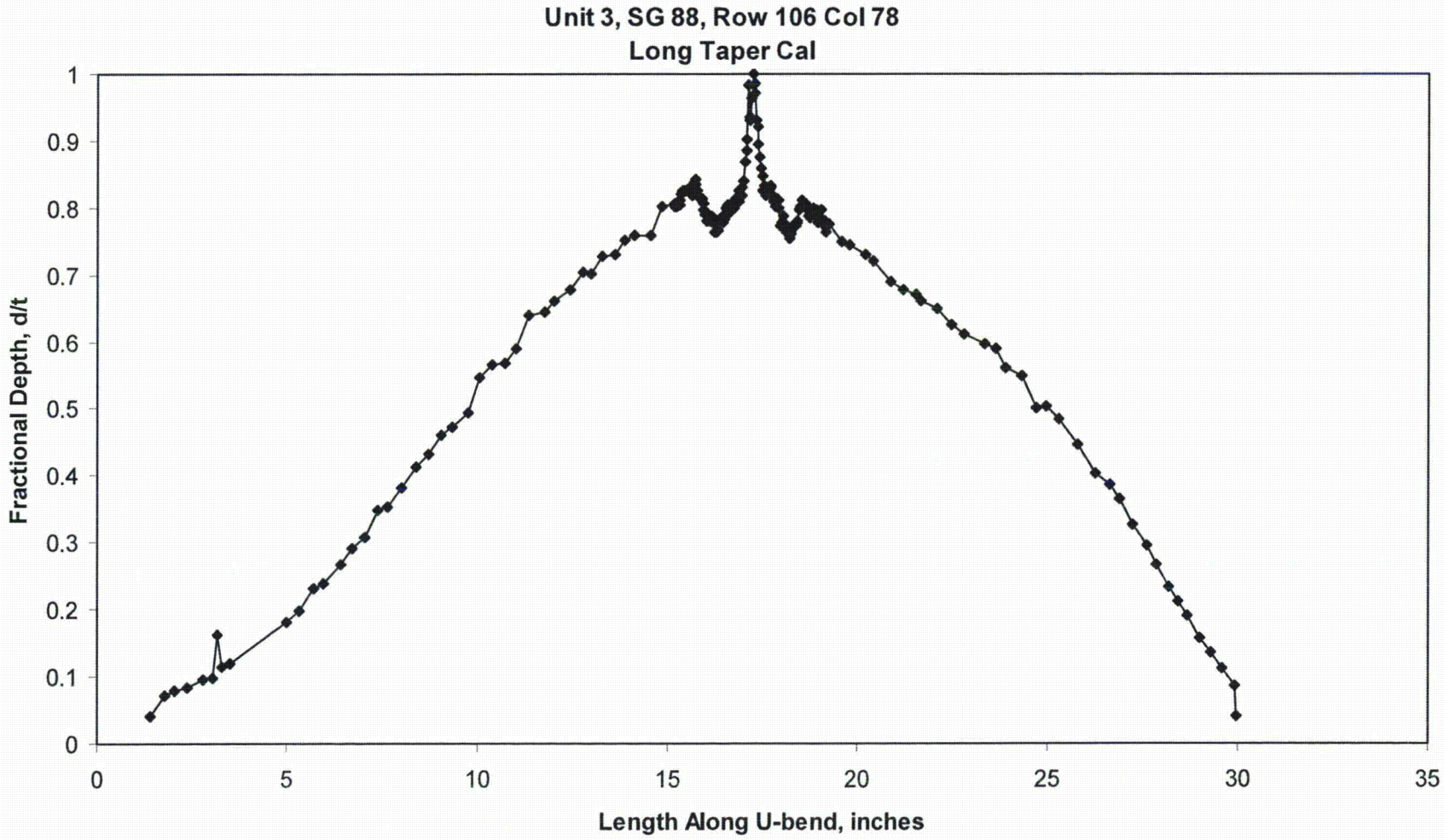

Figure 4-1: Depth versus Axial Length Profile for the Leaking Tube in Unit 3, SG E-088

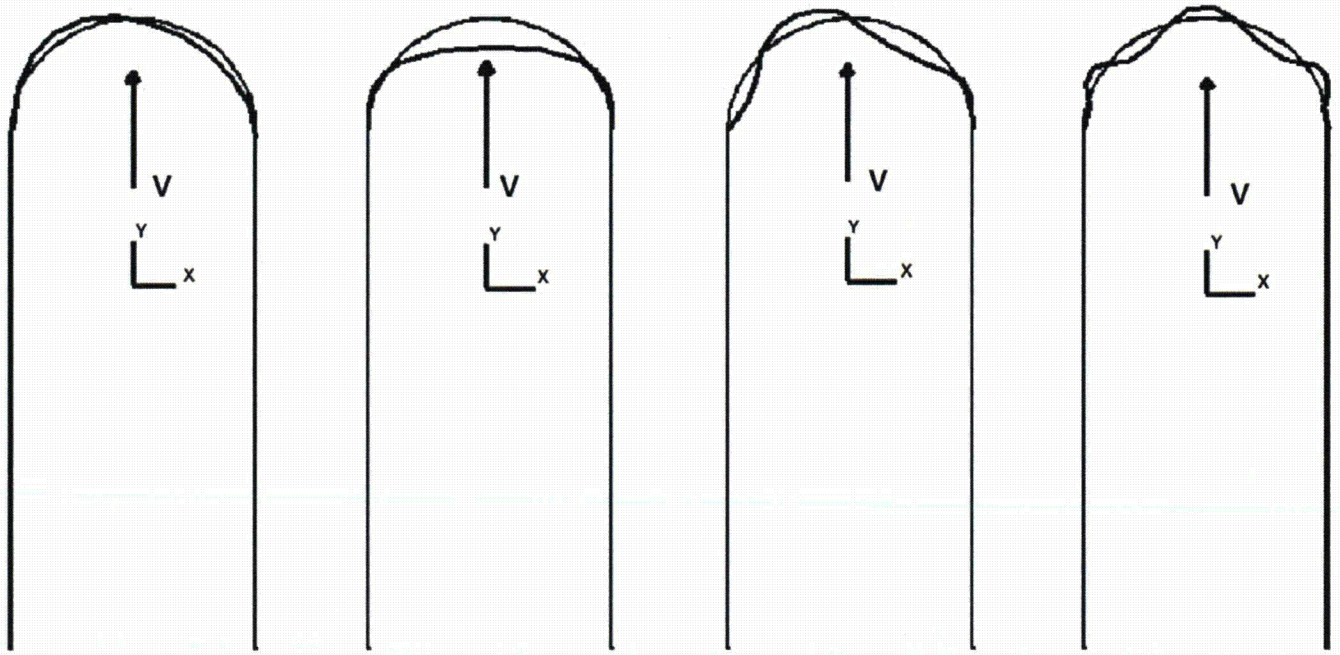

In-plane modes that have never been observed to be unstable even though the computed fluid-elastic stability margins are well below 1.0. (with FSM = 1/SR, SR>>1.0)

Figure 4-2: Figure from a Book by M. K. Au Yang, "Flow Induced Vibration in Power and Process Plant Components", ASME Press, 2001

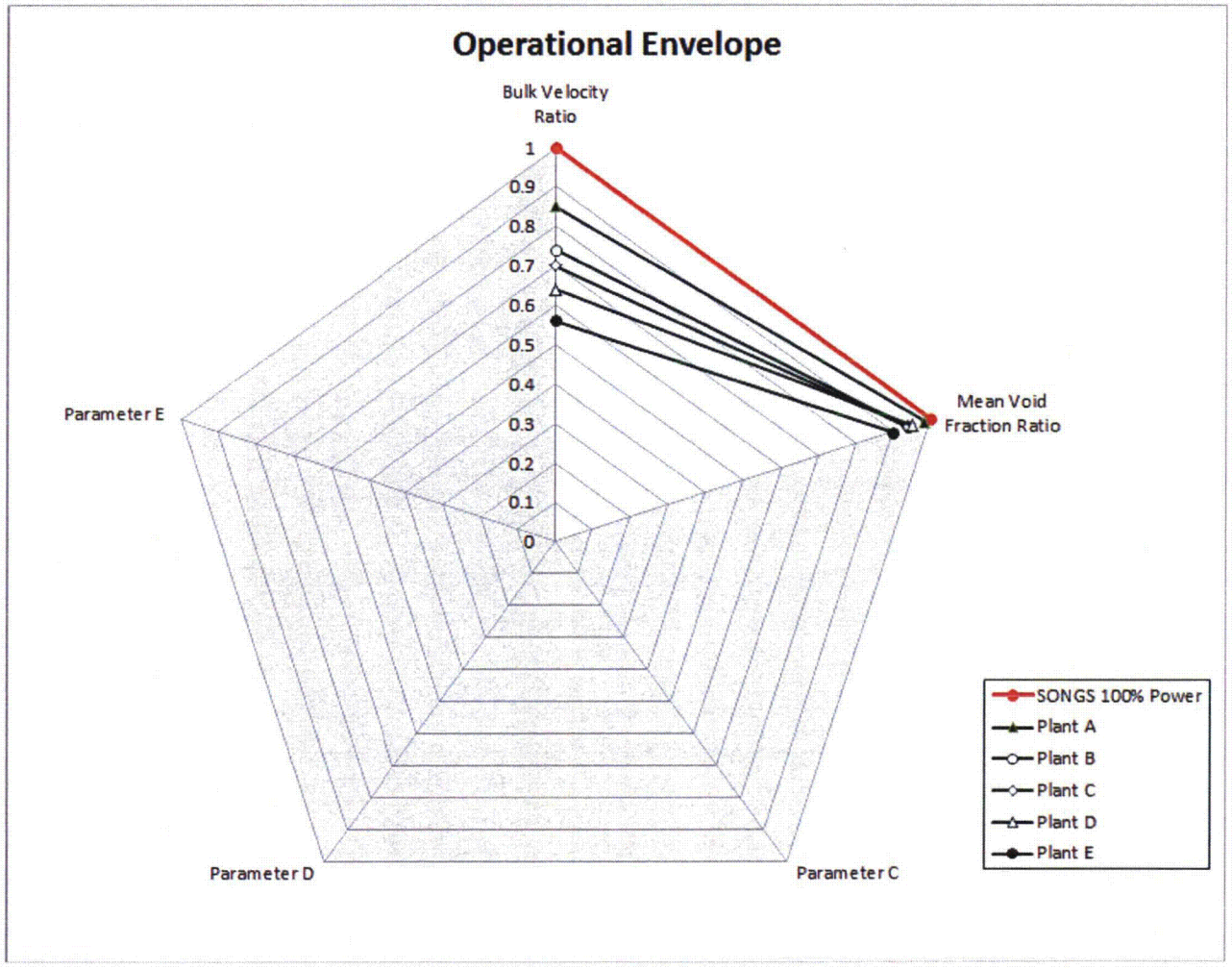

Figure 4-3: Spider Diagram of the Operational Envelope for Large U-bend Steam Generators

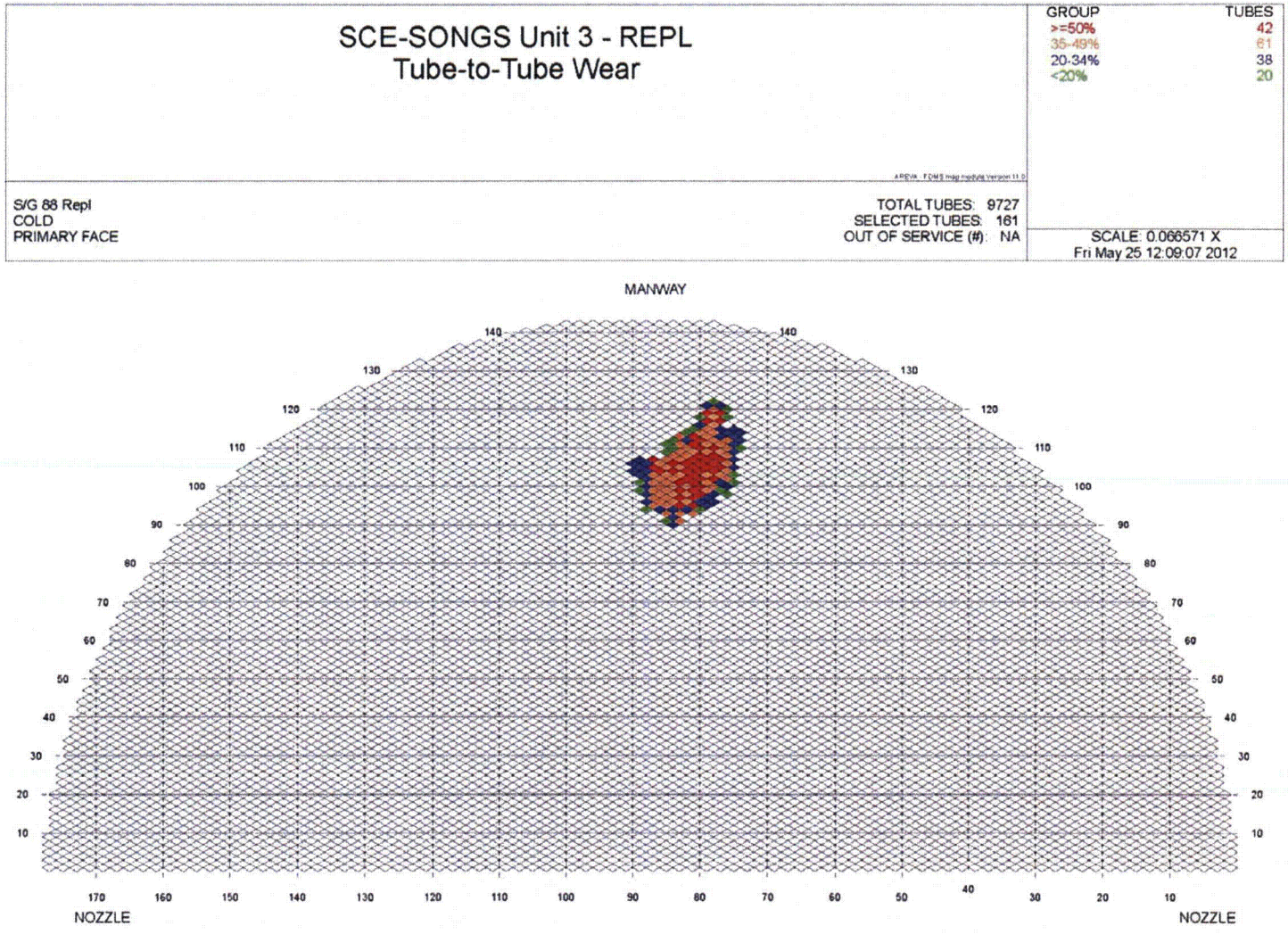

Figure 4-4: Tubesheet Map of TTW Indications, Unit 3, SG E-088

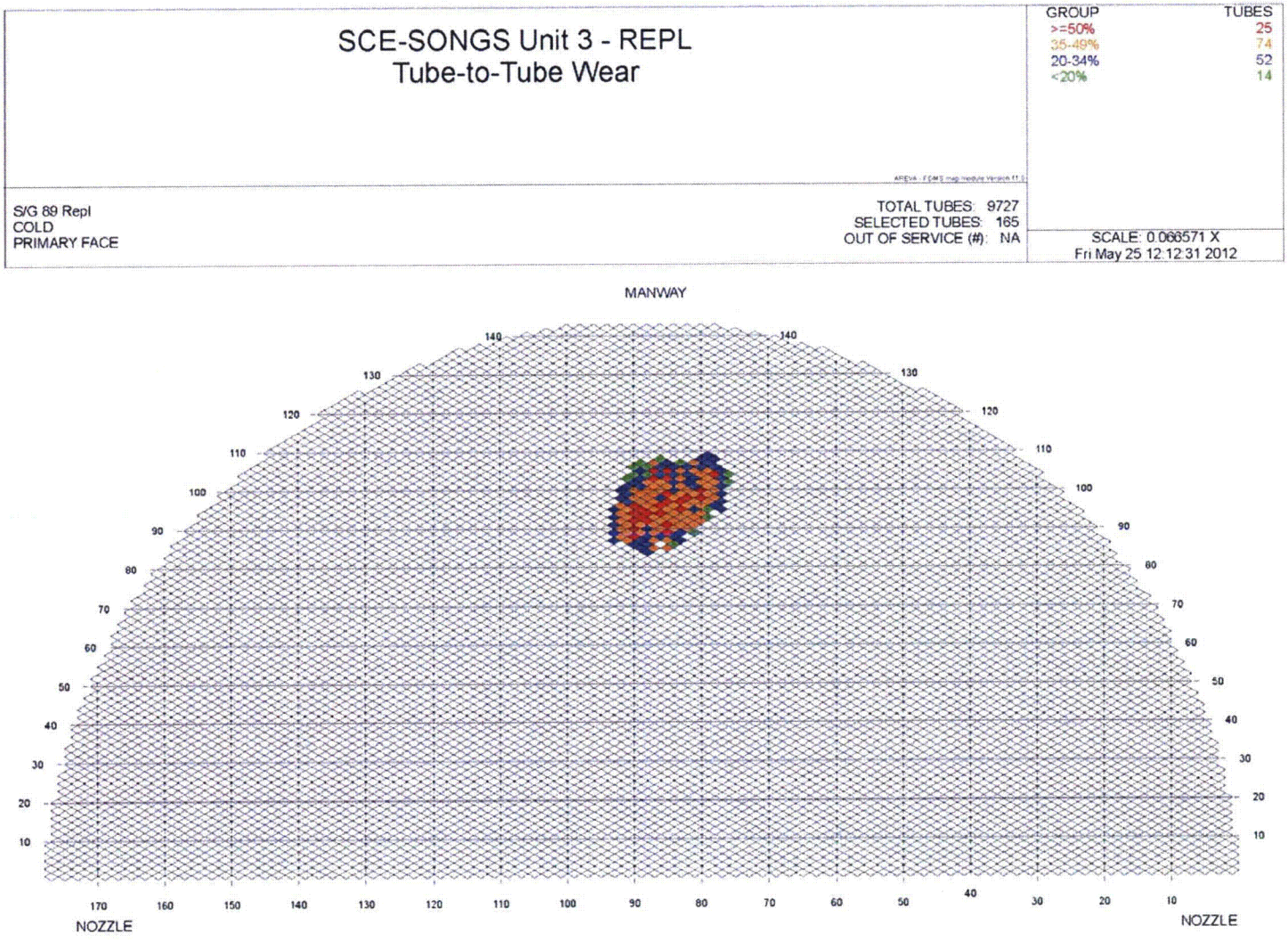

Figure 4-5: Tubesheet Map of TTW Indications, Unit 3, SG E-089

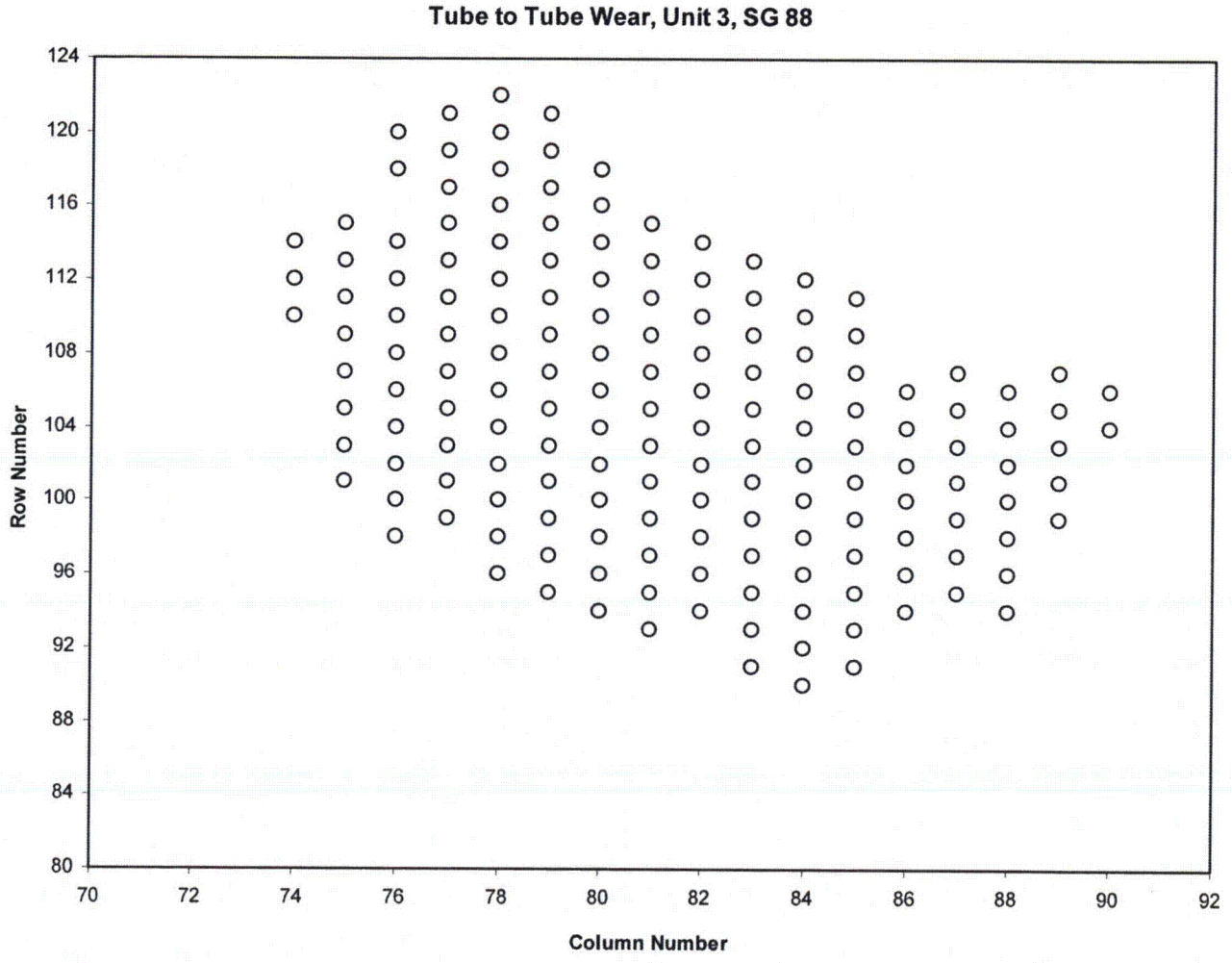

Figure 4-6: Expanded View of TTW Indications, Unit 3, SG E-088

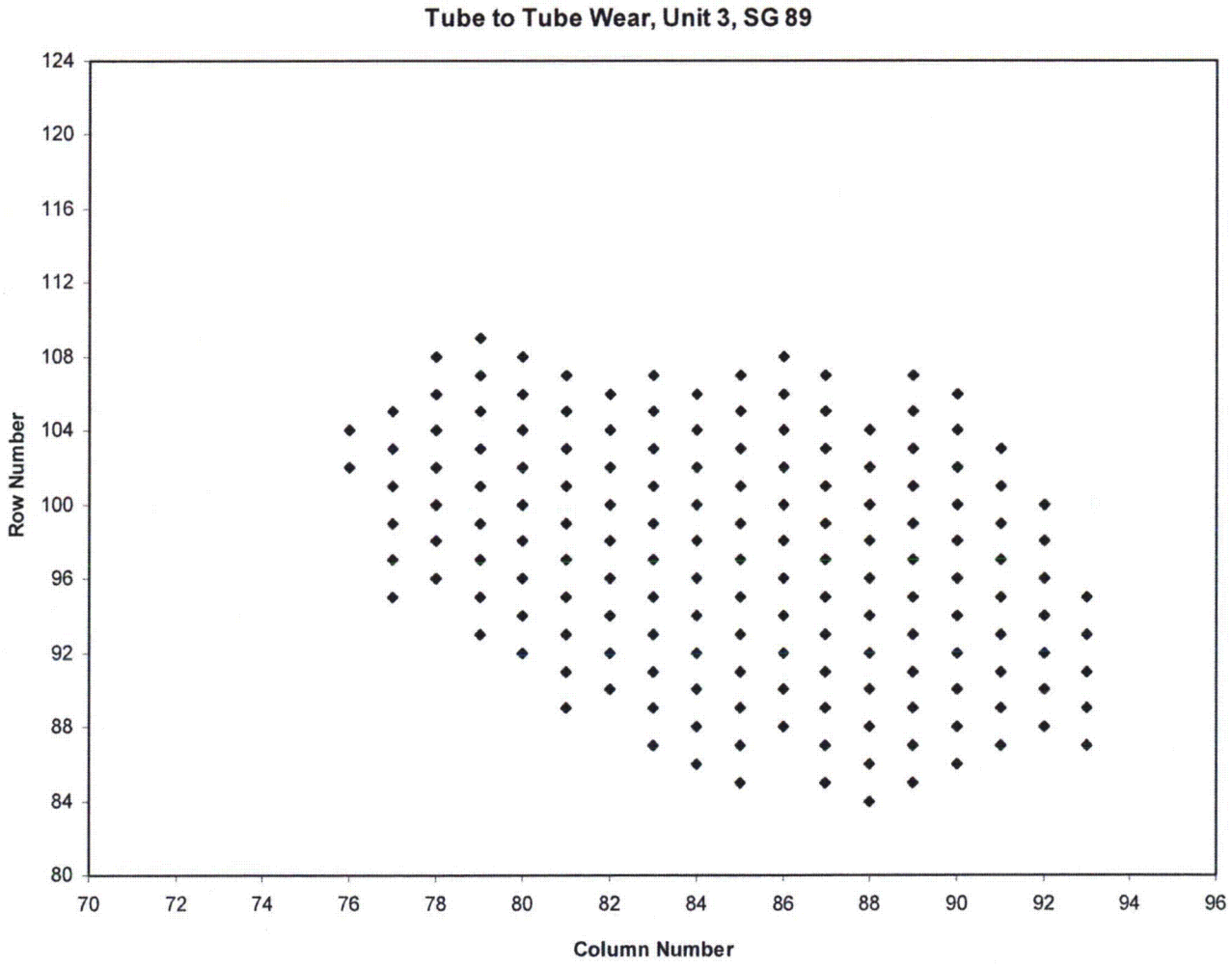

Figure 4-7: Expanded View of TTW Indications, Unit 3, SG E-089

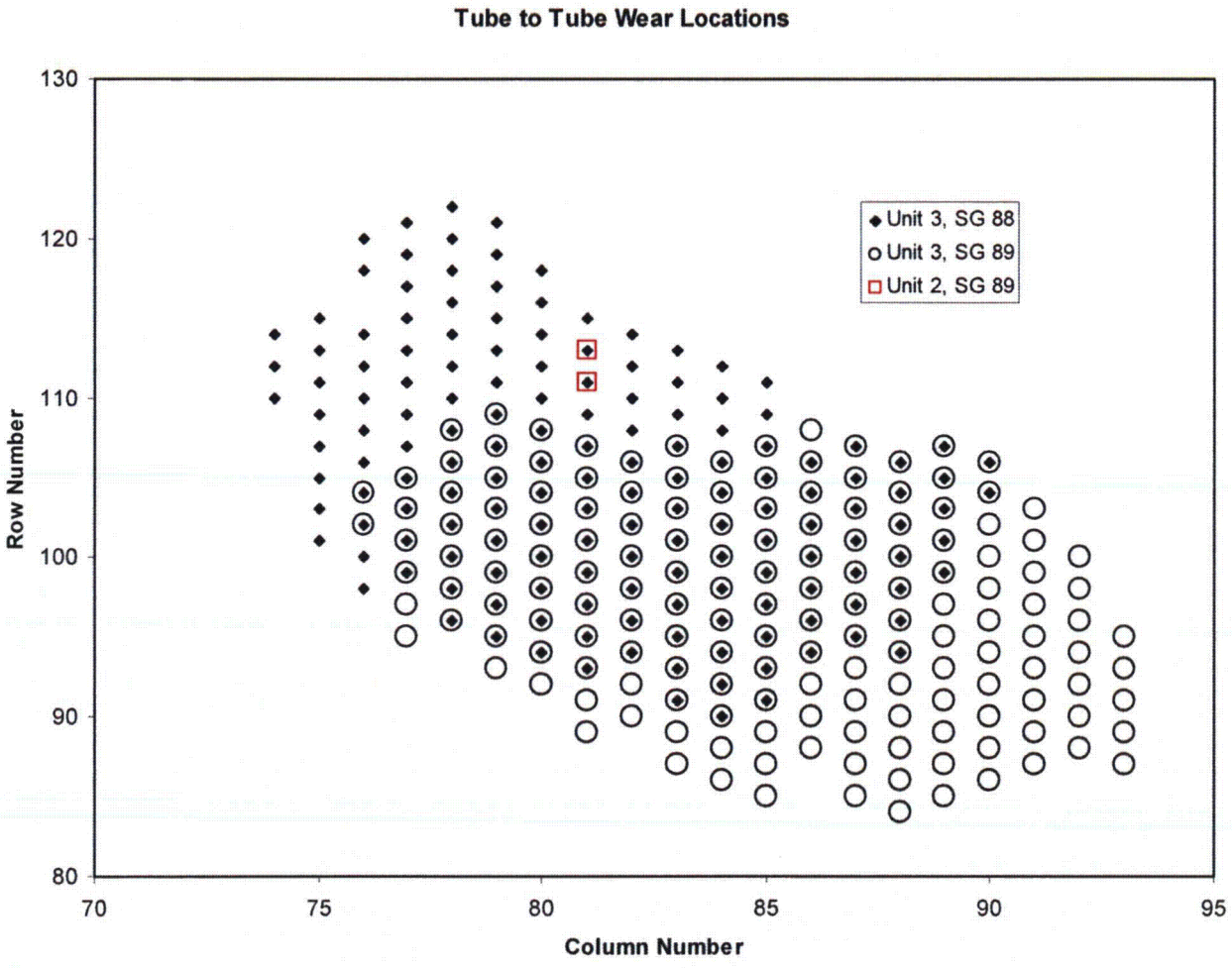

Figure 4-8: Combined View of TTW Indications

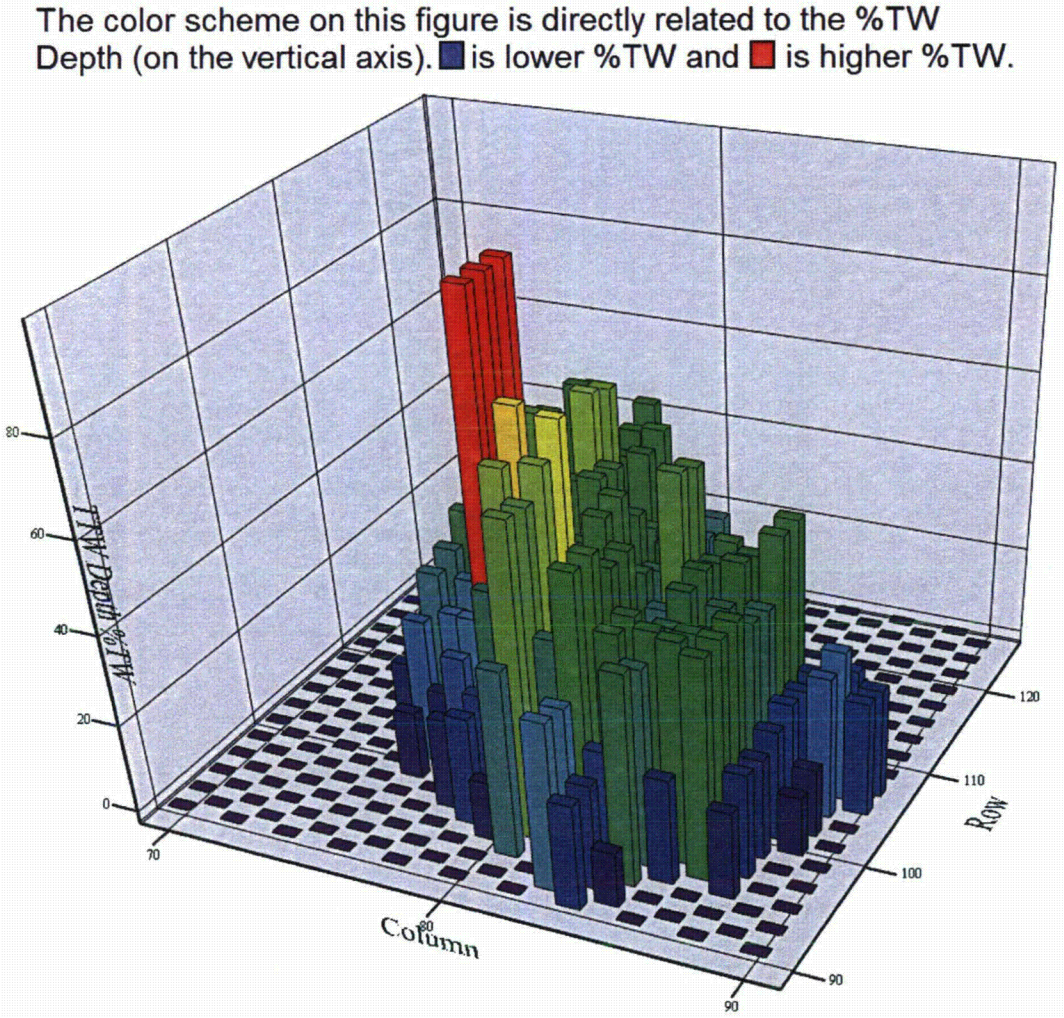

Figure 4-9: TTW Depth versus Row and Column, Unit 3 SG E-088

The color scheme on this figure is directly related to the %TW Depth (on the vertical axis). ■ is lower %TW and ■ is higher %TW.

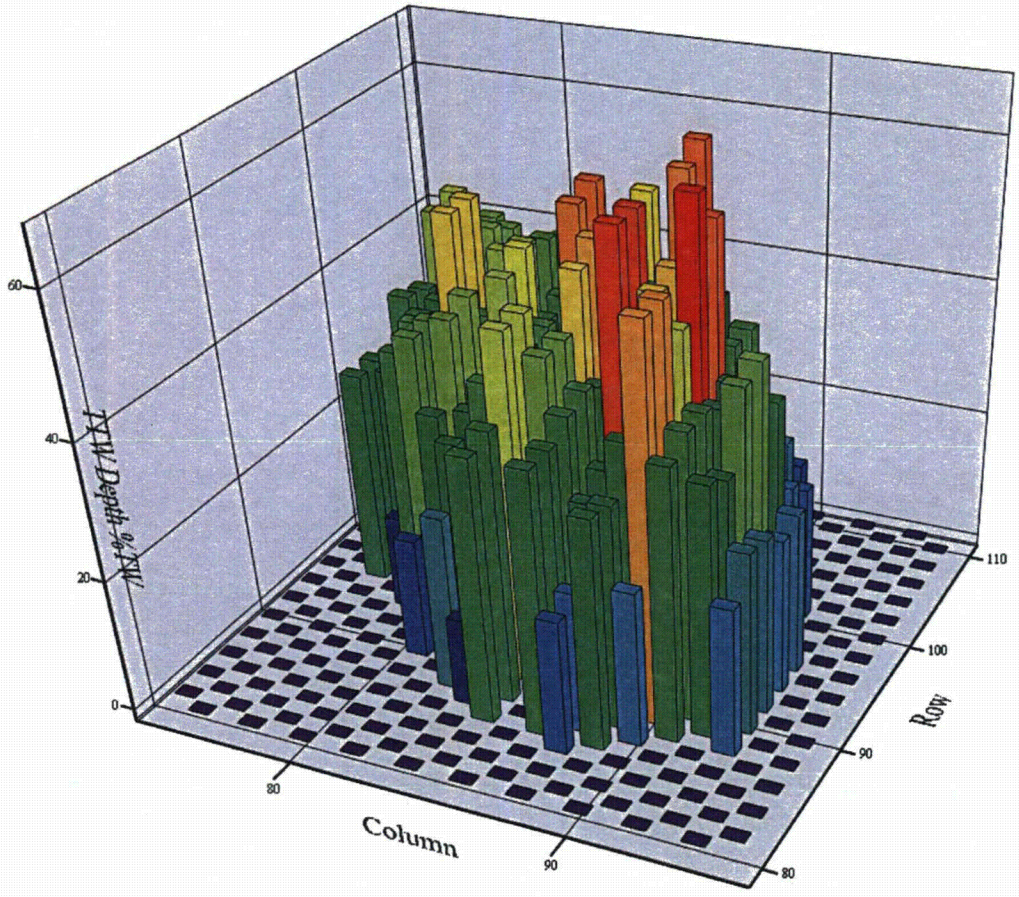

Figure 4-10: TTW Depth versus Row and Column, Unit 3 SG E-089

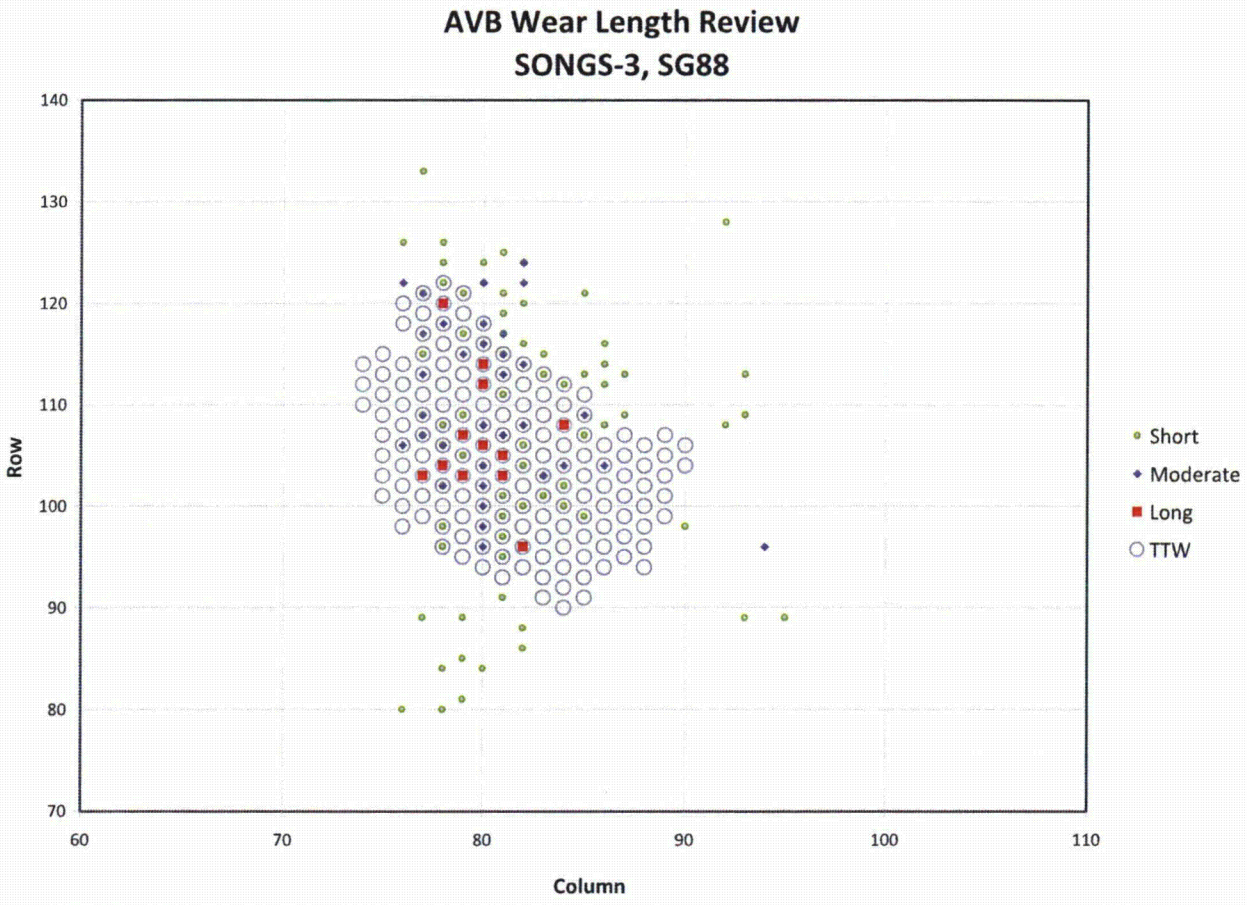

Note: This Figure is based on a +Pt™ probe evaluation of the AVB wear scar length compared to a bobbin probe evaluation of the AVB width.

Figure 4-11: No Elongated AVB Wear Found Beyond the Region of TTW, Unit 3 SG E-088

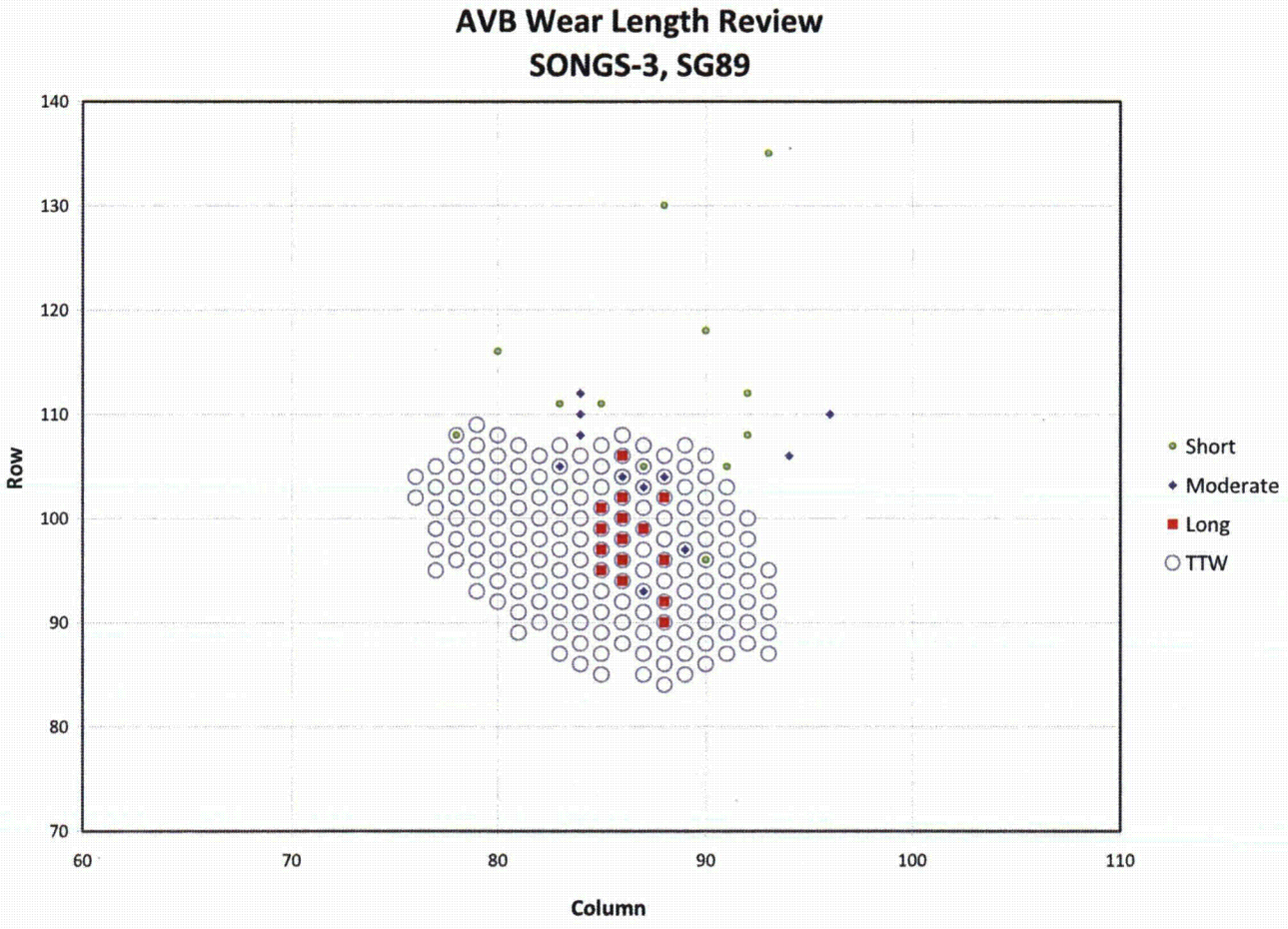

Note: This Figure is based on a +Pt™ probe evaluation of the AVB wear scar length compared to a bobbin probe evaluation of the AVB width.

Figure 4-12: No Elongated AVB Wear Found Beyond the Region of TTW, Unit 3 SG E-089

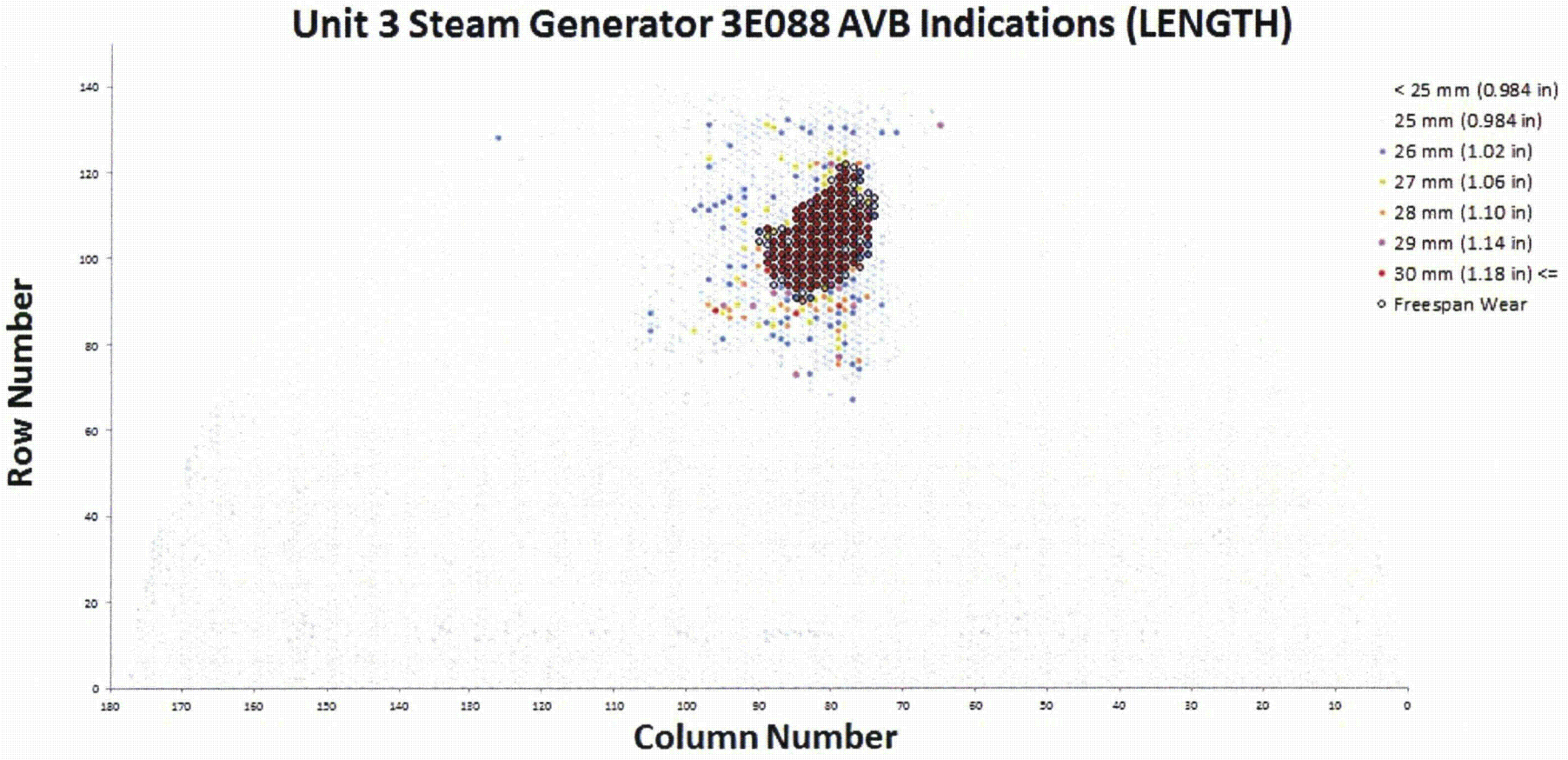

Figure 4-13: Tube Wear Length at AVBs for Unit 3 SG E-088

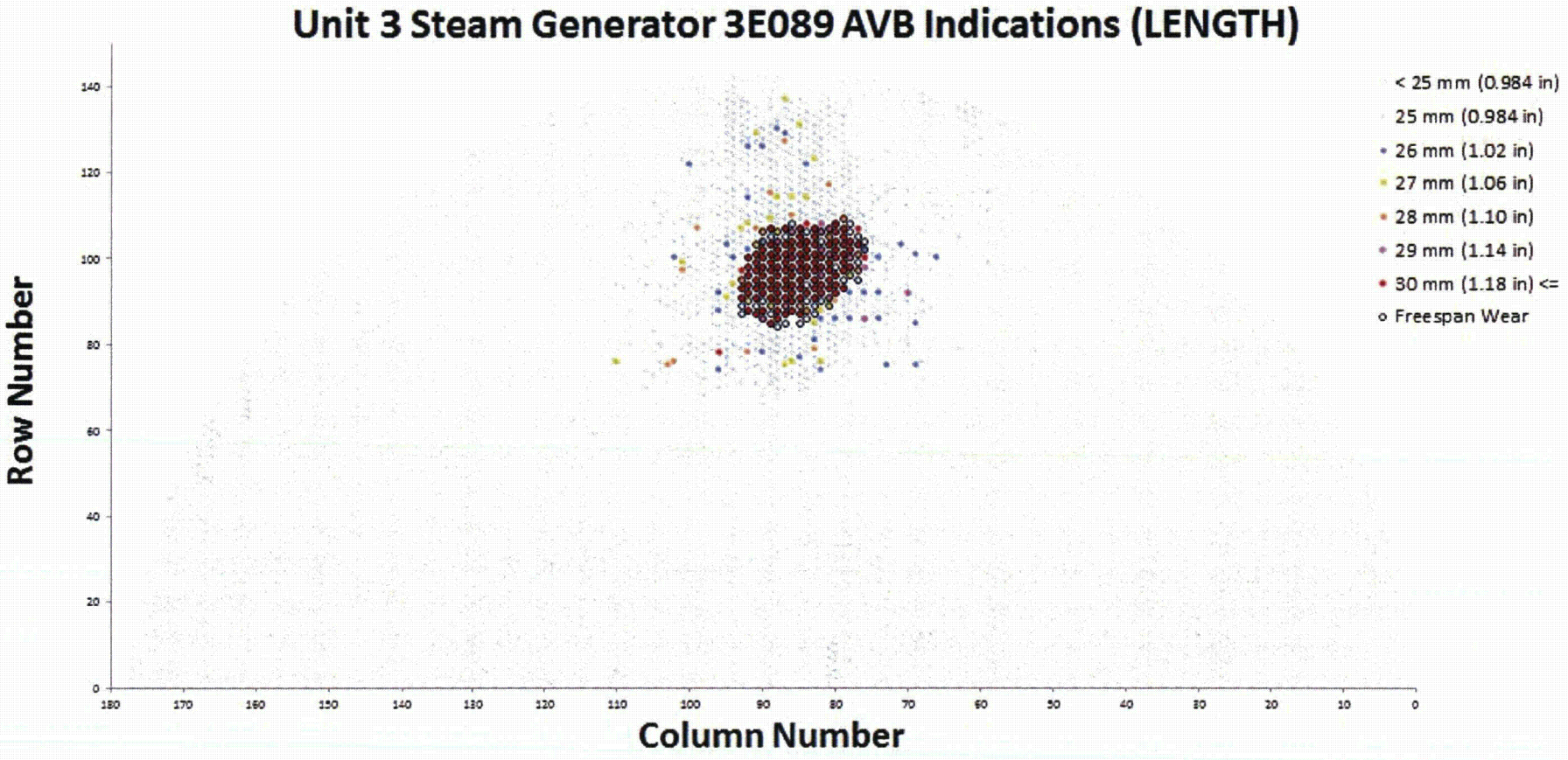

Figure 4-14: Tube Wear Length at AVBs for Unit 3 SG E-089

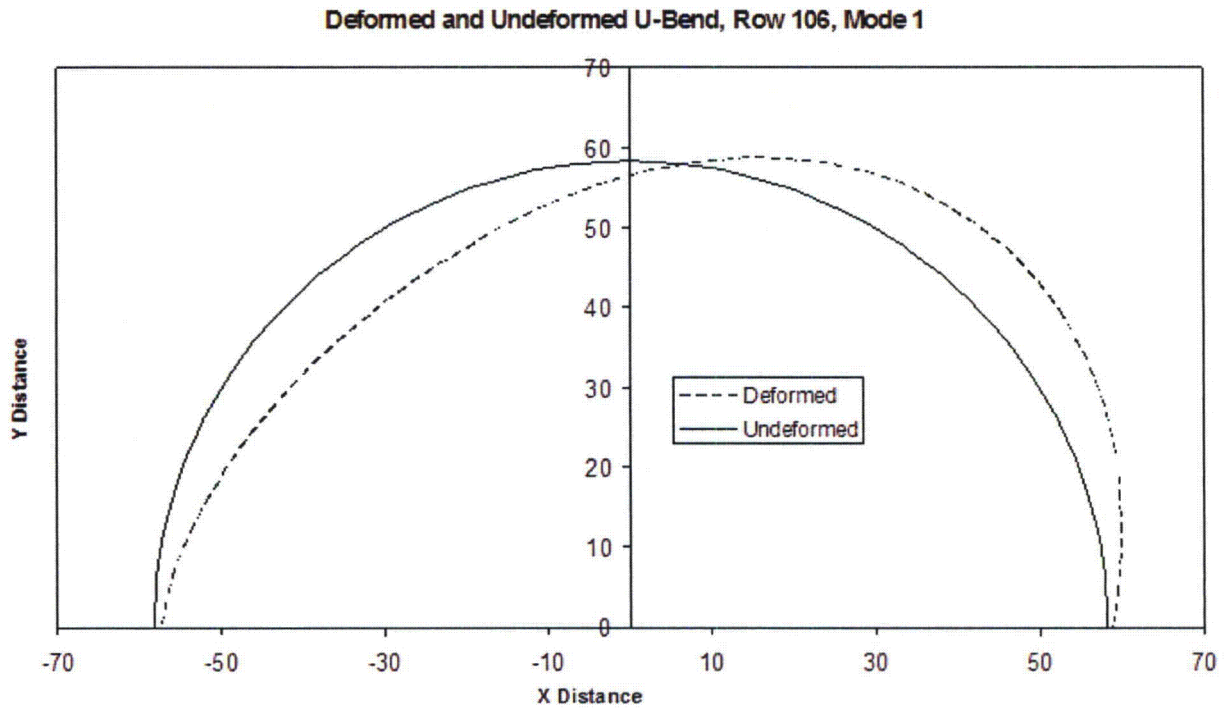

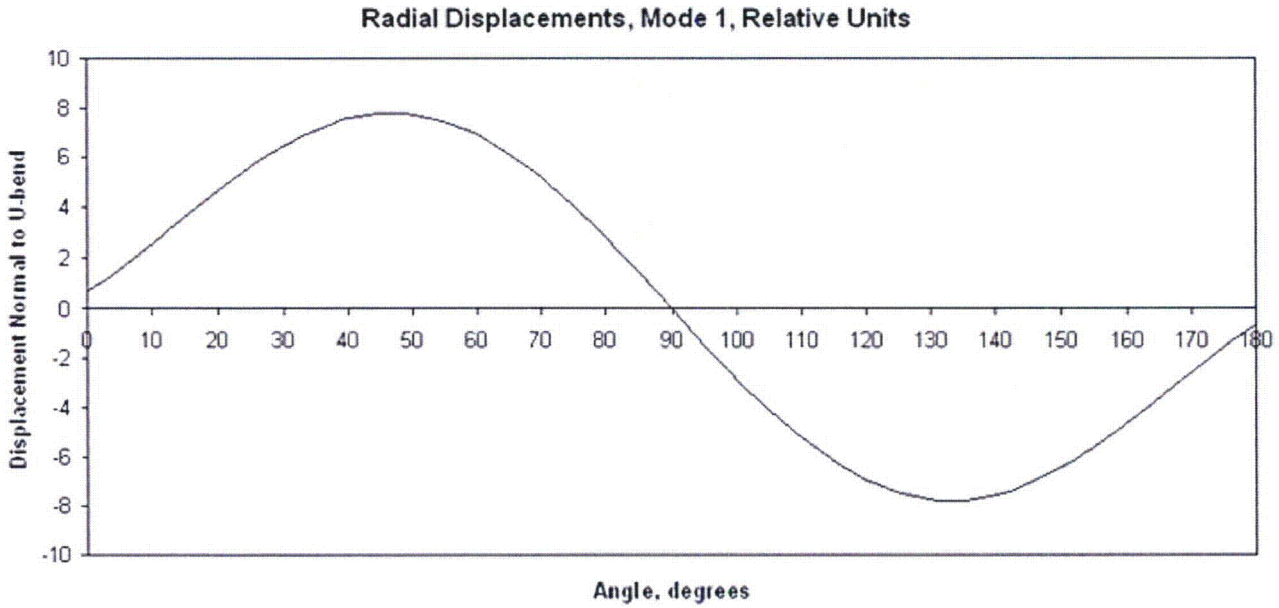

Figure 4-15: Mode 1 Displacement Pattern

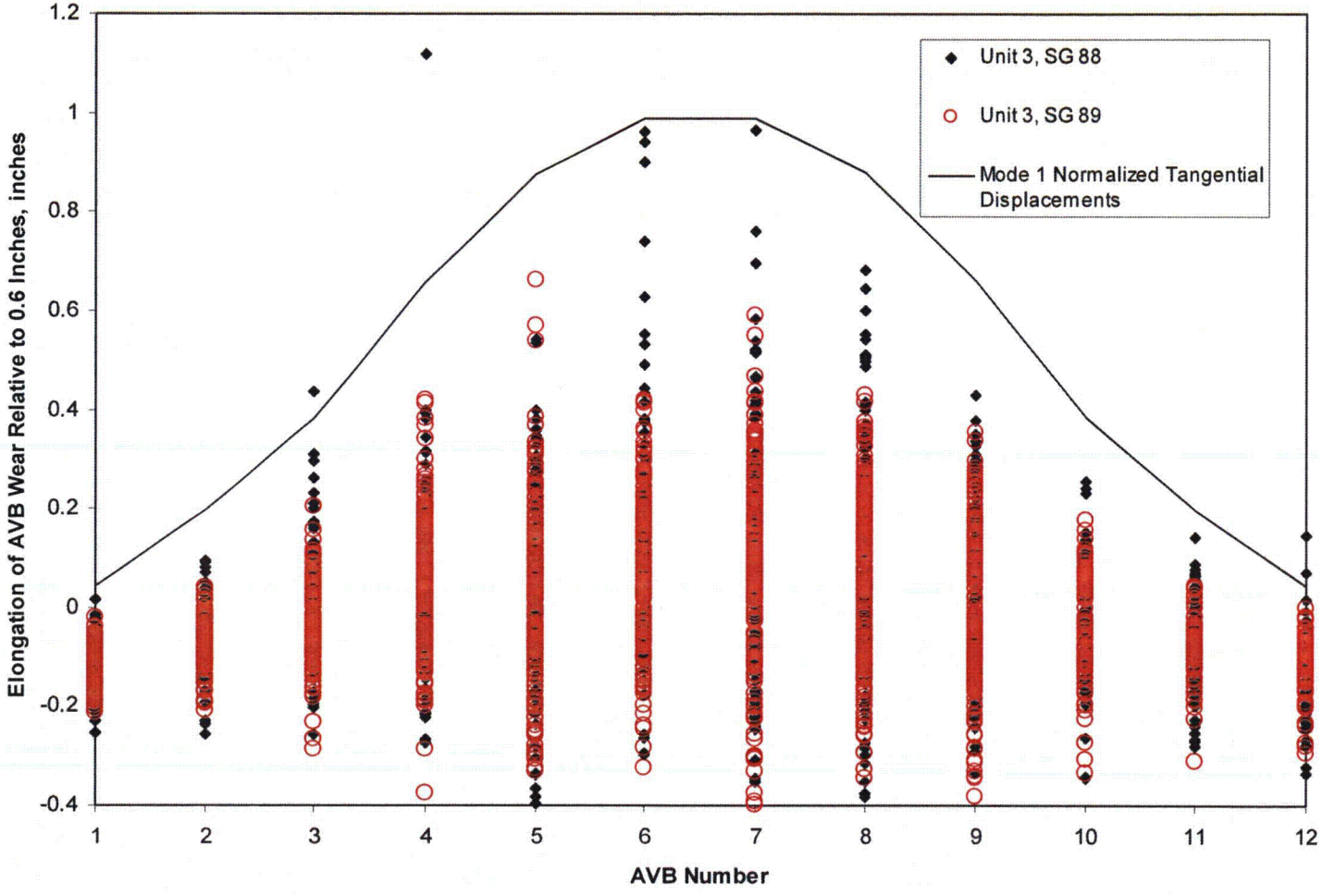

Figure 4-16: Elongation of AVB Wear at Each AVB

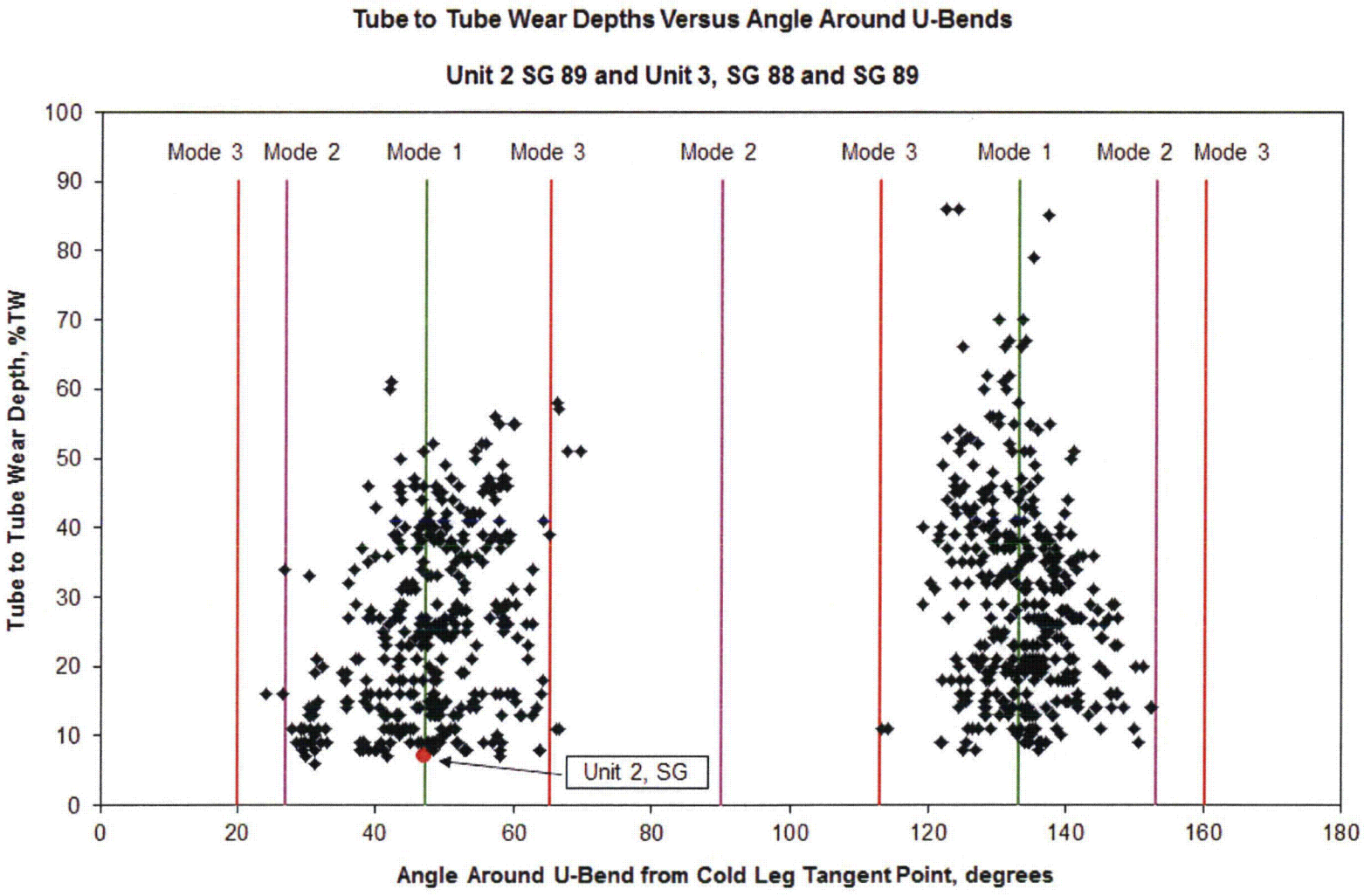

Figure 4-17: Impact Locations of Unstable Tubes

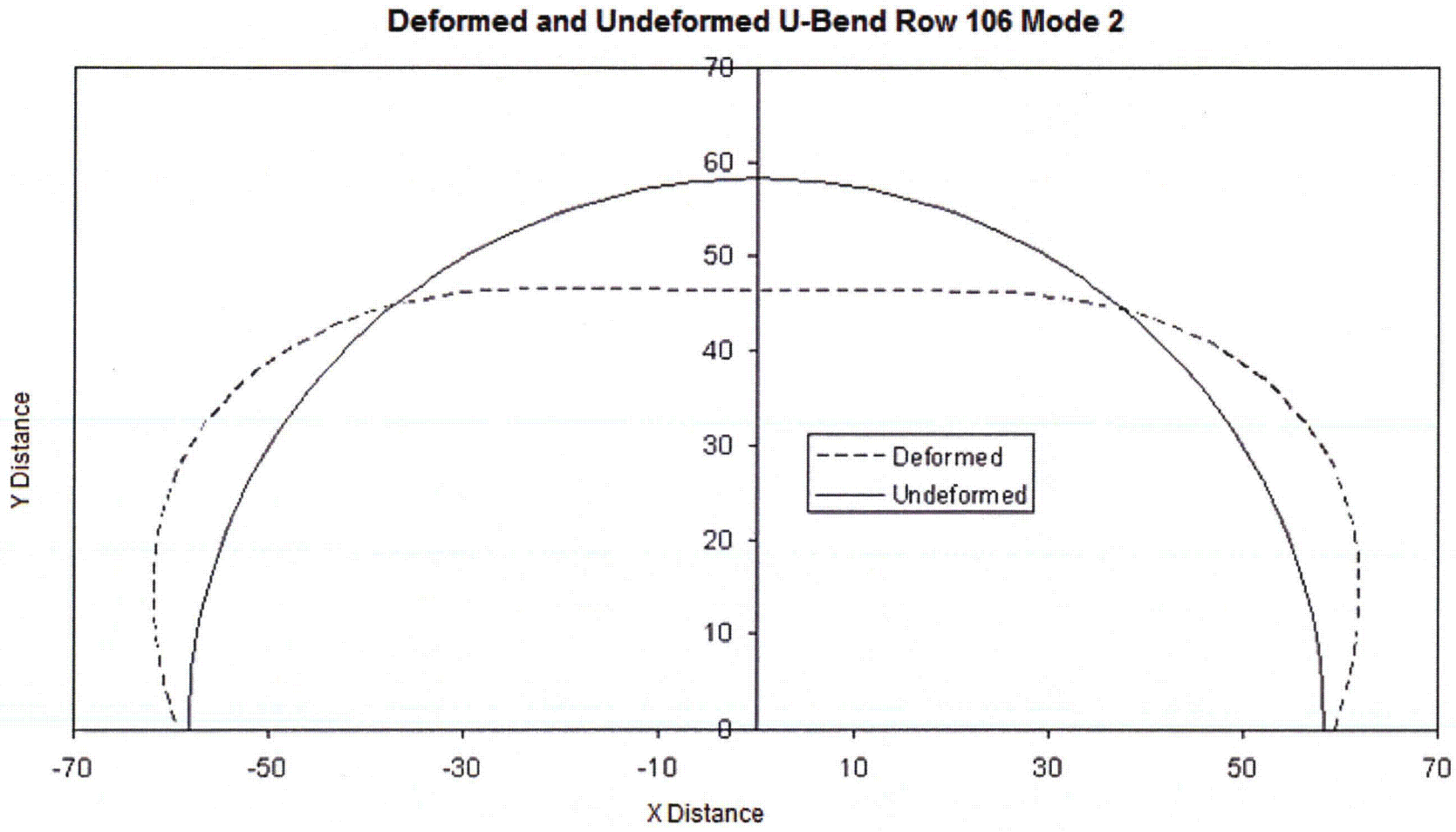

Figure 4-18: Mode 2 Displacement Pattern

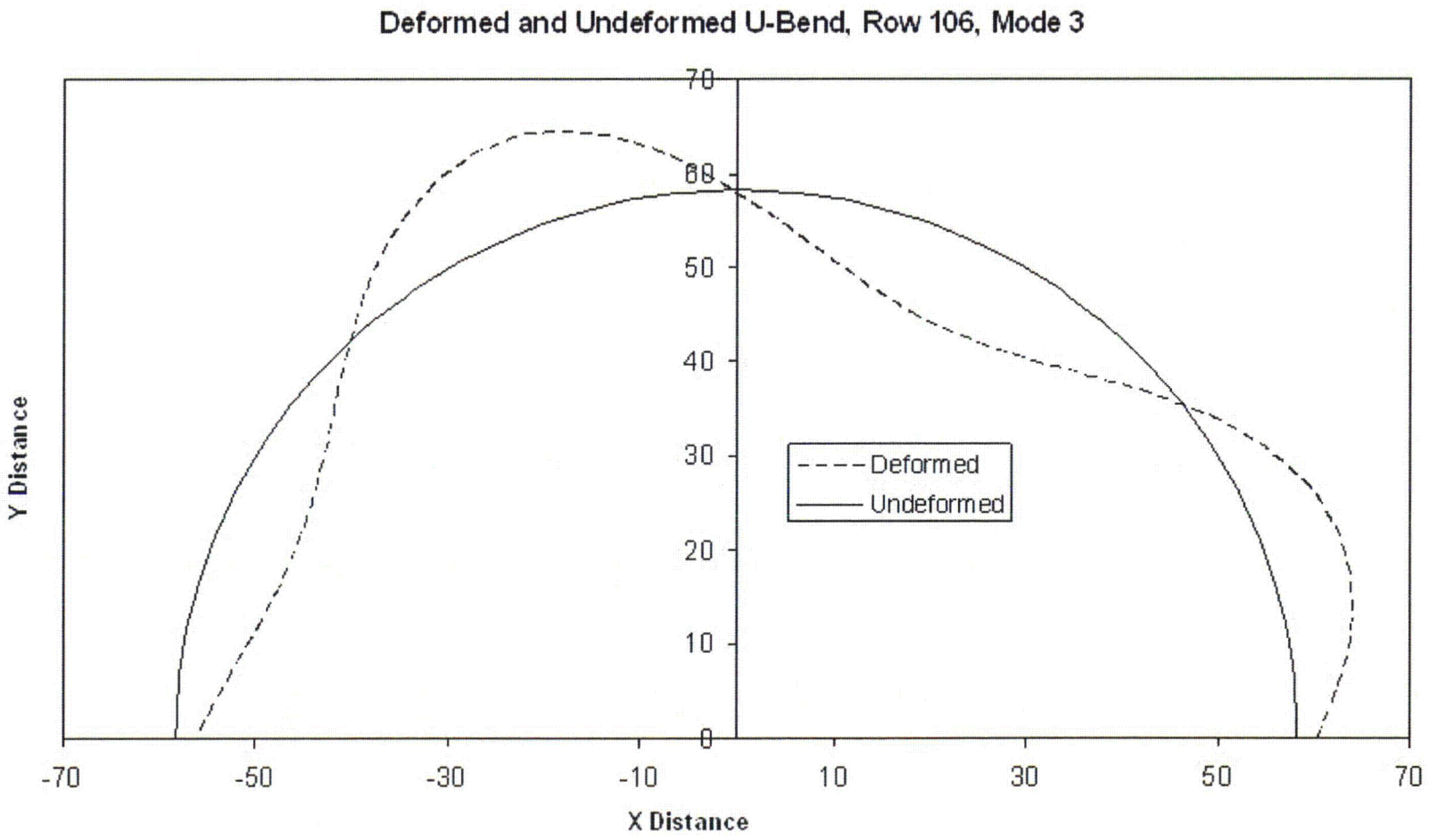

Figure 4-19: Mode 3 Displacement Pattern

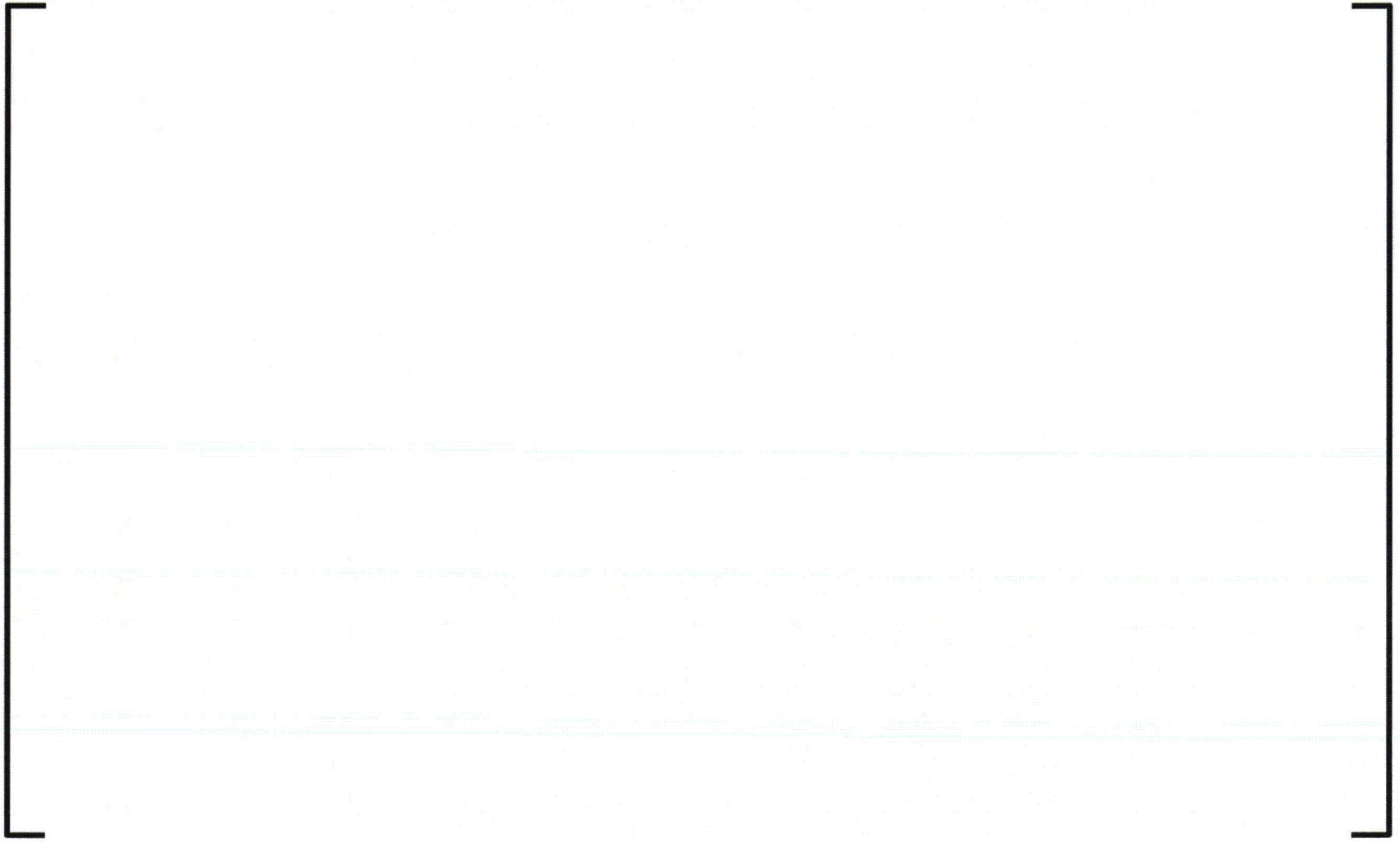

5.0 STABILITY RATIOS

An extensive effort was devoted to defining and refining the basis for the calculation of stability ratios. Calculation procedures and results are described in [20]. These results compare very well with independent calculations performed by Westinghouse [21]. It is important to state that stability ratio results are reported for the following conditions:

- 100% Power with an Upper 95th Percentile Stability Ratio
- 70% Power with an Upper 95th Percentile Stability Ratio
- 100% Power with an Upper 99th Percentile Stability Ratio
- 70% Power with an Upper 99th Percentile Stability Ratio

Basic conclusions regarding stability of U-bends at SONGS are based on the 95th percentile stability ratios. The more conservative 99th percentile ratios are presented only to demonstrate margin and degree of conservatism. The same holds true for references to instability developing at a stability ratio of 1 or more in contrast to maintaining a maximum stability ratio of 0.75. Again this later value is discussed in terms of margin and degree of conservatism.

Before beginning the discussion of the effect of power level on in-plane fluid-elastic stability, a more general engineering observation is pertinent. A decrease to 70% power places the SONGS steam generators back inside the operational envelope of demonstrated successful performance relative to in-plane fluid-elastic stability of nuclear steam generators with large U-bends. This is illustrated in Figure 5-1.

A stability ratio is a calculated value which depends on several inputs. A calculation of burst pressure of a degraded tube is exactly analogous. Uncertainties in input values lead to uncertainties in the output calculation. When all inputs are at mean values, a mean value of the output parameter is obtained. [

]

As previously stated, stability ratios depend on U-bend size, thermal-hydraulic conditions along the U-bend and the number of consecutive ineffective in-plane supports. Hence, stability ratios vary with position in the bundle and with the number of consecutive ineffective supports. This information is presented by means of a color coded tubesheet map, which was created by calculating stability ratios at 316 different locations and then interpolating between tube positions to develop a stability ratio for each tube. Figure 5-3 denotes the number of consecutive ineffective supports in-plane by color coding stability ratios equal to or greater than 1 for the SONGS-2 steam generators at 100% power and the no plugging condition at the beginning of life. At low rows, no in-plane supports are needed to maintain tube stability; therefore they have no effect on the probability calculations. In the highest susceptibility regions, instability is predicted if there are 5 consecutive ineffective supports. A decrease to 70% power produces dramatic effects; no in-plane effective supports are needed to maintain a stability ratio less

than 1, and as a result, the tubesheet map for instability is a blank sheet as shown in Figure 5-4. Thus demonstration of stability at 70% power is an appropriate basis for Unit 2 return to service.

There are two additional important considerations included in the 70% power result which are specific to Unit 2. Based on the measured wear at AVB locations, the comparisons with Unit 3 AVB wear patterns and the elevated risk of susceptibility to in-plane fluid-elastic instability, Unit 2 tubes will be plugged. These plugged tubes have an effect on local thermal-hydraulic conditions upon returning the SG to operation and have been included in the stability ratio calculations. [

] R113 C81 is shown because it has slightly higher computed stability ratios than does R111 C81. Stability ratio varies with amplitude as shown. All stability ratios are less than 1.0, assuming zero effective AVBs.

The remaining paragraphs of this section deal with margin, sensitivity and degree of conservatism arguments. These are necessary elements of a complete evaluation of in-plane fluid-elastic stability. [

]

[

]

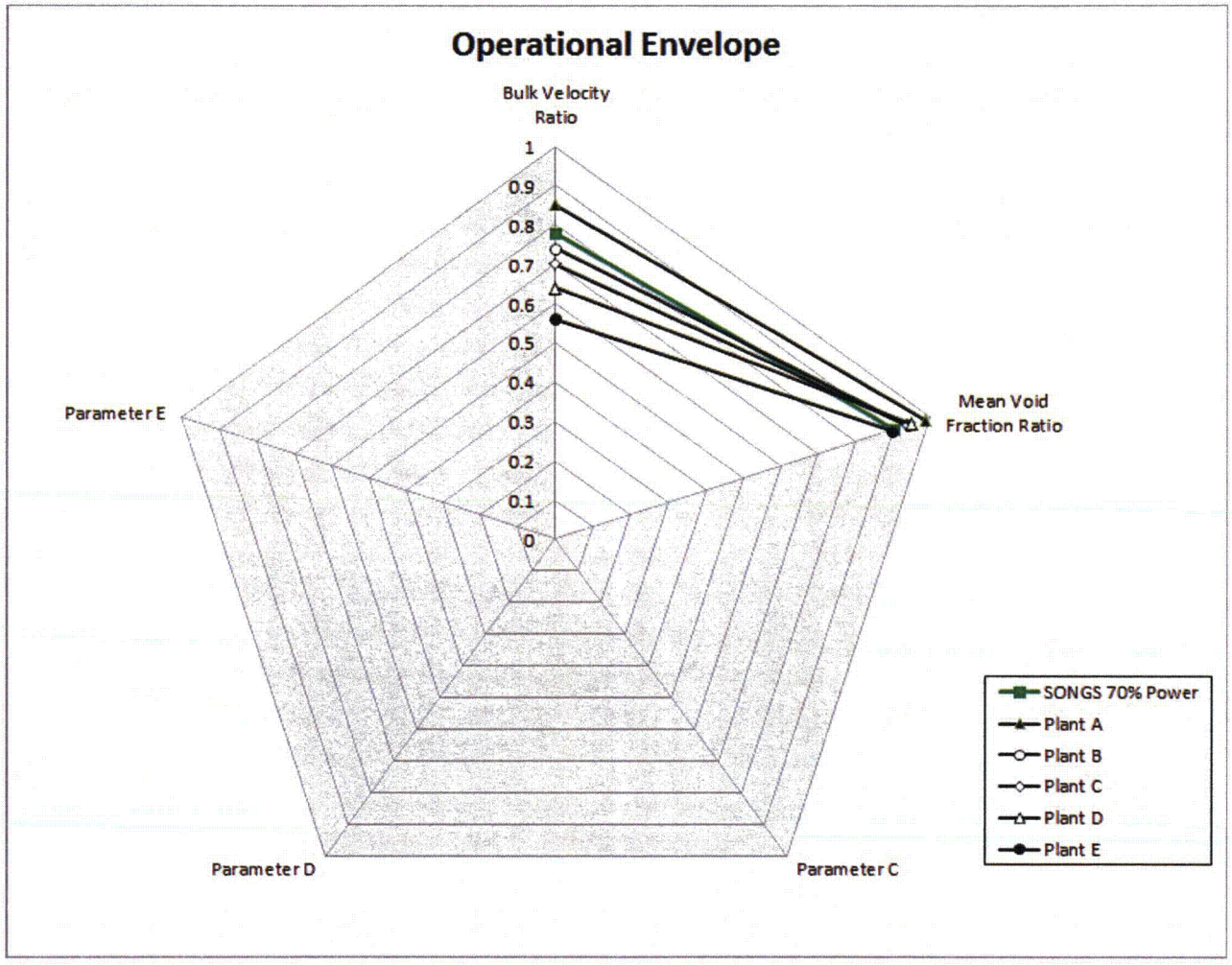

Figure 5-1: Spider Diagram of the Successful Operational Envelope for Nuclear Steam Generators with Large U-bends

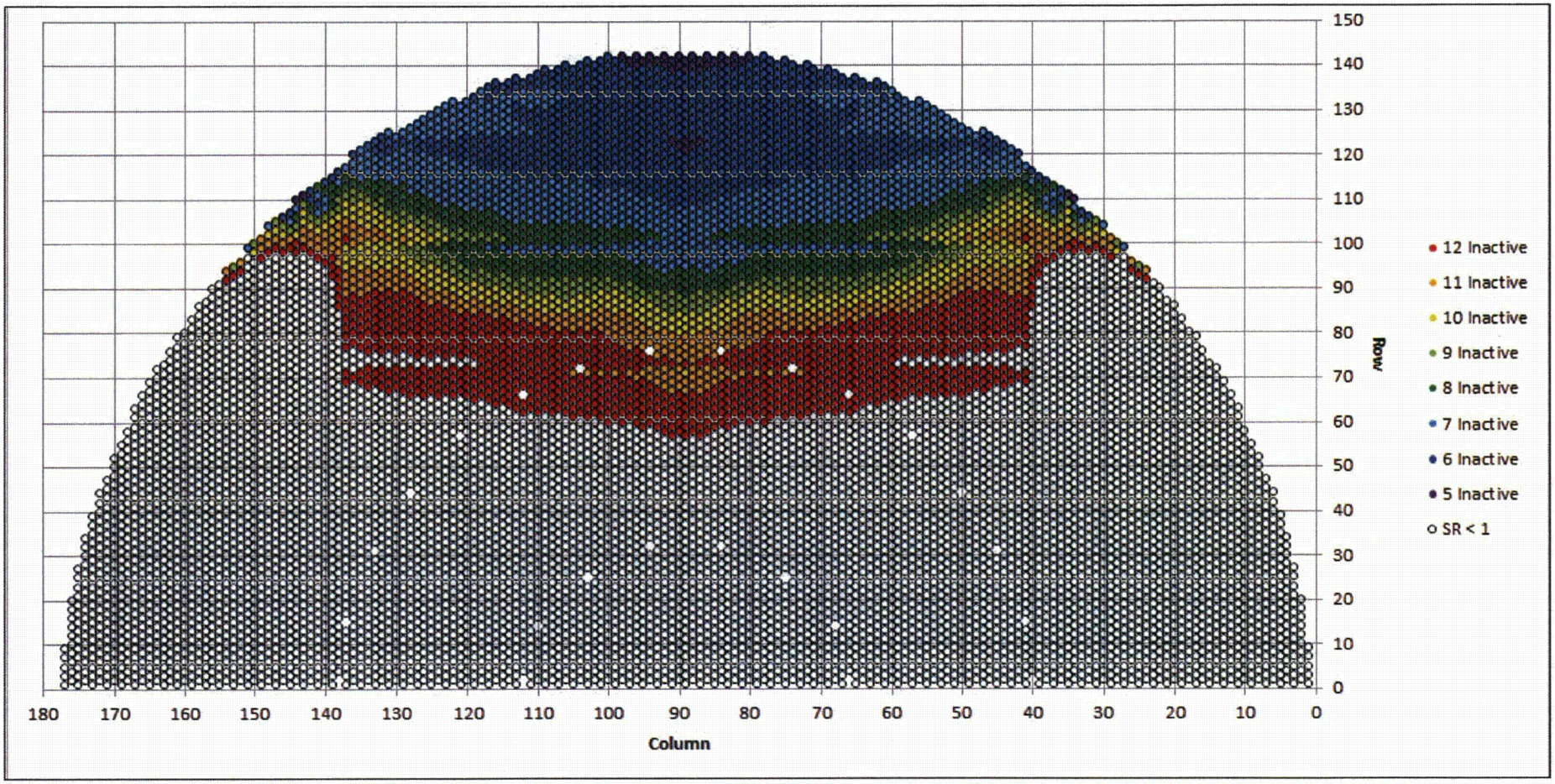

Figure 5-3: Stability Map at 100% Power, No Plugging, 95th Percentile SR, SR ≥ 1

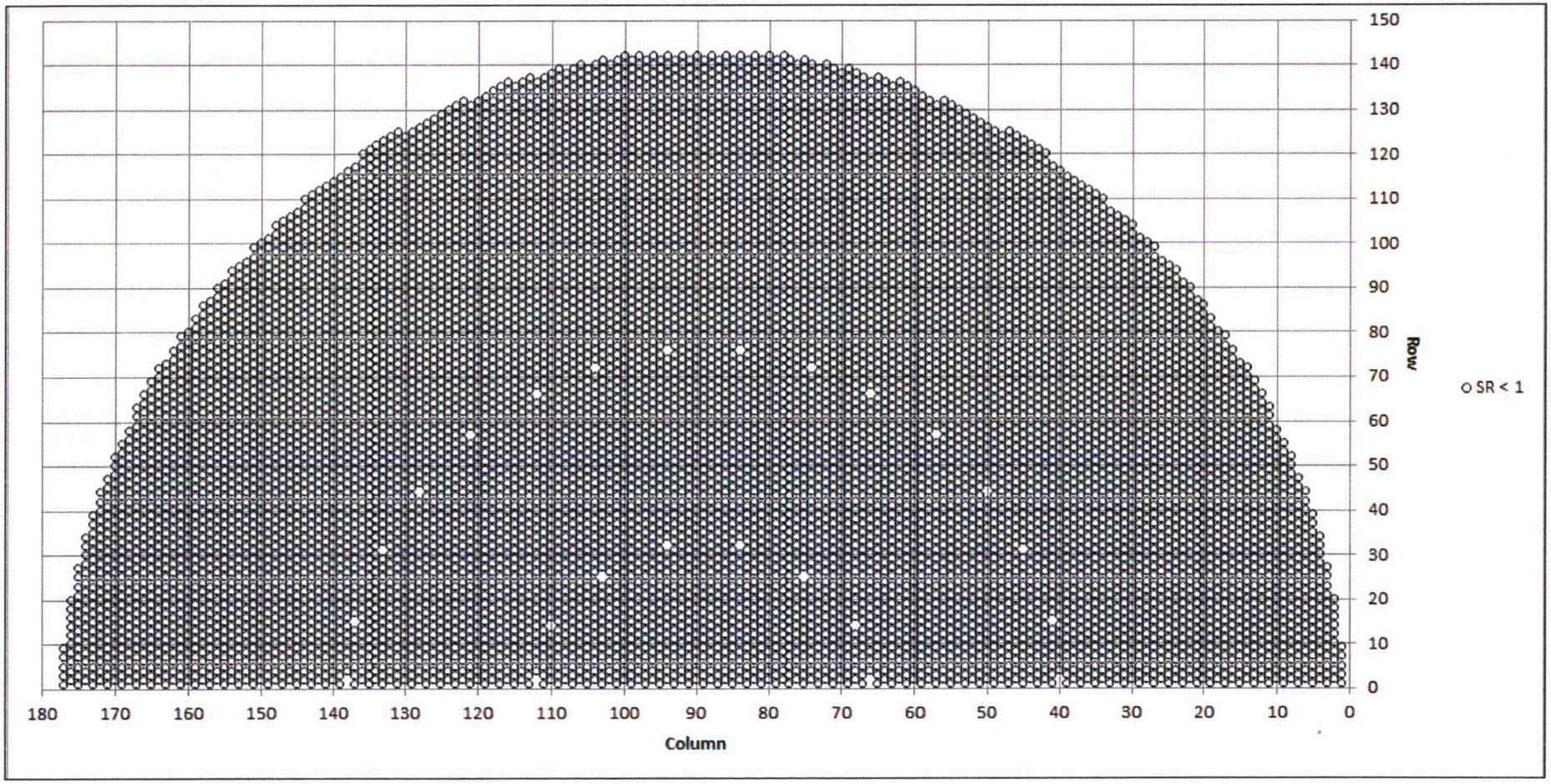

This blank figure is not an error. Even with no effective in-plane supports there are no unstable U-bends at 70% power

Figure 5-4: Stability Map at 70% Power with Plugging and Split Stabilizers, 95th Percentile SR, SR ≥ 1

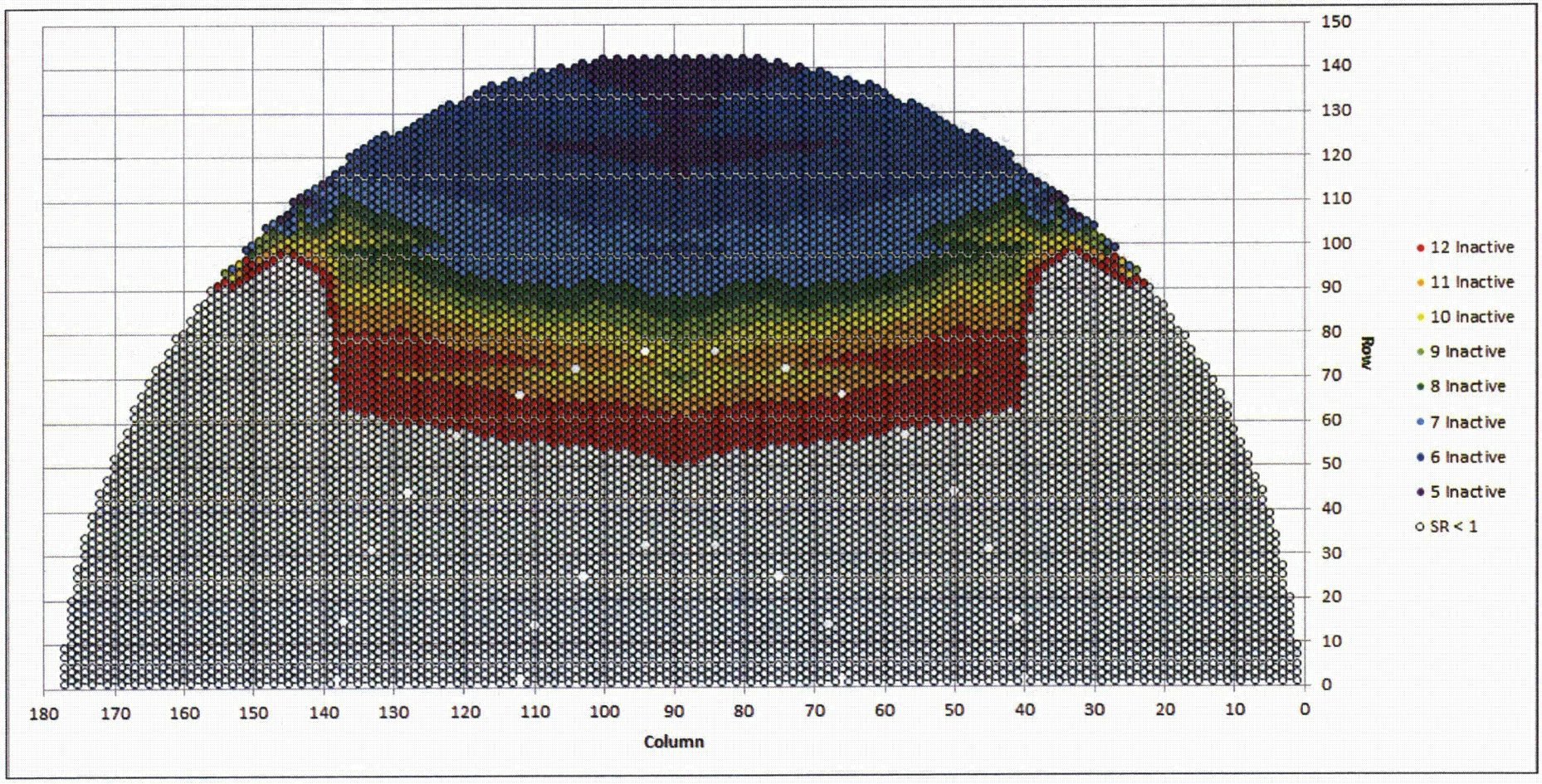

Figure 5-6: Stability Map at 100% Power, 99th Percentile SR, SR ≥ 1

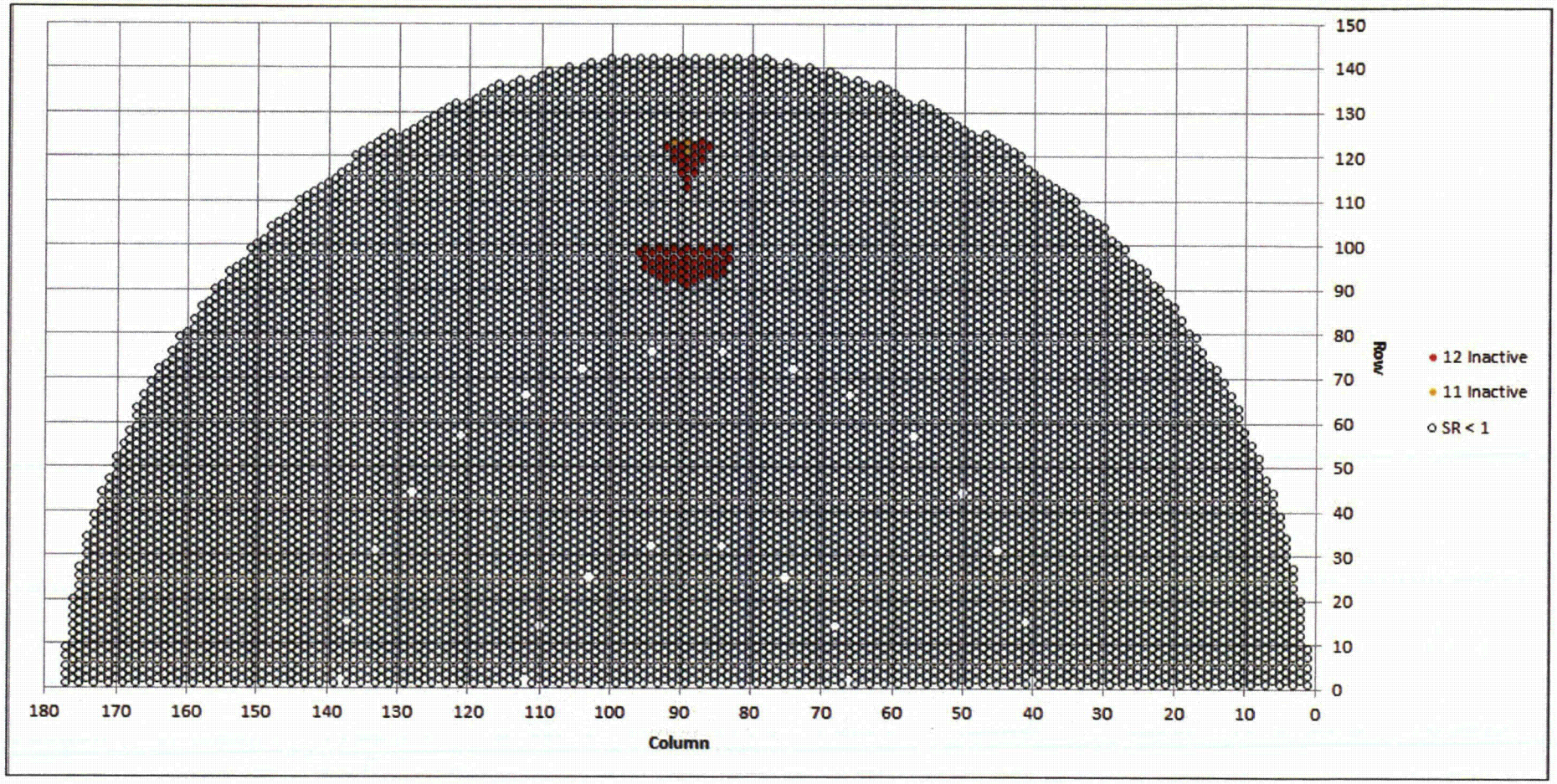

Figure 5-7: Stability Map at 70% Power with Plugging and Split Stabilizers, 99th Percentile SR, SR ≥ 1

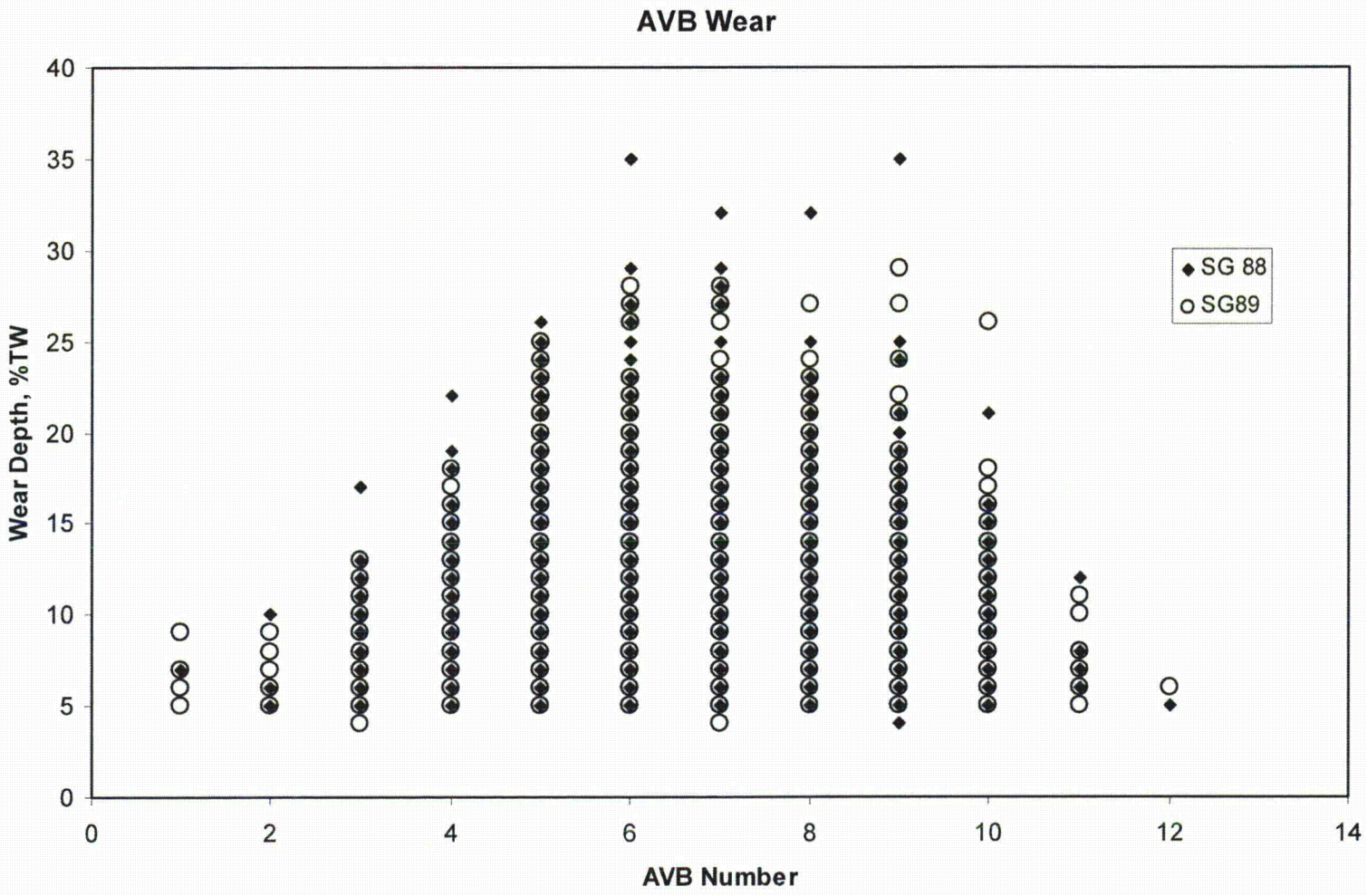

Figure 5-8: Depth of AVB Wear Indications versus AVB Number, Unit 2, SG E-088 and SG E-089

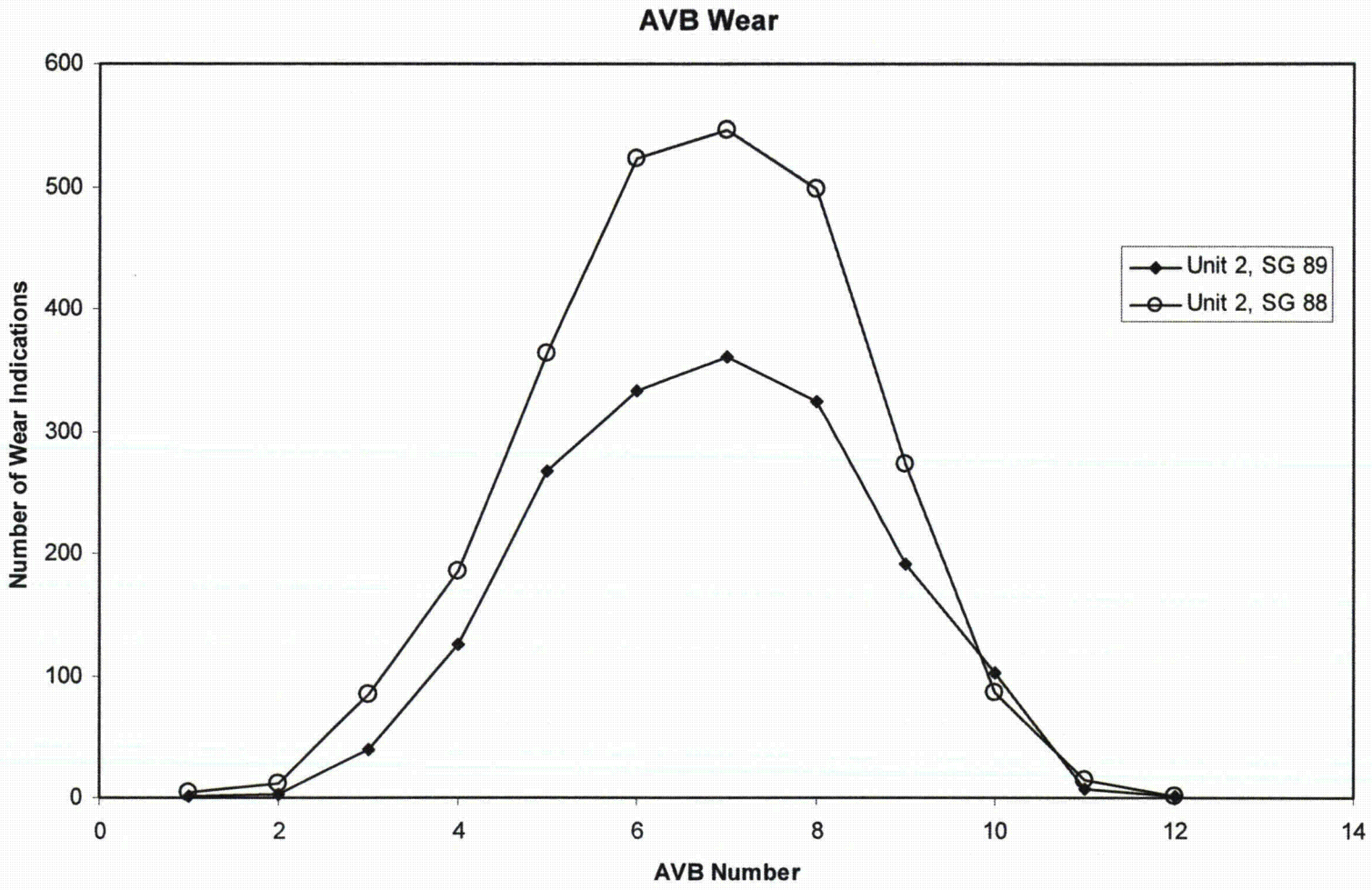

Figure 5-9: Number of AVB Wear Indications versus AVB Number

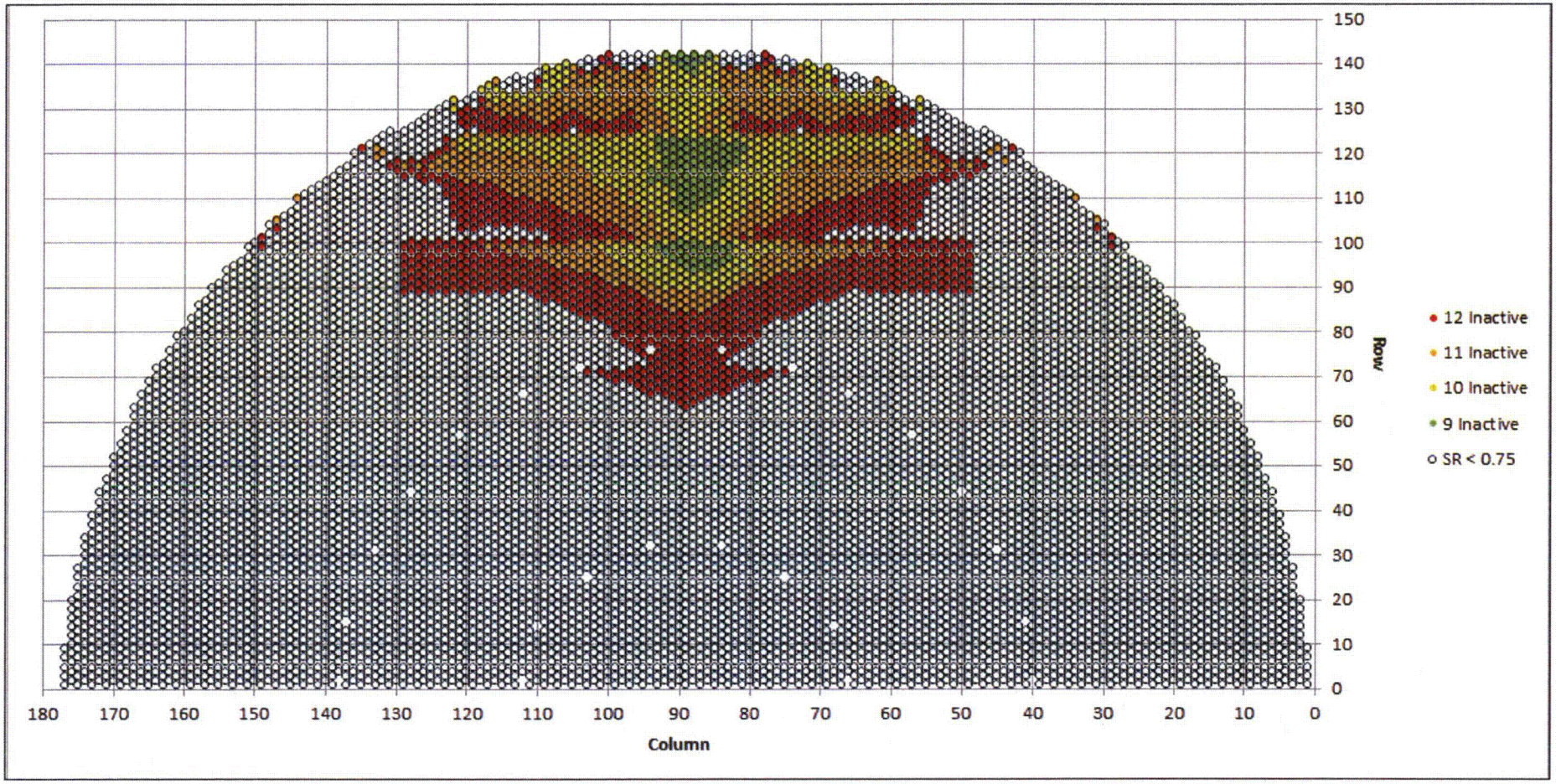

Figure 5-10: Stability Map at 70% Power with Plugging and Split Stabilizers, 95th Percentile SR, SR ≥ 0.75

6.0 CONTACT FORCES

Estimations of tube-to-AVB contact forces are a key component in probability of instability calculations. The contact forces are calculated using a finite element computer model, which is explained in Section 6.1. Contact force distributions output from the model are summarized in Sections 6.2 and 6.3. The calculated gap distributions compare well with observations from PSI and ISI data, as shown in Sections 6.4 and 6.5. Section 6.6 presents a summary of contact force and why the calculated forces are an appropriate basis for demonstrating margins to fluid-elastic instability at 70% power via probability of instability calculations.

6.1 MHI Quarter Bundle Steam Generator Model

[

] A gap distribution provides the input to the contact force problem. The quarter model then computes the interactions between all tubes and AVBs. The contact force on either side of a tube is part of the output along with the resulting balanced gaps which are considerably different from the input gaps. [

]

The contact forces are calculated based on the principle that the sum of the forces in the bundle is equal to zero; the nominal tube bundle geometry; and the random dispersion of the tube bundle component dimensions. Also used as input are the elastic material properties of the tube bundle components. A set of initial gaps is chosen for the model, the bundle geometry constraints are added, and the finite element model is solved to balance all of the forces. The primary source of tube-to-AVB contact forces is the restraint provided by the retaining bars and bridges, reacting against the component dimensional dispersion of the tubes and AVBs. Contact forces are available for both cold and hot conditions. Contact forces significantly increase at normal operating temperature and pressure due to diametric expansion of the tubes and thermal growth of the AVBs.

The initial gaps that are input to the MHI finite element model have a distribution that is approximately normal with a mean of zero. Six factors contribute to the gap distribution:

- Tube diameter
- AVB thickness
- TSP hole mislocation
- AVB twist
- AVB flatness
- Tube flatness

[

MHI Proprietary

Figure 6-1 shows a 3D plot of the AVB locations in the quarter model. Each run of the quarter model inputs gaps randomly selected from the input distribution. The output of one run is one of many possible states of contact forces and final gaps at each location shown in Figure 6-1. Given lengthy computation times, it is not practical to use an individual run of the quarter bundle model as a single Monte Carlo trial for contact forces. It is necessary to combine runs of the quarter model to define the state of contact forces and gaps in small zones of the bundle. A zone size of ten rows by ten columns was found to be practical. Each zone contains approximately 50 tubes. By combining multiple runs of the quarter model, cumulative distributions of contact forces can be constructed for each AVB in a particular zone. These cumulative distributions are characteristic of the zone and hence Monte Carlo trials for contact forces in the zone can be performed. Four runs of the quarter model are used in constructing cumulative distributions of contact forces for each AVB in the zone.

A wide variety of cases were examined to select the best description of the distributions of the contact forces that best match the NDE data and observations of the Unit 2 and Unit 3 steam generators. The six factors that contribute to the input gap distributions set the scale of the problem but additional guidance is needed. The main benchmark used by MHI is the number and magnitude of classic dent signals found in the pre-service inspections (PSI) of Units 2 and 3. Systematic laboratory testing (Appendix 9 of Reference [22]) correlated both on load and off load dent signal amplitude with applied loads of an AVB pressed at a small angle against a tube. [

] The comparison of dents in the steam generators to the contact forces predicted by the model served as a primary benchmark of contact force calculations.

A post check of the reasonableness of contact force calculations was provided by an extensive program of AVB to tube gap measurements using ultrasonic and newly developed eddy current techniques [14]. While the primary purpose of gap measurements was to determine if there were highly heterogeneous spatial distributions of large gaps that are not included in contact force calculations, the gap measurements were used as a check, albeit subtle, of the reasonableness of contact force calculations and differences between Units 2 and 3. An additional check of differences between Unit 2 and Unit 3 is provided by the use of non-classical dent/contact signals that have been found to be eddy current footprints of contact between tubes and support structures in other steam generators. These checks are discussed after the presentation of contact force results for Units 2 and 3.

6.2 Contact Force Distributions – Unit 3

The zones used to develop characteristic distributions of contact forces for each AVB in the zone are plotted in Figure 6-2. Note that only zones for rows 63 and higher are shown. Contact forces are available for all regions of the steam generator but these are the zones of interest since lower rows have a negligible contribution to probability of instability calculations. Unit 3 is considered first. Figure 6-3 through Figure 6-6 contain plots of the cumulative distributions of contact forces for zones 1, 3, 5 and 8 for Unit 3 at BOC 16. Only AVBs 1 through

6 are shown since quarter model results are used. By symmetry AVBs 12 to 7 correspond to AVBs 1 through 6 respectively. The tubes included in these zones are as follows:

- Zone 1, Rows 133 to 142, Columns 80 to 89
- Zone 3, Rows 113 to 122, Columns 80 to 89
- Zone 5, Rows 93 to 102, Columns 80 to 89
- Zone 8, Rows 63 to 72, Columns 80 to 89

All of the above zones are adjacent to the center column. Zone 1 is at the periphery and Zone 8 begins at row 63. Figure 6-3 shows that contact forces are relatively high at the periphery. This is a high stiffness region since here the ends of AVBs are welded to the retaining bars which essentially are arranged as longitudinal lines across the hemispherical top of the bundle. At approximately 10 column intervals the retaining bars are welded to bridges which are essentially arranged as latitude lines. See Figure 2-2. Nominal clearances between AVBs and tubes (0.001 inches each side cold) are set by the distances between bridges when the bridges are welded to the retaining bars. Other high stiffness locations are at the noses of AVBs, see Figure 2-1, and the top tube support plate. AVBs 1 and 12 are closest to the top tube support plate.

The cumulative distribution function (CDF) of contact force for a given AVB is read as follows. Select any given contact force and read the value of the cumulative distribution. This is the fraction of all possible contact forces for that AVB in that zone that lie at or below the selected value. If, for example, the selected contact force is identified as the value needed to provide an effective AVB support then the value of the CDF distribution is the probability that the support is ineffective. The rule is simply high CDF plots indicate a higher probability of support ineffectiveness than lower CDF plots. In terms of interpreting CDF plots, a rough figure of merit for effective AVBs is a contact force in the vicinity of 10N. Consider Figure 6-3, all CDF plots at 10N are below a CDF of 0.1. Using the rough figure of merit, the AVBs would be effective more than 90% of time. As one moves away from the high stiffness periphery, contact forces decrease. Note the relatively high CDF plots for Zones 3 and 5 in Figure 6-4 and Figure 6-5. AVBs 4 and 5 exhibit relatively high CDF plots. This is true of AVBs 4 and 5 in almost all zones. These are two of the longest AVBs with a relatively large separation between high stiffness regions at the periphery and the nose of the AVB. Additionally, the longest AVBs have the smallest bend angles at the nose sections. This leads to less distortion and consequently a smaller AVB twist. AVB 1 is as long as AVB 4 but remains relatively close to the top tube support plate. AVBs 1, 2 and 3 usually exhibit the lowest CDF plots. AVB 6 is the shortest AVB and usually exhibits an intermediate CDF plot prior to wear considerations.

As one moves radially outward from Zone 8 toward the periphery, CDF plots lower in Zone 29 and then drop significantly in the periphery in Zone 35. Moving from Zone 8 directly across to lower columns, CDF plots exhibit small changes (see Zone 32 in Figure 6-9 and Zone 56 in Figure 6-10), before decreasing significantly at the periphery in Zone 64 which is comparable to Zone 35.

The introduction of wear at AVB locations produces large changes in contact forces particularly for Unit 3. The wear zone extends approximately from row 70 to row 140 and from the center column out to about column 65. The zones of most interest are 3, 4 and 5. Zone 5 is chosen for illustrative purposes. Comparing Figure 6-5 with Figure 6-11, note the dramatic elevation gain of CDF plots for all AVBs in Zone 5 after 3 months of wear in Unit 3. Note specifically the high fractions of zero contact forces. After 3 months of wear Unit 3 has much fewer effective in-plane supports in Zones 3, 4 and 5. After 11 months of wear, as shown in Figure 6-12, contact forces have been virtually eliminated in Zone 5.

6.3 Contact Force Distributions – Unit 2

Contact force distributions for Unit 2 at the beginning of life are shown in Figure 6-13, Figure 6-14, Figure 6-15 and Figure 6-16 for Zones 1, 3, 5 and 8 respectively. As with Unit 3, CDF plots for Unit 2 are lower near the periphery and increase in elevation for Zones 3 through 5. AVBs 4 and 5 again exhibit the highest CDF plots. The CDF plots are considerably lower for AVB 6 for Unit 2 compared to Unit 3. This is a consequence of increased AVB twist in Unit 2 at the nose of AVBs. Overall, low CDF plots are noted for AVB 1, 2, 3 and 6 for Unit 2.

The contact force distributions developed for Unit 2 are more resistant to the effects of wear. After 22 months of operation the severity of wear in Unit 2 is similar to that experienced by Unit 3 after 11 months of operation. Similar does not mean the same. The worst case steam generator in Unit 2 had about 2600 wear indications at AVBs [23] compared about 3400 wear indications in Unit 3 [12]. There was also significantly less wear in Unit 2 at the four lower AVB locations, 1, 2, 11 and 12.

The effects of wear are now considered in Zone 5 after 22 months of full power operation and then subsequently for 6 months of 70% power after restart. Zone 5 is characteristic of the most significant Zones, 3, 4 and 5. Figure 6-17 shows that wear after 22 months in Unit 2 has grossly altered the contact force distributions for AVB 5 and 6, particularly AVB 6 with very high fractions of zero contact forces. In contrast, AVB 1 and 2 maintain low CDF plots. Wear has moved AVB 3 from a low CDF plot to an intermediate position. Considering all AVB locations, wear has a less dramatic effect on contact force distributions in Unit 2 compared to Unit 3. Comparing Figure 6-17 and Figure 6-18 shows that conservatively projected wear after restart at 70% power produces very little noticeable change in contact force distributions after 6 months of operation at reduced power. This augurs well for demonstration of continuing margin over time at reduced power from probability of instability calculations.

6.4 Dent Evaluation

The following paragraphs describe checks of contact force calculations from observations of PSI dents, ISI contact forces and AVB to tube gap measurements.

6.4.1 Pre-Service Dents

Figure 6-19 and Figure 6-20 present tubesheet maps of dents detected in the pre-service inspections of Unit 3, SG E-089 and Unit 2 SG E-089 respectively. The dent eddy current signal amplitudes vary for 0.5 to 1.5 volts. The larger dents are plotted with enlarged symbol size. In production, minimum reporting levels for dents during eddy current analysis are about 1.0 volts. Dents with lower signal amplitudes are often used as a diagnostic tool. [

] Figure 6-19 shows there are relatively few of these locations in Unit 3 SG E-089 with the same observation being true for SG E-088. In stark contrast, Figure 6-20 shows that there are very many locations of 0.5 volt dents and high loads in Unit 2 SG E-089. These dents occur at the noses of AVBs 6 and 7 near row 48. AVBs 2, 3, 11 and 10 near row 27 have sporadic dents in the vicinity of the noses of AVBs 1, 4, 9 and 12. The larger amount of AVB twist in Unit 2 compared to Unit 3 is illustrated by the presence of these dents. Only classic dents with a magnitude of 0.5 volts and greater were used as a guide to benchmark and optimize MHI contact force calculations. Patterns of dents and associated high contact forces are in good agreement with the final quarter model calculations. Comparisons were naturally made with cold condition quarter model results for Unit 2 and 3 as these are the forces relevant for the pre-service inspection observations.

6.4.2 Non-Classical Dents

Two other sets of observations serve as checks of the reasonableness of contact force calculations. These observations are non-classical dent/contact eddy current signals and AVB to tube gap measurements. They were not used in benchmarking or optimizing calculations. Non-classical dent/contact signals have been found to be eddy current footprints of contact between tubes and support structures in other steam generators. In very broad terms, classic dents are usually reported on the differential mix channel [

]

Non-classical dent/contact signals have been found to be a valuable diagnostic tool in root cause evaluations. They are found by automated analysis of mix residual signals with specified sorting parameters and occasional analyst review. [

] Signals are reported down to a signal amplitude of [ ]. This low reporting threshold is possible in the newer replacement steam generators having tube material with low noise levels. Non-classical dent/contact signals have been found to an eddy current footprint of either past or current contact of tubes with support structures. [

]

Typical amplitude growth of non-classical dent/contact signals from another plant is illustrated in Figure 6-21. [ ]

A three dimensional plot of non-classical dent/contact signals is shown in Figure 6-22 for Unit 2 SG E-088 at the first in-service inspection. [

] The same observations apply to Figure 6-23, a three dimensional plot of non-classical dent/contact signals for Unit 2, SG E-089. [

]

Figure 6-24 and Figure 6-25 illustrate three dimensional plots of non-classical dent/contact signals for Unit 3, SG E-088 and then for Unit 3, SG E-089. [

] More importantly, comparison of the relative numbers of contact signals in the upper bundle for Units 2 and 3 provides a graphic, visual demonstration that contact forces are more significant in Unit 2 than in Unit 3. Unit 2 and 3 are significantly different and different behavior with respect to the development of in-plane FEI is expected.

Calculated contact force distributions are in reasonable agreement with eddy current non-classical dent/contact signals. Significant differences between Unit 2 and Unit 3 are confirmed. Additionally contact signal densities in the upper bundle suggest that calculated contact forces are underestimated somewhat, particularly for AVBs 4 and 5 in Unit 2. This would lead to an overestimated probability of instability for Unit 2. [

] While support effectiveness is not needed in demonstrating a stability ratio less than 1 at 70% power, it is important relative to demonstration of margin by having a high probability of maintaining a maximum stability ratio that is less than 0.75.

6.5 Tube-to-AVB Gap Evaluation

An extensive campaign of gap measurements was undertaken in all steam generators using both eddy current and ultrasonic techniques. The ultrasonic technique is more accurate and can measure smaller gaps but is very time consuming. The eddy current technique is much faster [

] Field inspections are more challenging than laboratory conditions and some degradation of detection thresholds and resolution is expected in field inspections. Figure 6-28 from Reference [14] compares in generator gaps measurements using eddy current and ultrasonic techniques. The overall agreement is very good. In fact, it is quite comparable to the agreement of AVB wear depths using bobbin and +Pt™ eddy current probes when both are setup according to standard EPRI ETSS procedures. For gaps on the order of [ ] the eddy current gap measurements significantly overestimate the gap size. At larger gap sizes, eddy current measurements are larger than ultrasonic measurements by an average factor of [ ]. Sizing uncertainties increase by about [ ] from laboratory to in generator conditions. Since the primary purpose of gap measurements was to determine if there were highly heterogeneous spatial distributions of large gaps, eddy current measurements are well suited to this purpose and much more accurate than previous eddy current techniques.

Over 117,000 eddy current gap measurements were performed. Only global findings are reported here. It should be noted that gaps and hence contact forces are significantly affected by wear at AVB locations. Hence it is difficult to make any but the most general inferences about differences in gaps and contact forces between Unit 2 and Unit 3 at the beginning of life. Further, there are plugged tubes in the regions of interest in all steam generators that could not be inspected.

6.5.1 Unit 2 Tube-to-AVB Gaps

Figure 6-29 and Figure 6-30 present tubesheet maps of the total of all measured gaps on a given tube for Unit 2, SG E-088 and Unit 2, SG E-089 [14]. All AVB locations are included in the total reported gap. The distinction noted for wear versus no wear locations indicates that wear was present at one or more AVB locations on a tube. It is important to note that some of the points indicated as "wear influenced" exhibited very low wear signals that are below the reporting level for standard inspections for wear. The presence of wear, particularly standard wear calls, tends to lead to an underestimate of the gap size. Figure 6-29 shows that the spatial distribution of gaps in Unit 2, SG E-088 is unexceptional. Naturally, wear at AVB locations open up gaps. The average 10% depth wear indication represents a material loss of 0.004 inches. In Unit 2, SG E-089 with approximately 800 more wear indications than Unit 2, SG E-088, larger total gaps are observed. See Figure 6-30. Here there is one area where there is some indication of a local spatial heterogeneity in gap sizes. Note the linear sequence of red data points in column 71 centered near row 120. This area was examined in detail. It is the column boundary of AVB wear for the rows in the vicinity of row 120. In this vicinity, column 71 and, to a lesser extent, column 73 have a noticeable row sequence of AVB wear indications. This has created a larger local region of total gap values. The contact force model for Unit 2 is based on wear in SG E-089 with wear locations each discretely modeled based on eddy current inspection results; thus, the contact force model actually includes this local region of heterogeneous gap sizes as part of the calculation of contact forces. Since quarter model results are mirrored to the other side of the steam generator, worst case wear conditions are double counted. With all of the above, the end results are not particularly important for this OA since the lower AVB supports are relatively unaffected and thus there is no challenge from this region to maintaining a maximum stability ratio of 0.75 at 70% power.

6.5.2 Effect of Gap Size on Tube-to-AVB Wear

Before proceeding to a discussion of Unit 3 gap results a consideration of the implication of gap sizes relative to expected wear rates at AVB locations is worthwhile. Figure 6-31 presents a synthesis of viewpoints relative to the relationship between wear rates and tube to support gap sizes. Both seek to explain high wear rates at support locations. One is termed the nil gap hypothesis. The other exclusively favors out-of-plane, gap limited, fluid-elastic excitation. Both have been applied successfully. The nil gap hypothesis maintains that a zero gap condition, perhaps maintained by a small bias force, results in continuously high wear rates from turbulence excitation. For large gaps, out-of plane fluid-elastic excitation is admitted as a consideration but not expressly used. The nil gap hypothesis has been successfully applied and correctly predicts that many individual wear sites will exhibit constant wear rates over multiple cycles of operation. Westinghouse has demonstrated success with the out-of-plane, gap limited, fluid-elastic excitation approach. Figure 6-31 shows high wear rates from turbulence excitation at a nil gap condition and high wear rates at larger gap sizes. Negative gaps imply high contact forces. Conceptually, there is some contact force that hinders motion to the extent that wear effectively ceases. A tube can experience a contact force on one side with a larger gap on the other side. If the contact force is sufficient, out-of-plane gap limited fluid-elastic excitation will not be an important consideration. Hence, a tube with a large one sided gap may or may not exhibit a high wear rate. The support may still be an effective support. Conversely, a tube with a small gap on each side will not exhibit a high wear rate. For small gaps, it will be an effective support.

6.5.3 Unit 3 Tube-to-AVB Gaps

Substantial regions of gap heterogeneity are observed in the Unit 3 steam generators. Part of this heterogeneity is the results of increased wear in Unit 3 compared to Unit 2, particularly at lower AVBs. This is perhaps exacerbated by lower contact forces in Unit 3 and less effective rebalancing of gaps and contact forces as wear was introduced. A very substantial region of large gaps appear under retainer bars in both steam generators from column 40 across to column 50. See Figure 6-32 for Unit 3, SG E-088 and Figure 6-33 for Unit 3, SG E-089 for

gap measurement results. Large gaps are much more pronounced in Unit 3, SG E-089. As advanced by MHI, these gaps are interpreted as a result of downward movement of the entire support structure near the retainer bar locations with a consequent distortion of U-bends and AVBs. This distortion, which can be relatively small in absolute terms, has created substantial gaps. Recall that the upper support structure, to which the AVBs are attached at the periphery, is a floating structure. The weight of the upper support structure is resisted by the friction forces at AVB locations. A downward sagging of the support structures is interpreted as the end result of low initial contact forces further degraded by wear at AVB locations. Unit 3 is indeed different than Unit 2.

6.6 Conclusions – Contact Forces

The primary purpose of gap measurements was to determine if there were highly heterogeneous spatial distributions of large gaps that are not included in contact force calculations. For the purposes of this OA, this is more relevant to Unit 2 rather than Unit 3. In Unit 2 there were no highly heterogeneous spatial distributions of large gaps that challenge contact force calculations. In Unit 3 there are highly heterogeneous spatial distributions of large gaps under the retainer bars from column 40 across to column 50. This region is far enough removed from the region of in-plane fluid-elastic instability and thus probability of instability calculations are not grossly affected. Gap measurements are suggestive that contact forces were smaller in Unit 3 than in Unit 2 at the beginning of life. A far stronger argument is provided by observations regarding classic dent signals and non-classical low level dent/contact signals. Any measurements that could have been made to check contact forces calculations were made. Contact force calculations are appropriately reliable to demonstrate maintenance of adequate margins relatively to in-plane fluid-elastic instability at 70% power.

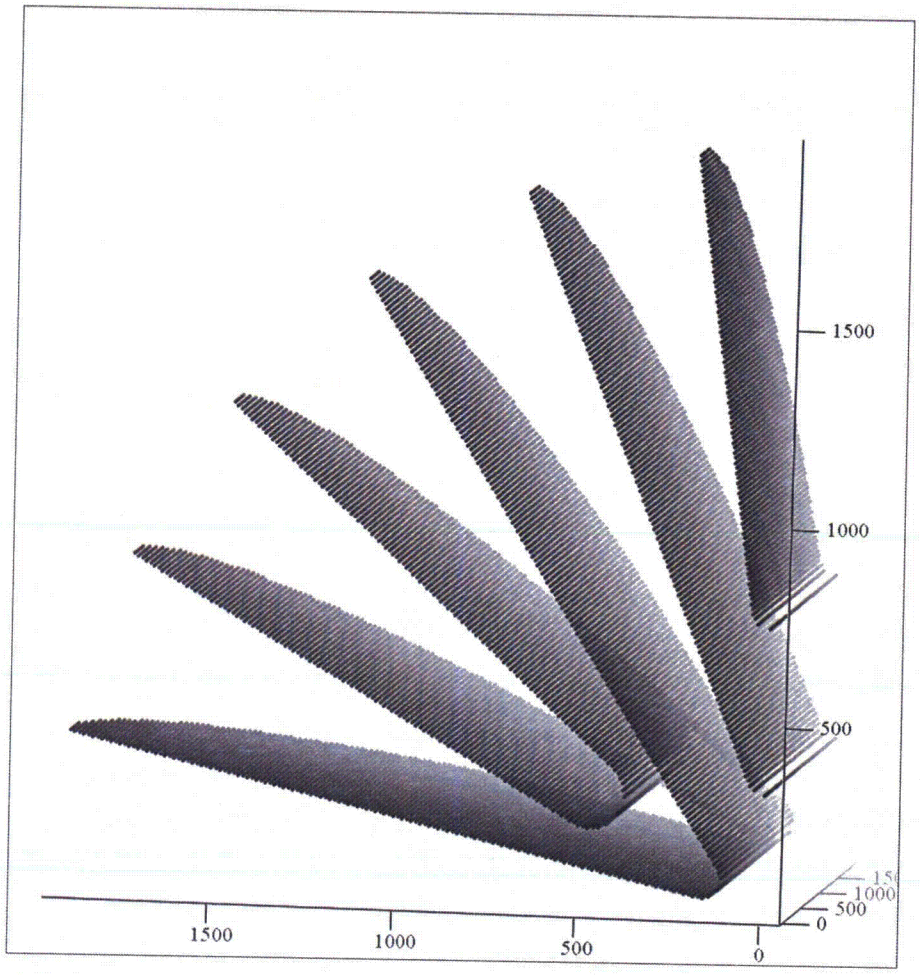

Figure 6-1: Quarter Model Contact Force and Gap Locations

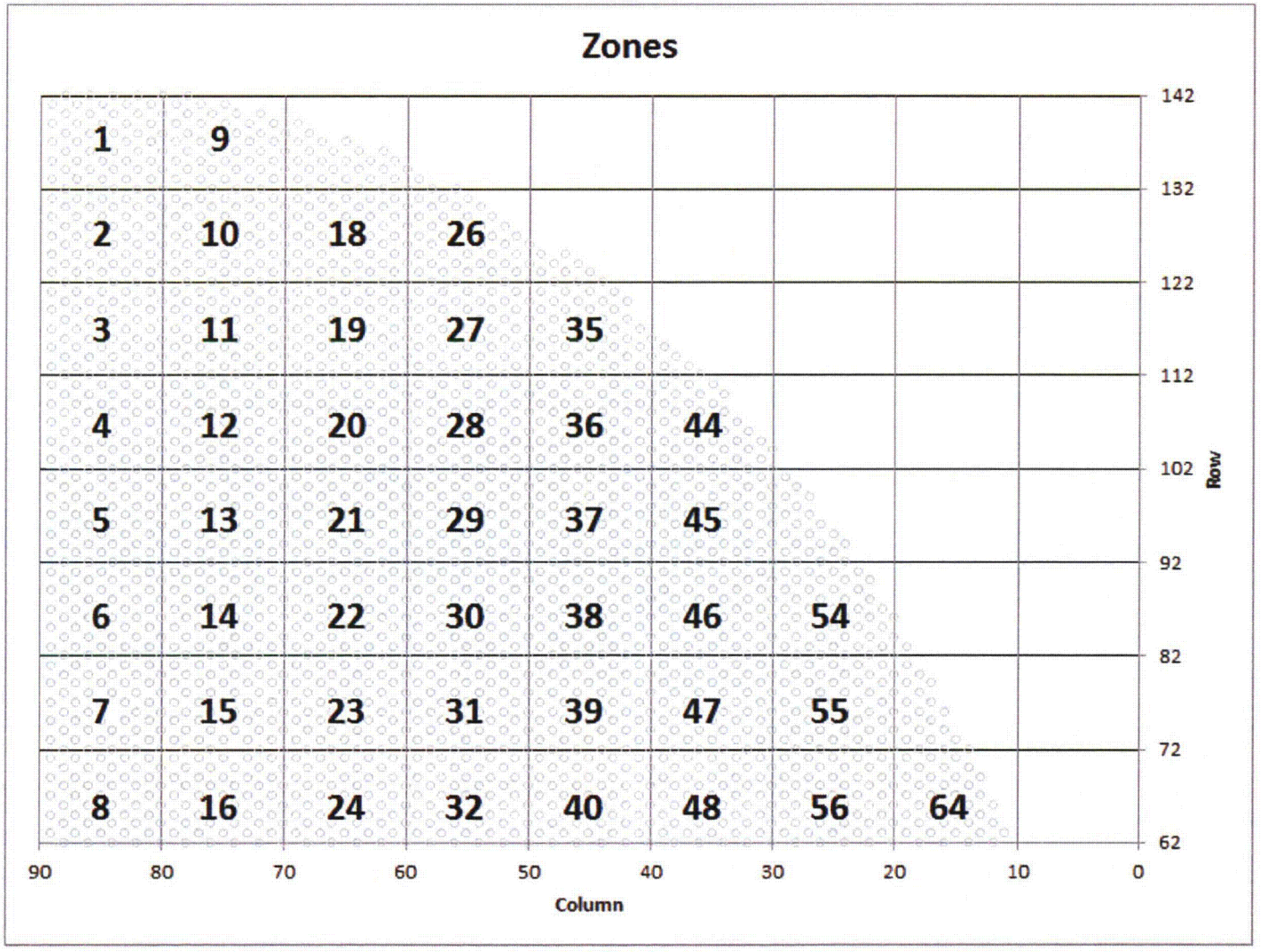

Figure 6-2: Zones Used to Develop Characteristic Distributions of Contact Forces for Each AVB in the Zone

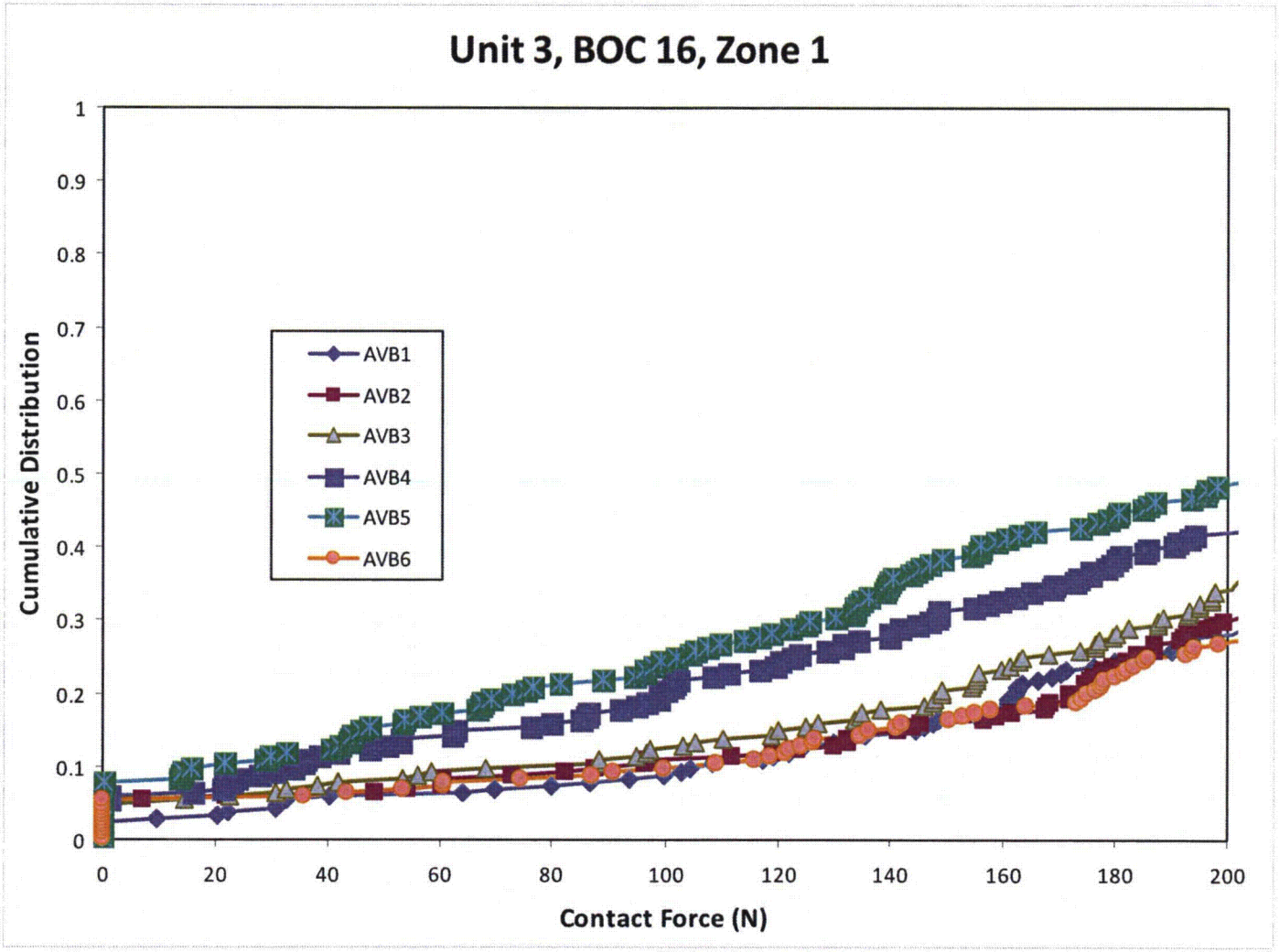

Figure 6-3: Cumulative Contact Force Distributions, Zone 1, Unit 3, BOC 16

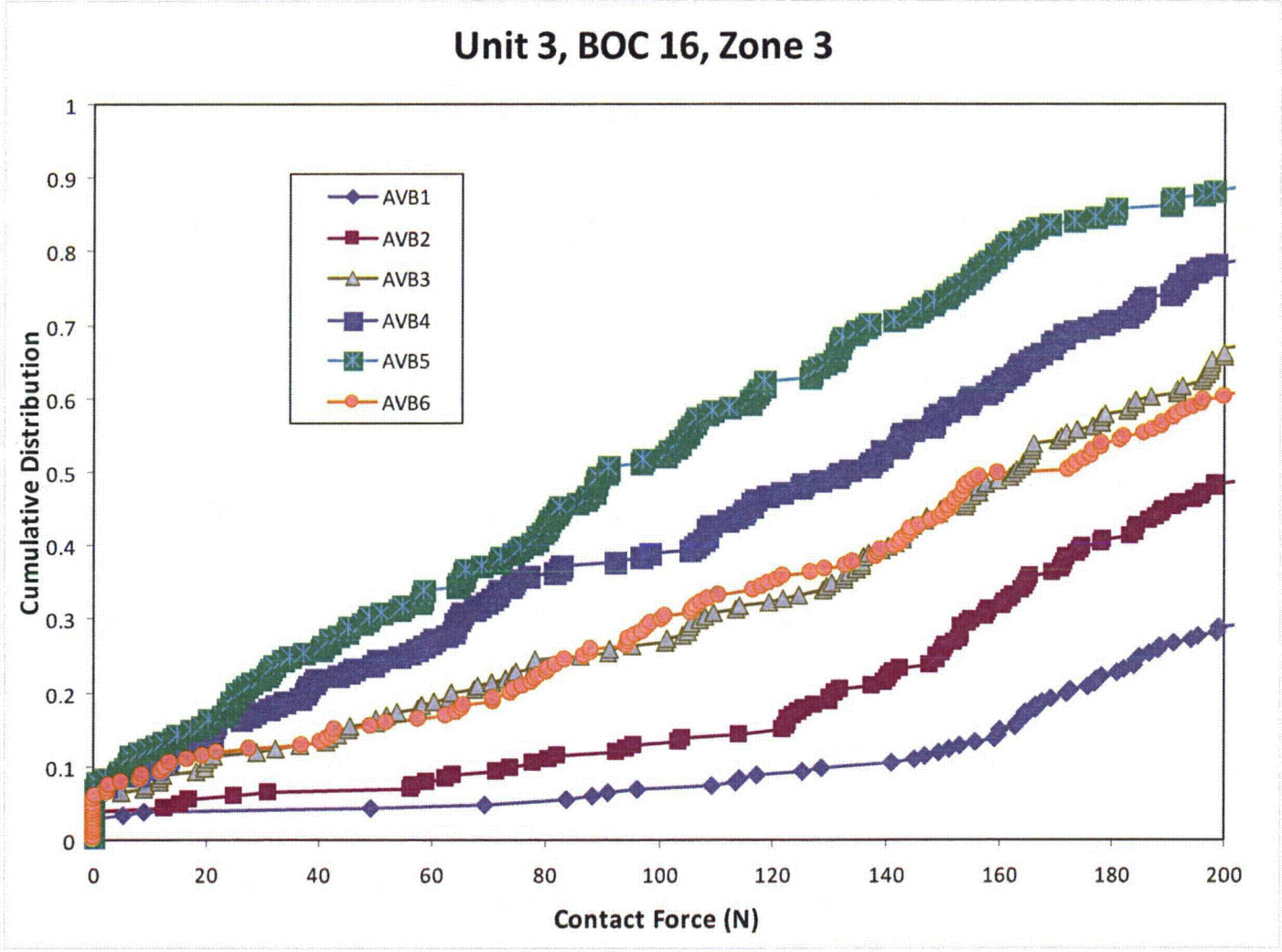

Figure 6-4: Cumulative Contact Force Distributions, Zone 3, Unit 3, BOC 16

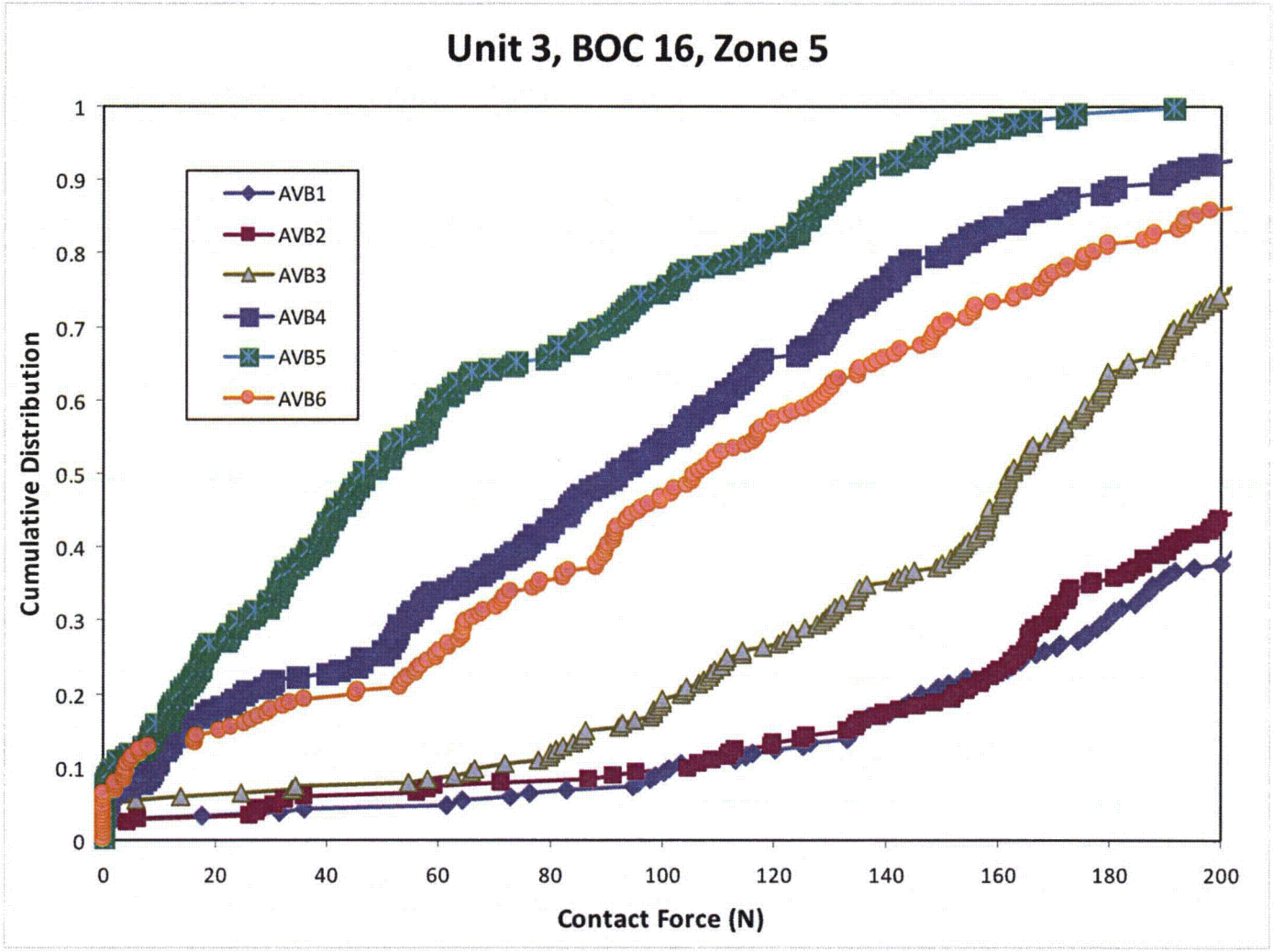

Figure 6-5: Cumulative Contact Force Distributions, Zone 5, Unit 3, BOC 16

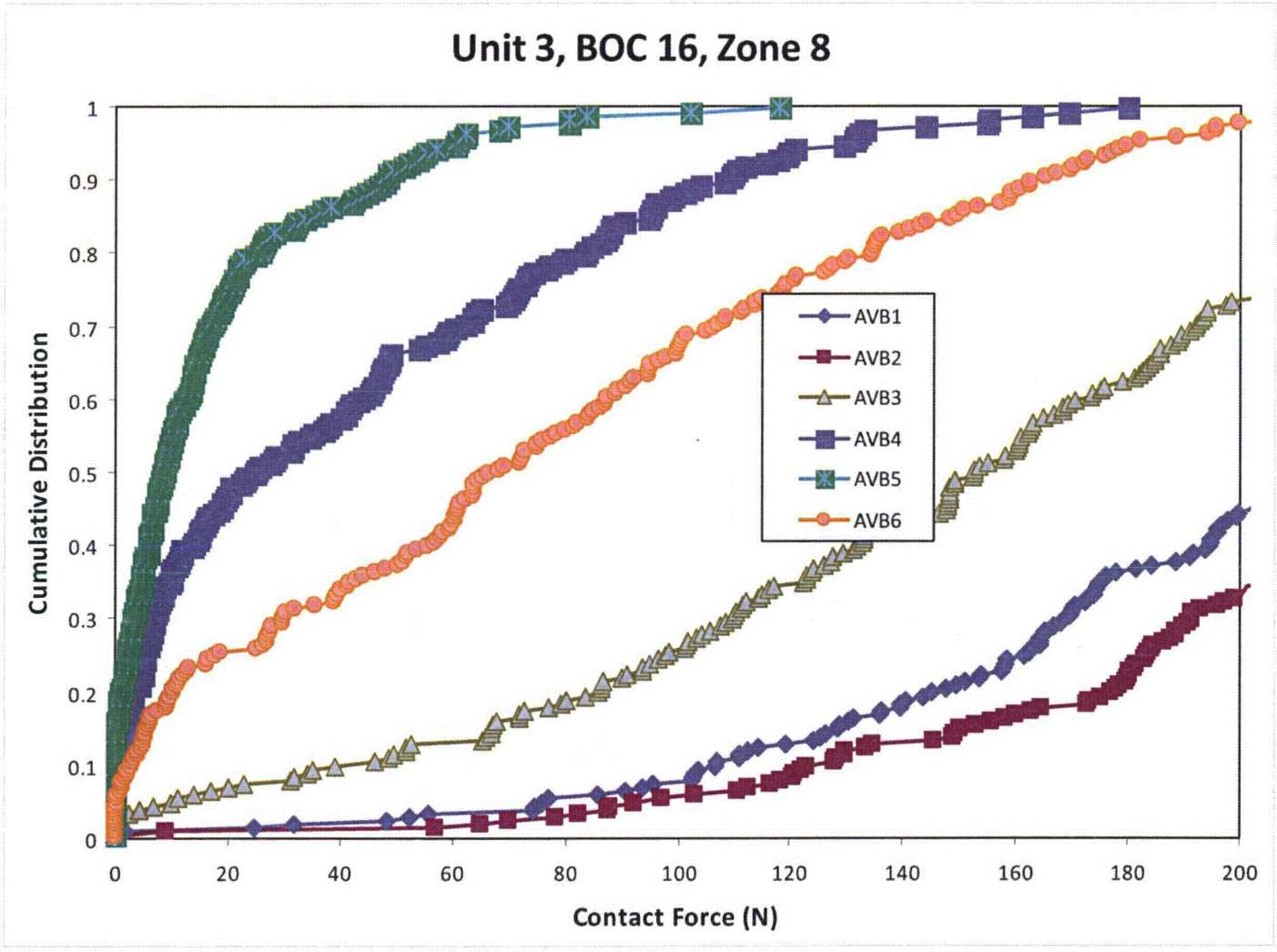

Figure 6-6: Cumulative Contact Force Distributions, Zone 8, Unit 3, BOC 16

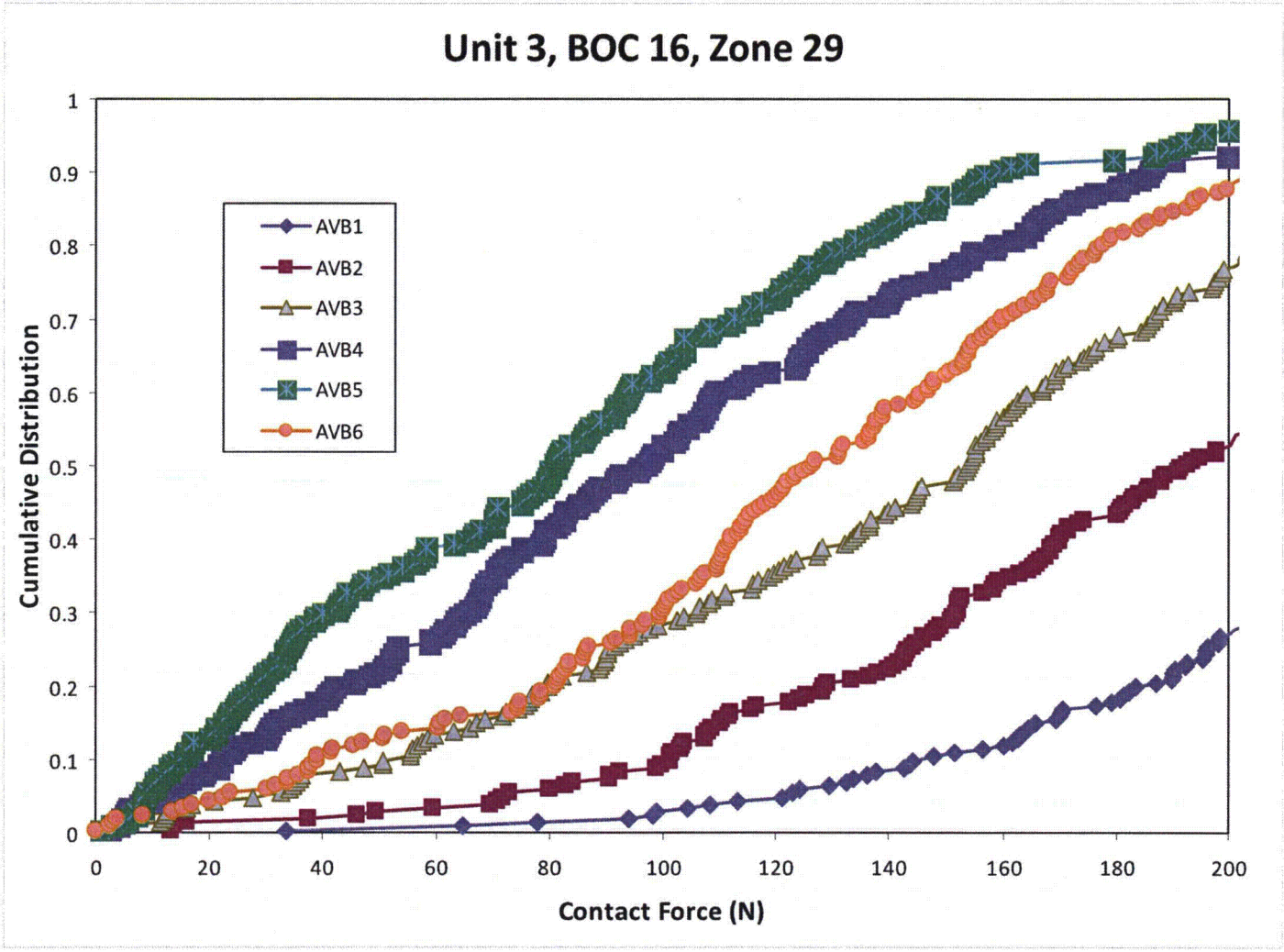

Figure 6-7: Cumulative Contact Force Distributions, Zone 29, Unit 3, BOC 16

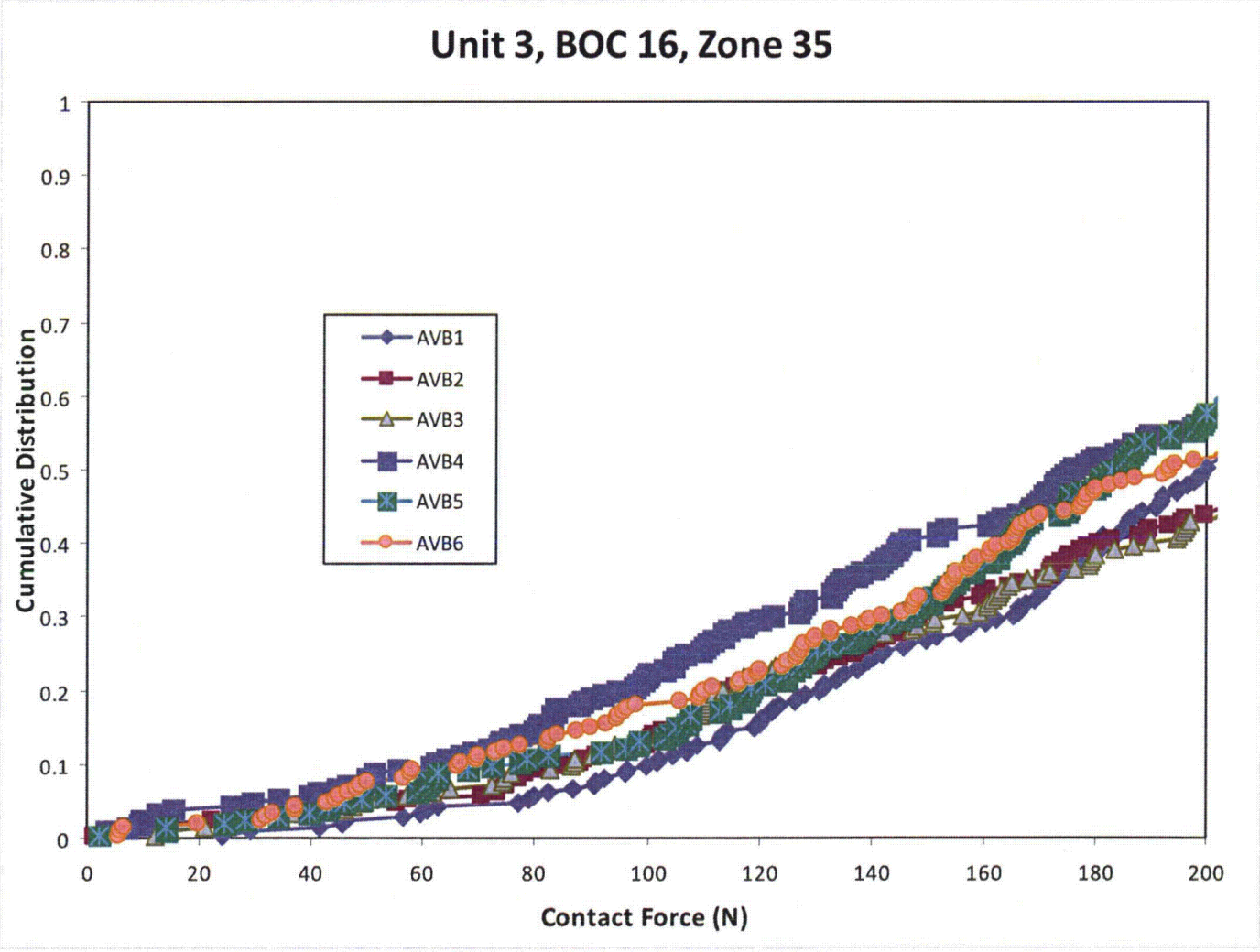

Figure 6-8: Cumulative Contact Force Distributions, Zone 35, Unit 3, BOC 16

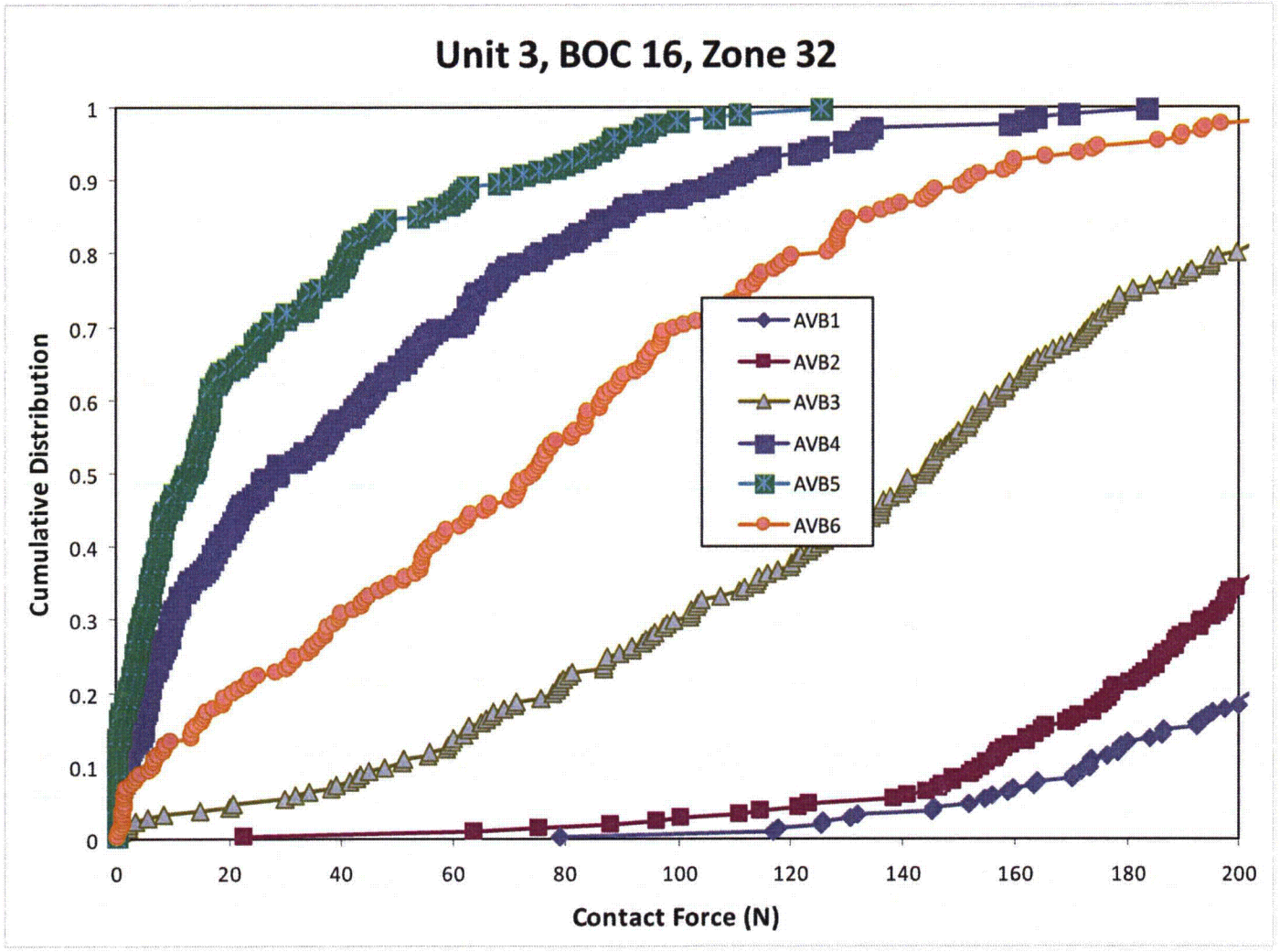

Figure 6-9: Cumulative Contact Force Distributions, Zone 32, Unit 3, BOC 16

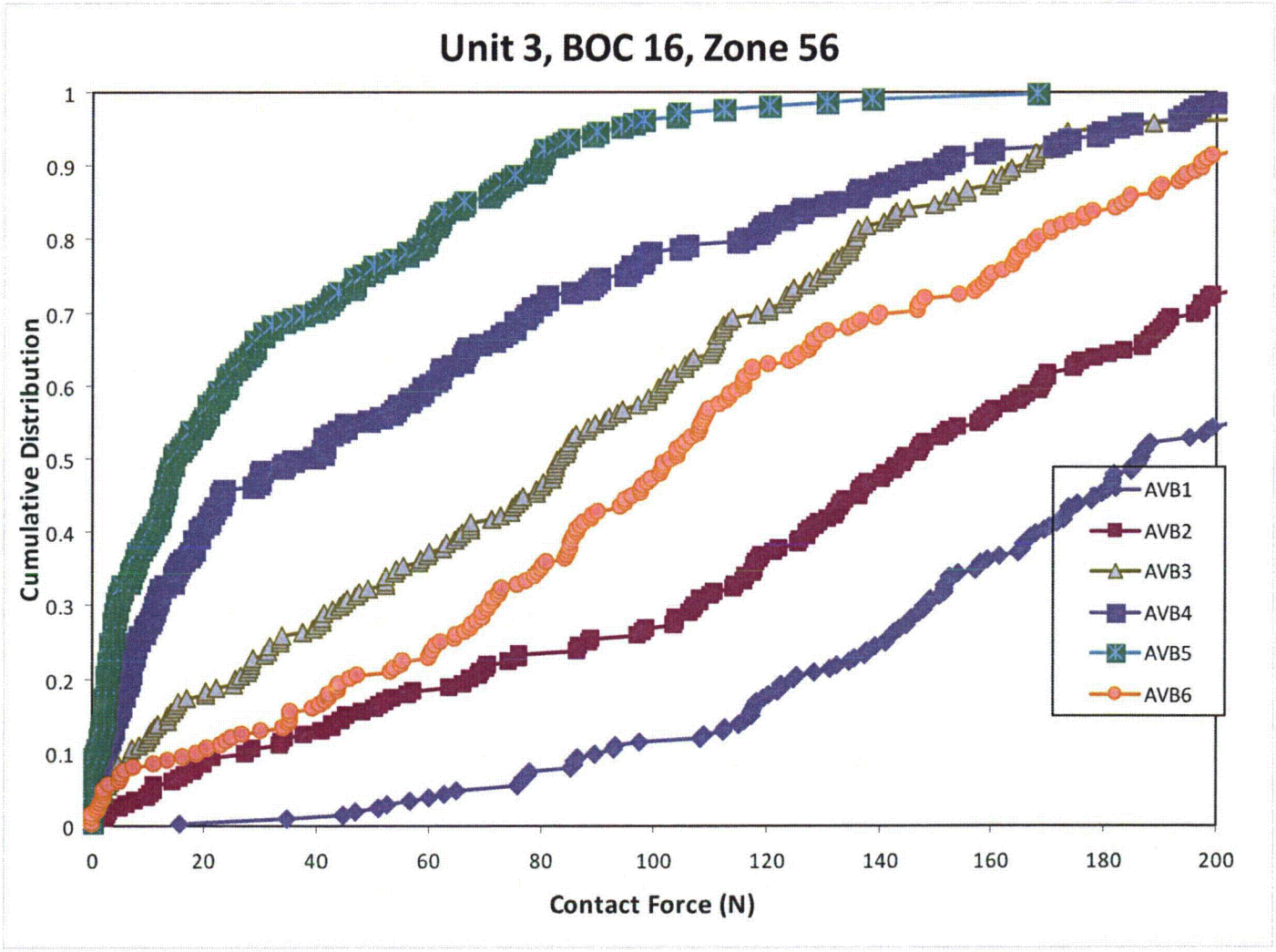

Figure 6-10: Cumulative Contact Force Distributions, Zone 56, Unit 3, BOC 16

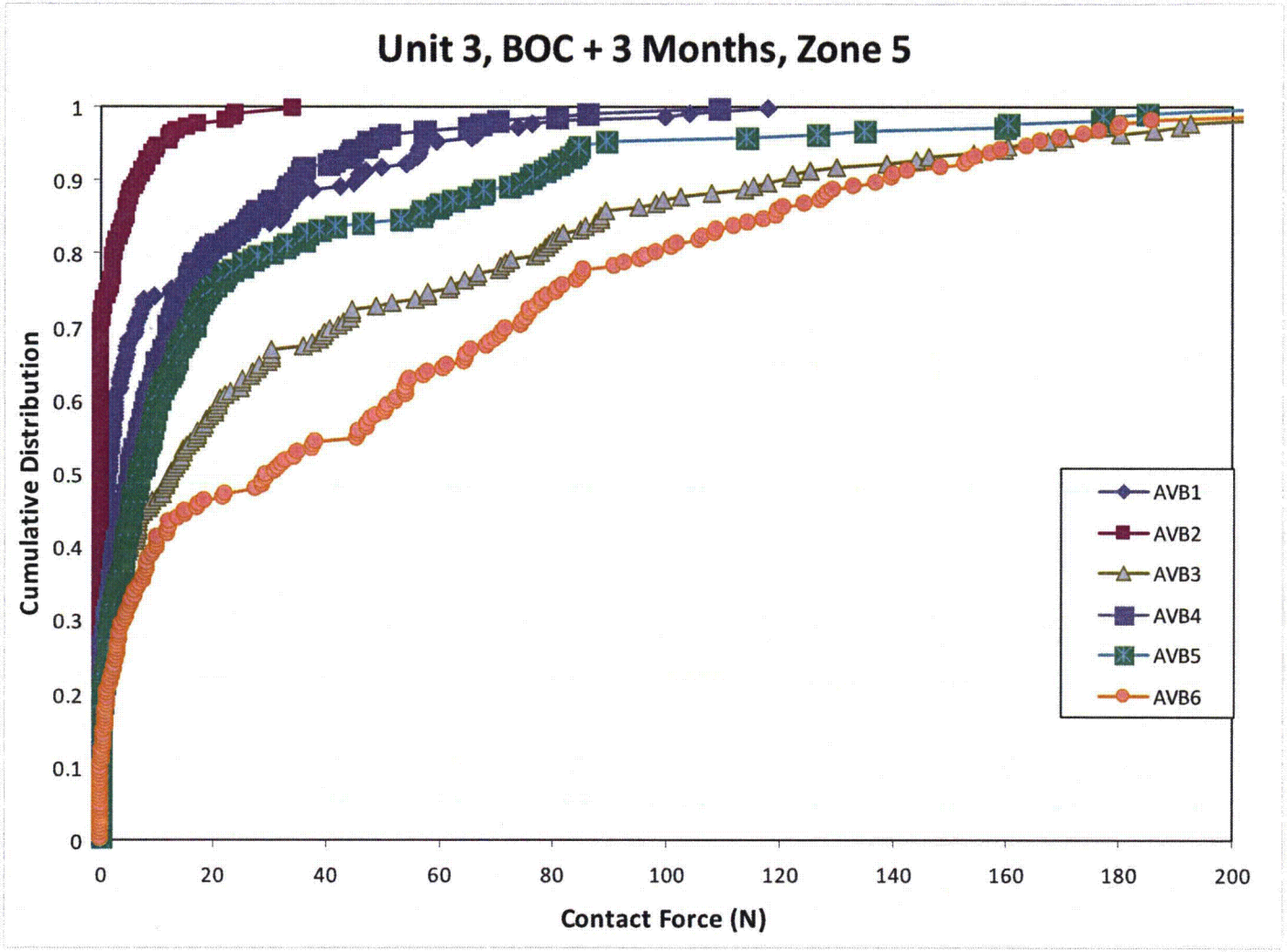

Figure 6-11: Cumulative Contact Force Distributions, Zone 5, Unit 3, BOC 16 + 3 Months

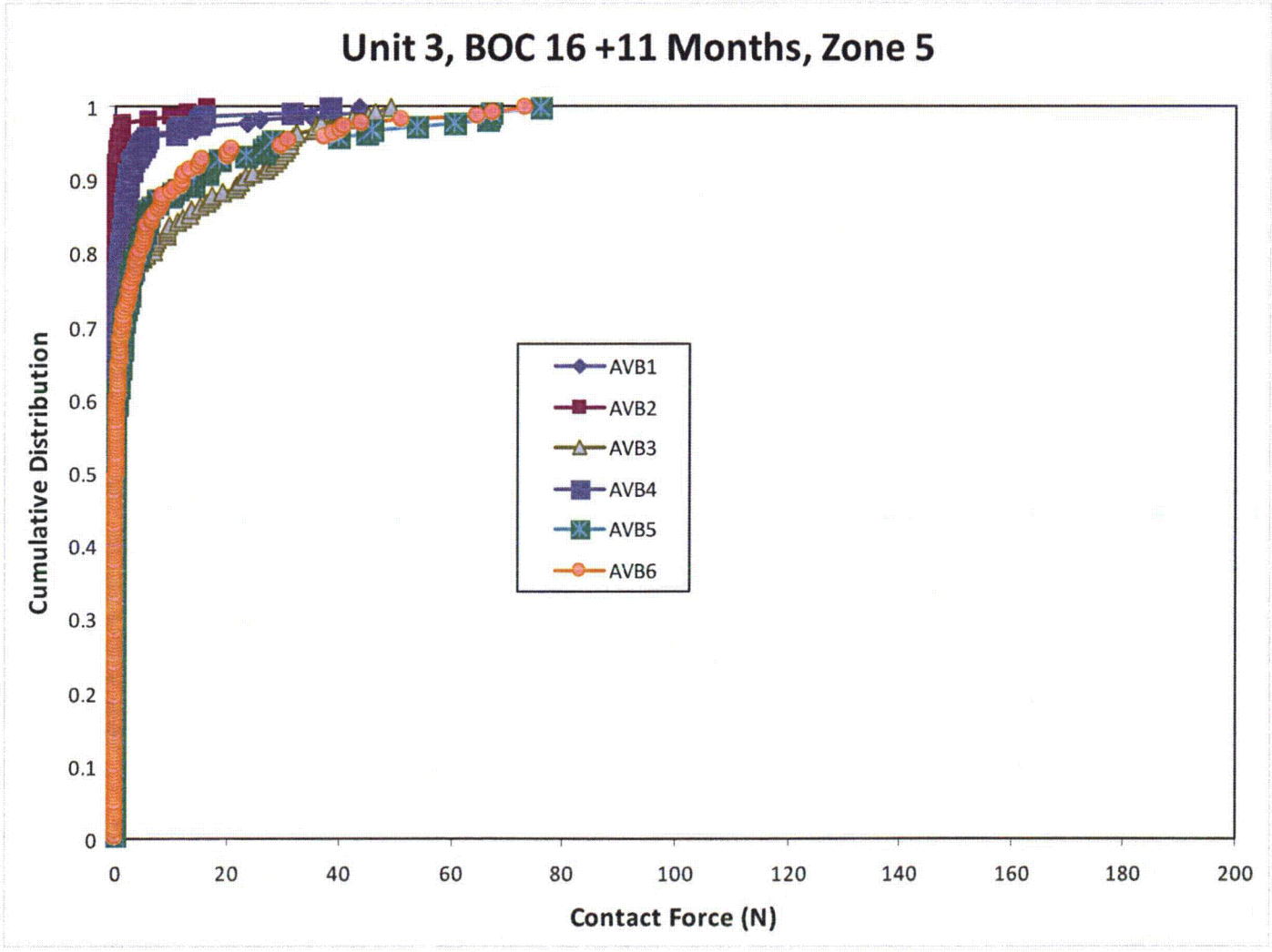

Figure 6-12: Cumulative Contact Force Distributions, Zone 5, Unit 3, BOC 16 + 11 Months

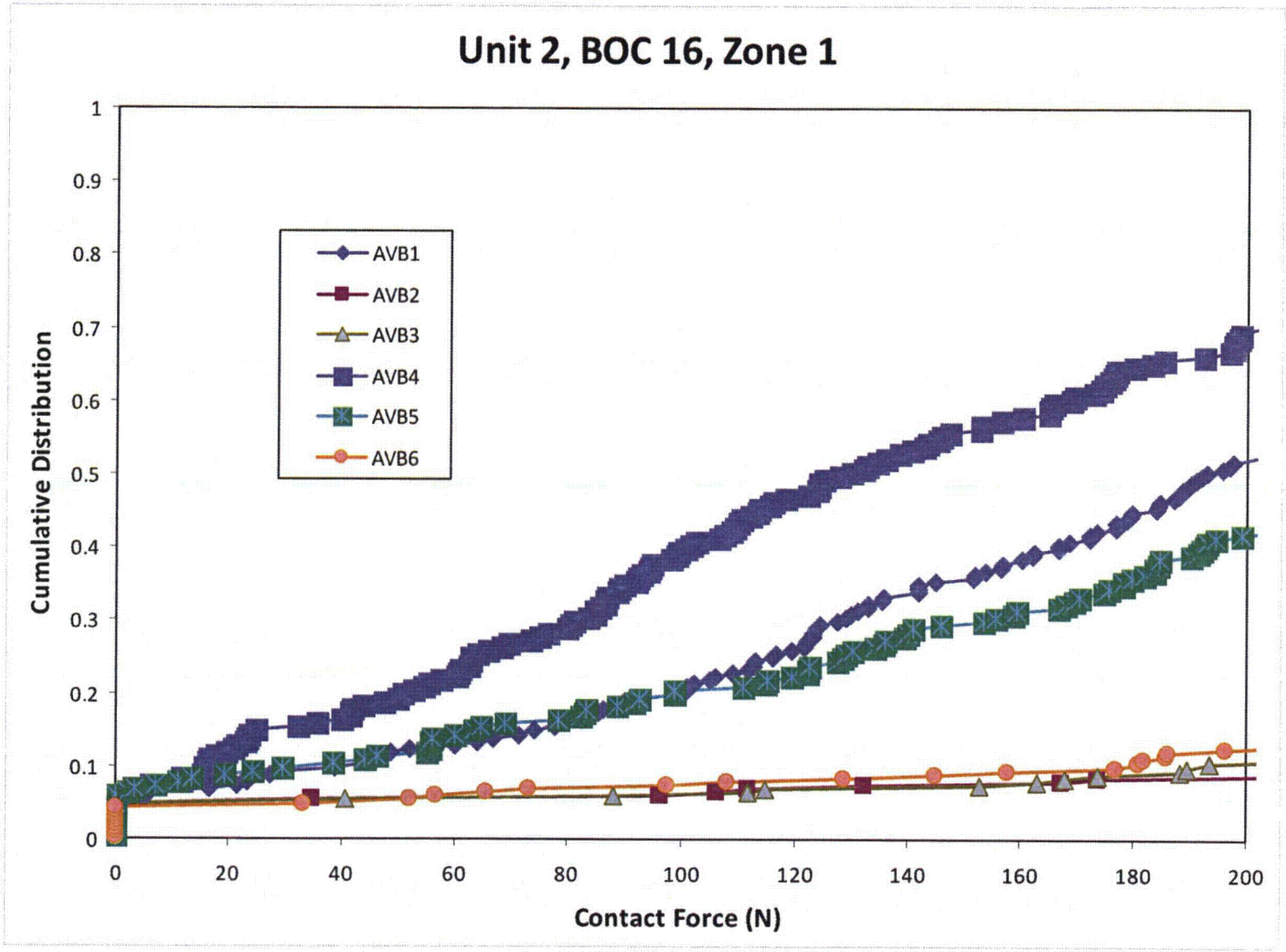

Figure 6-13: Cumulative Contact Force Distributions, Zone 1, Unit 2, BOC 16

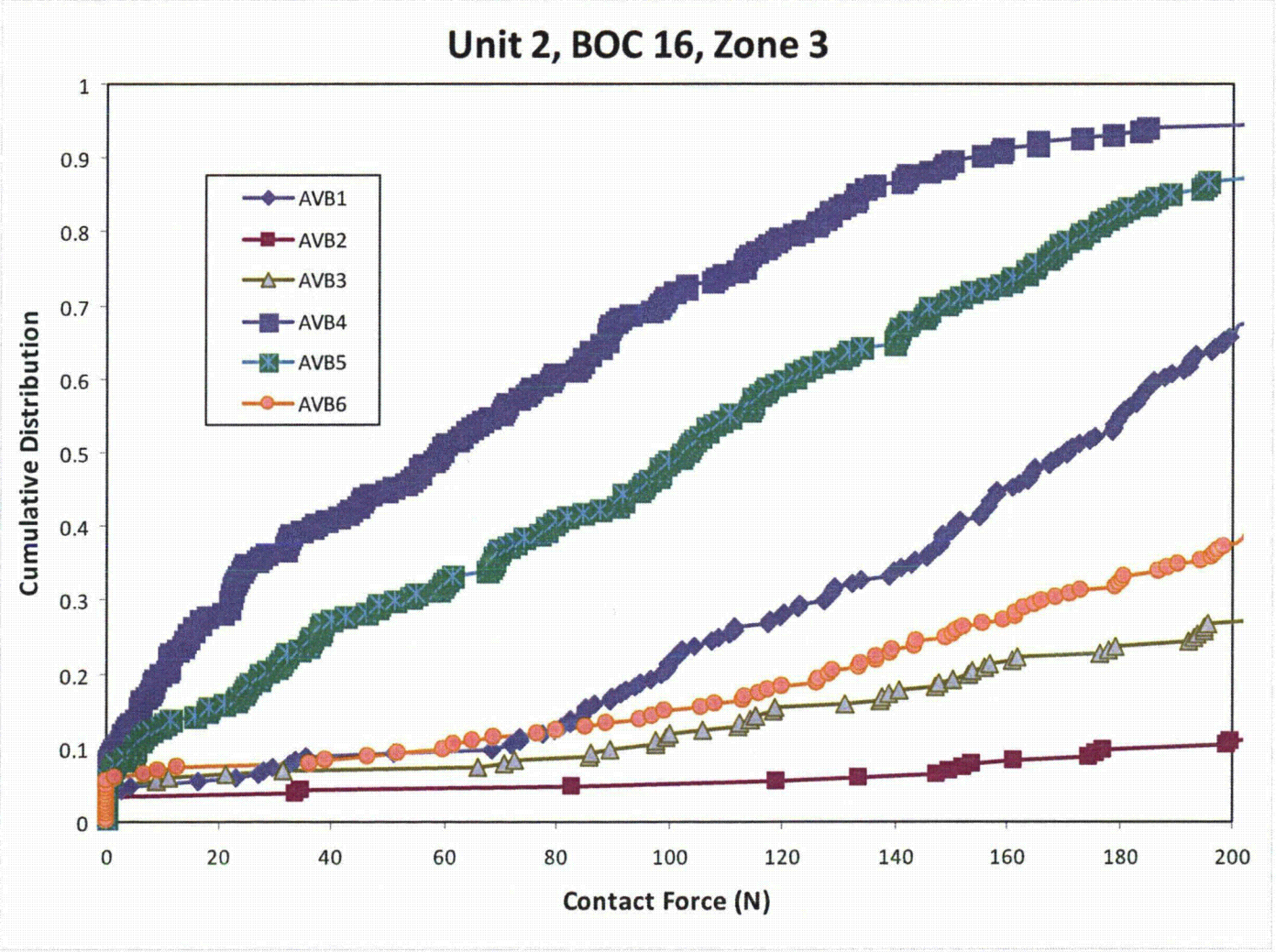

Figure 6-14: Cumulative Contact Force Distributions, Zone 3, Unit 2, BOC 16

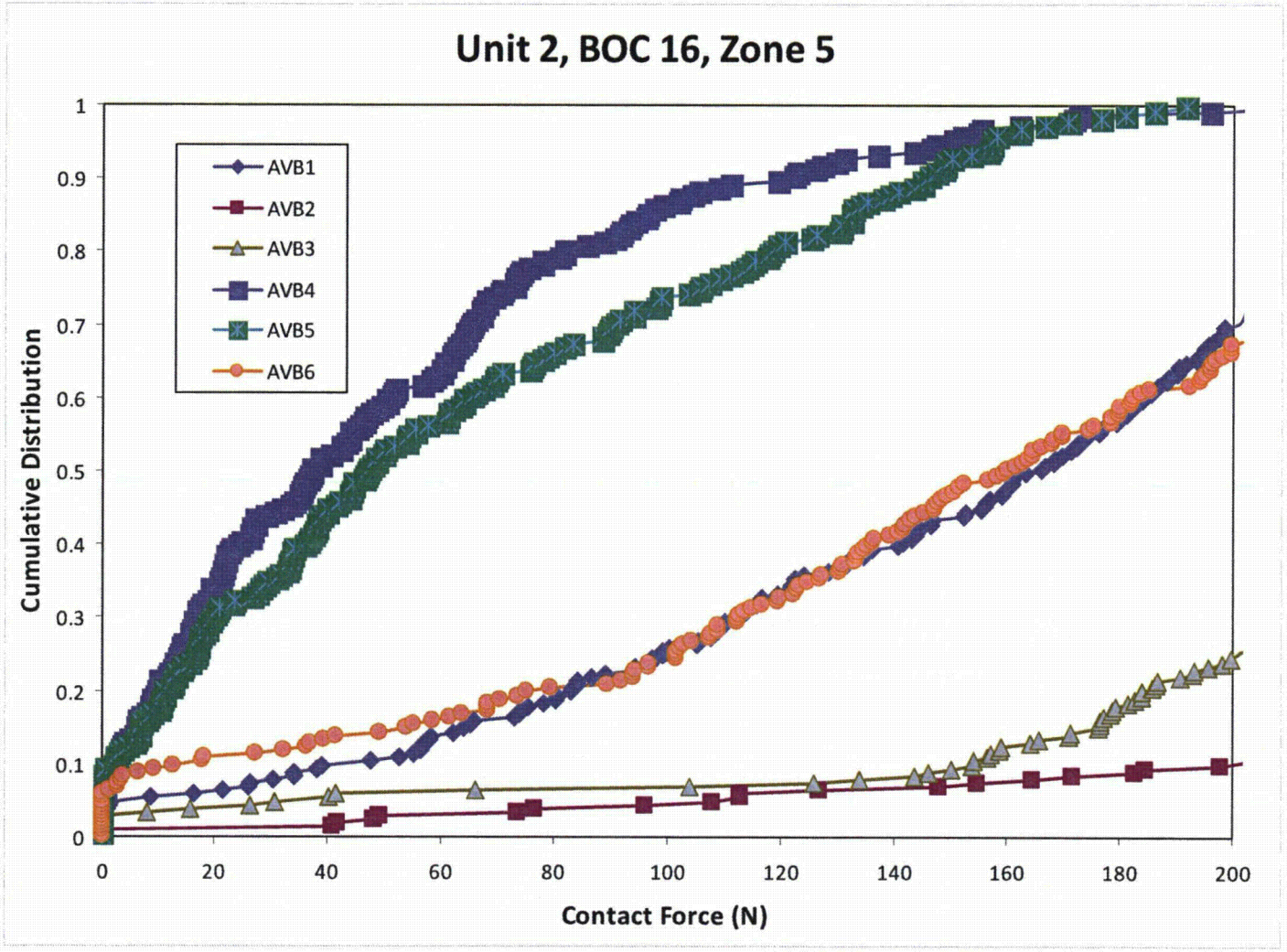

Figure 6-15: Cumulative Contact Force Distributions, Zone 5, Unit 2, BOC 16

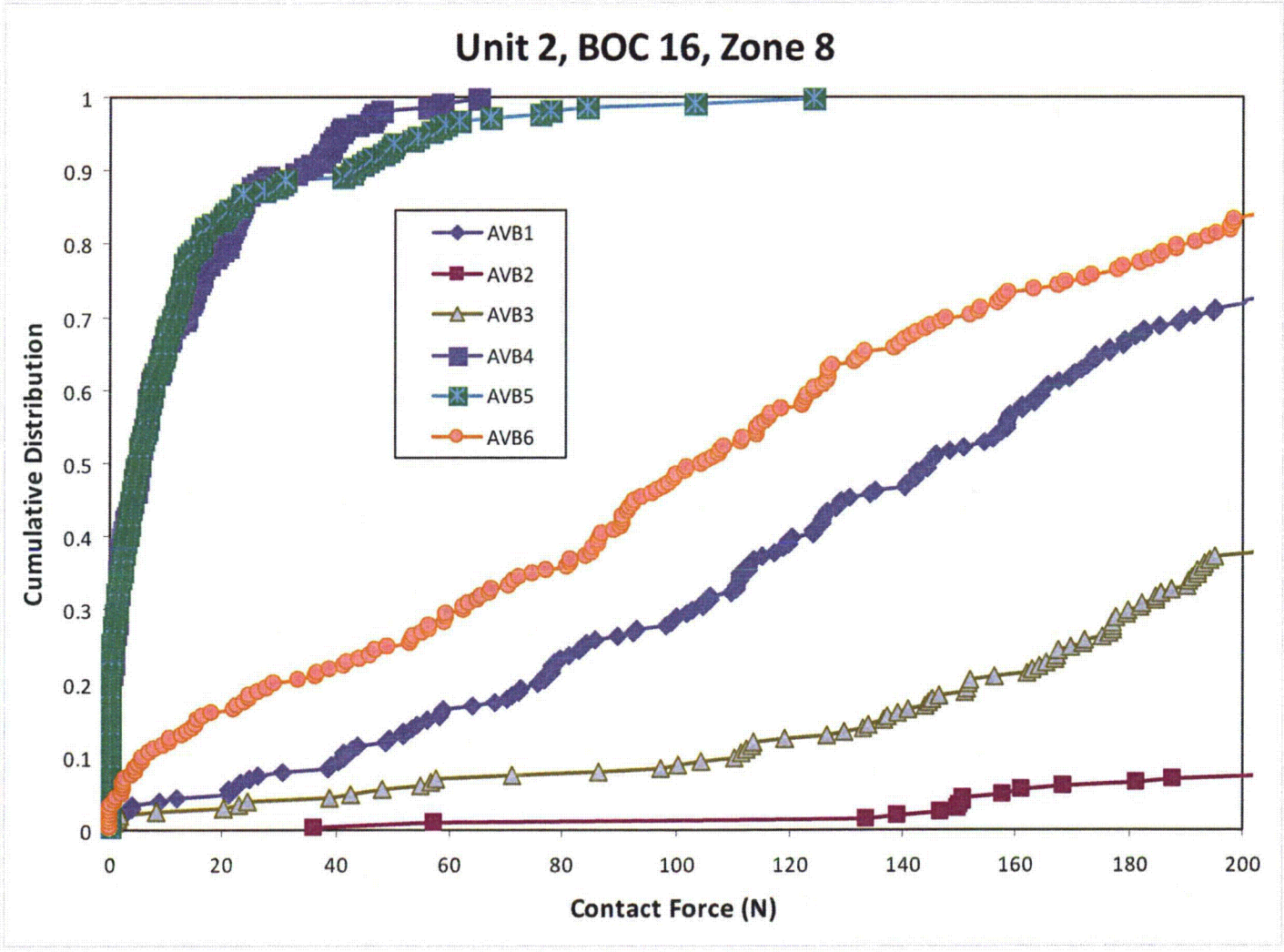

Figure 6-16: Cumulative Contact Force Distributions, Zone 8, Unit 2, BOC 16

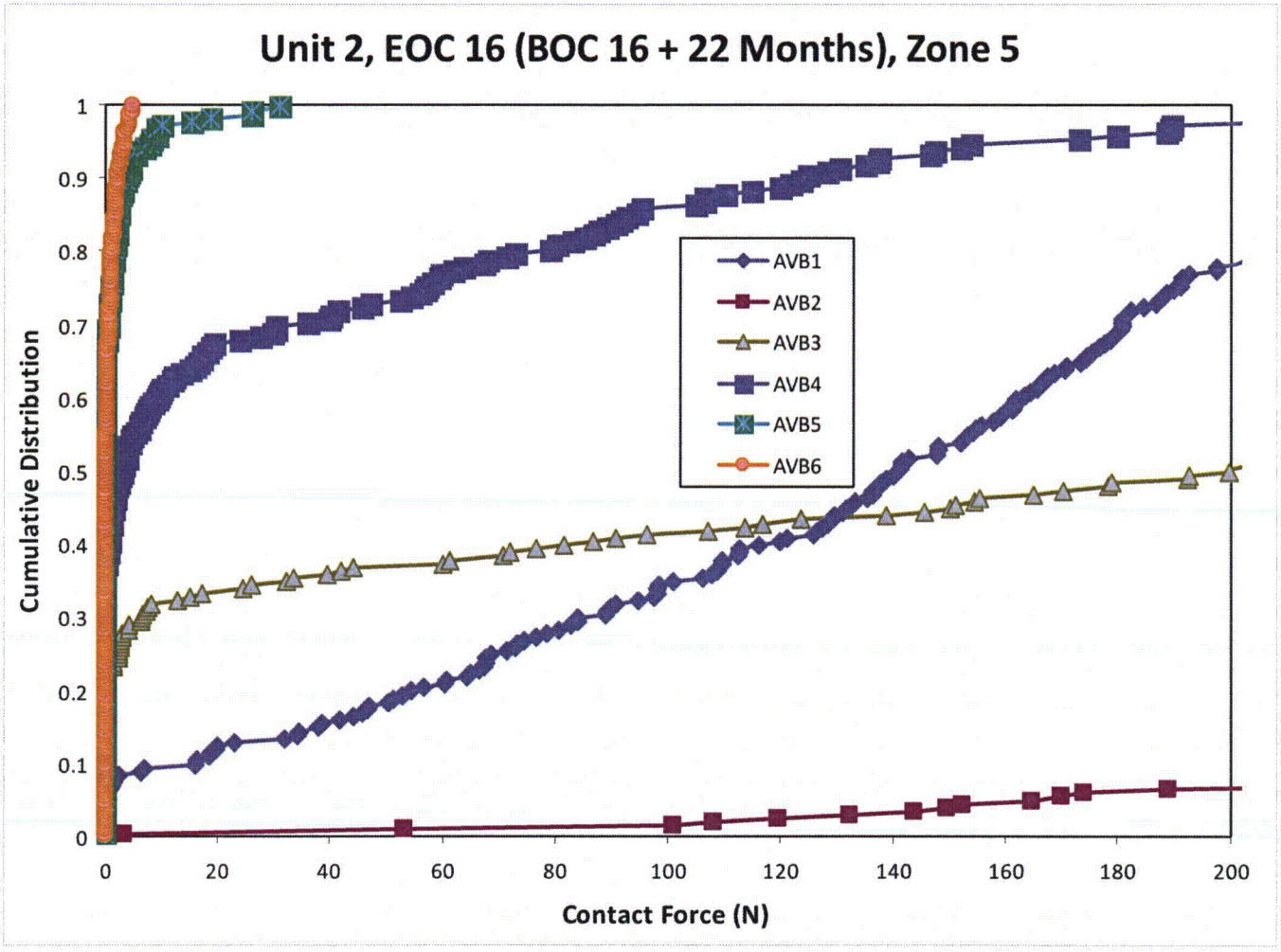

Figure 6-17: Cumulative Contact Force Distributions, Zone 5, Unit 2, EOC 16 (BOC 16 + 22 Months)

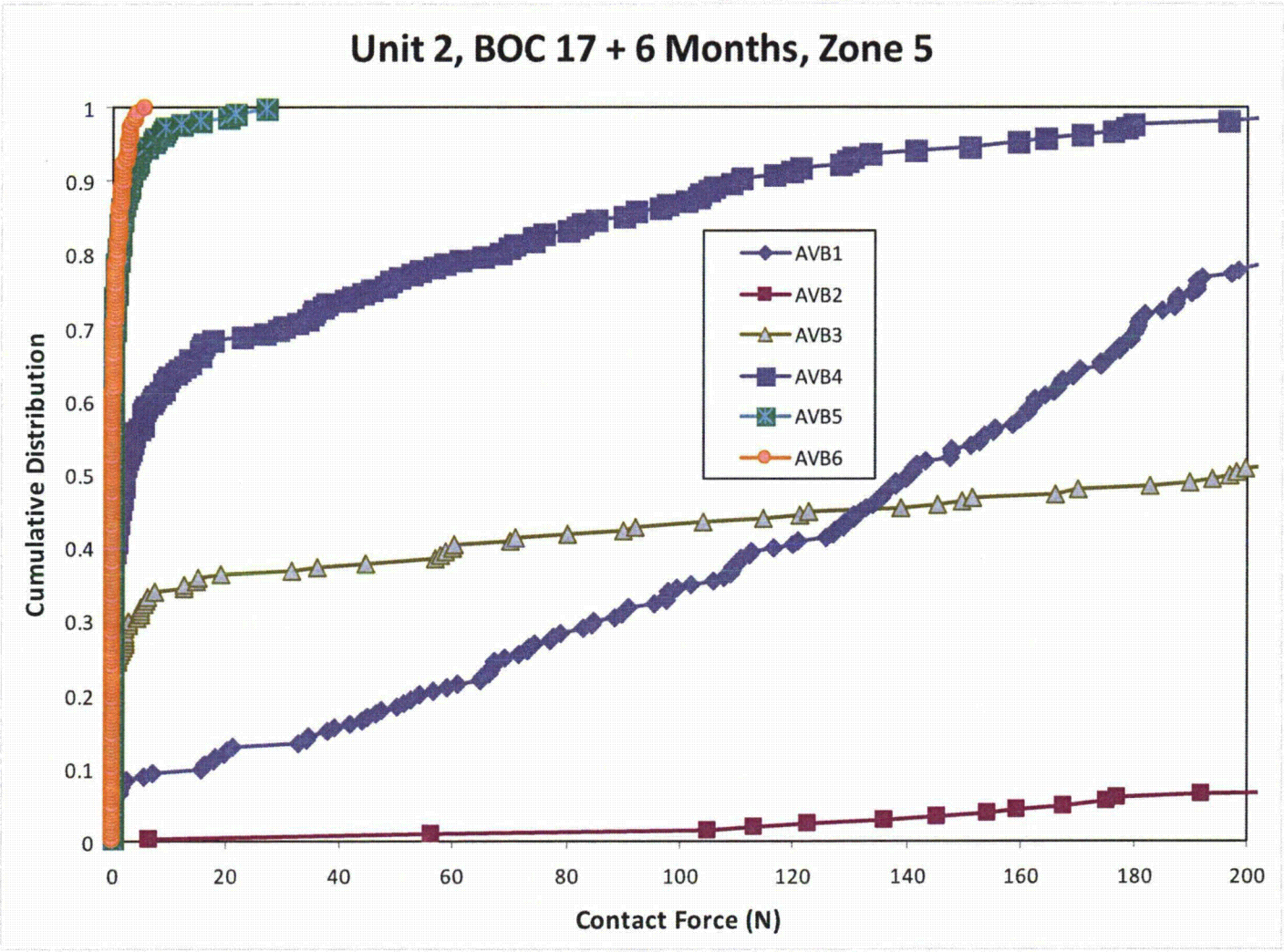

Figure 6-18: Cumulative Contact Force Distributions, Zone 5, Unit 2, BOC 17 + 6 Months

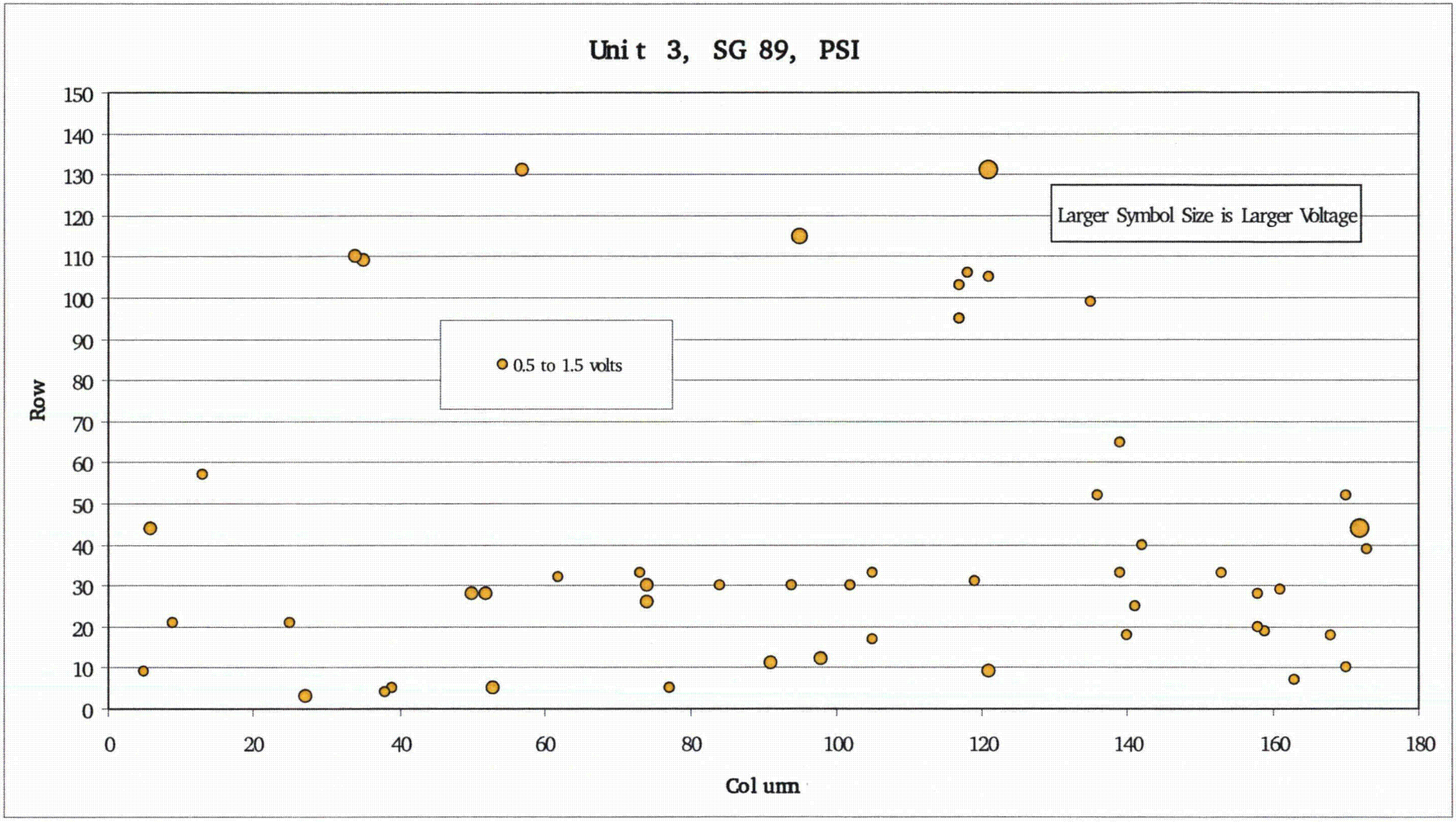

Figure 6-19: Tubesheet Map of Dents Found in Pre-Service Inspection, Unit 3, SG E-089

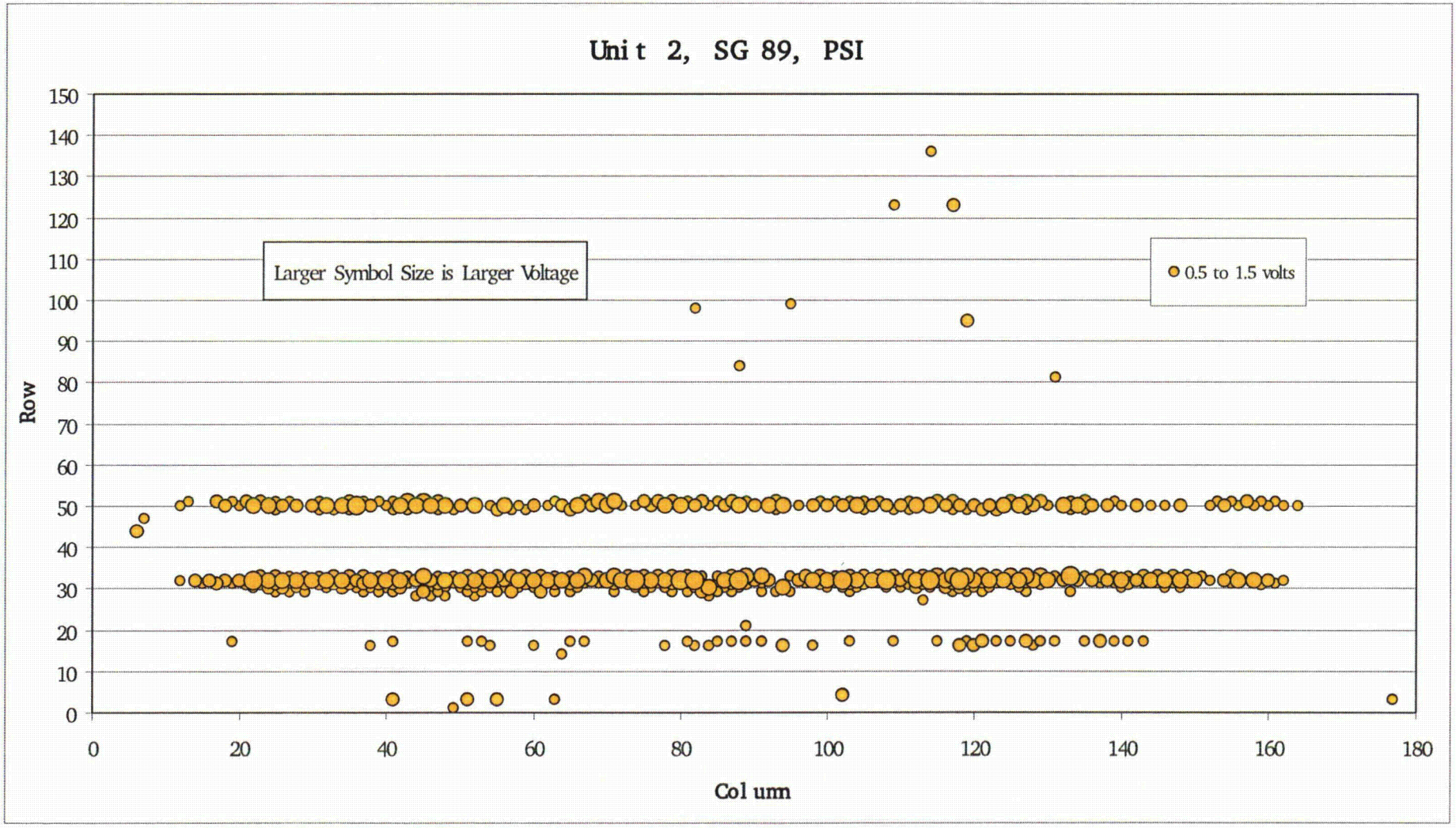

Figure 6-20: Tubesheet Map of Dents Found in Pre-Service Inspection, Unit 2, SG E-089

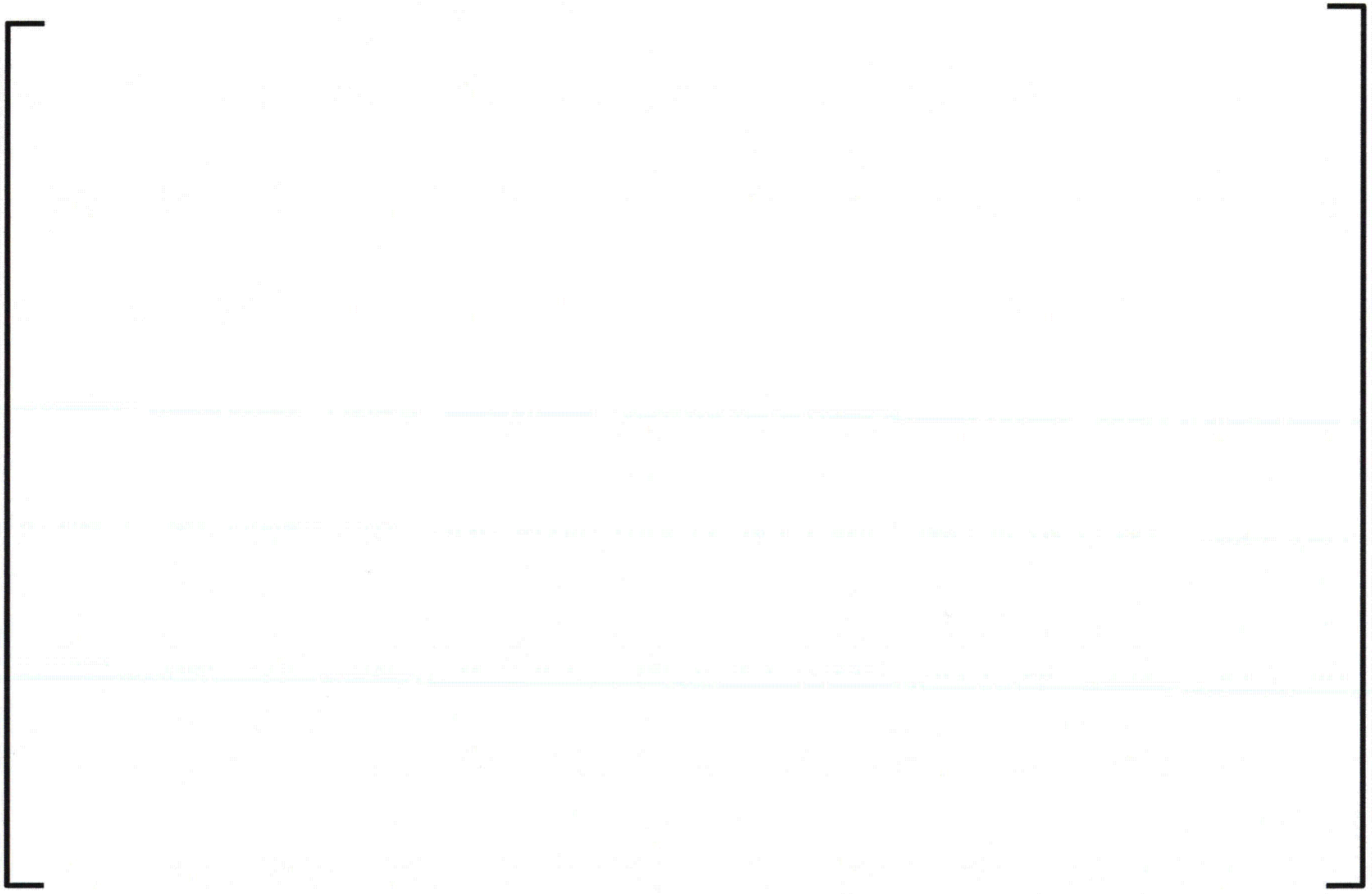

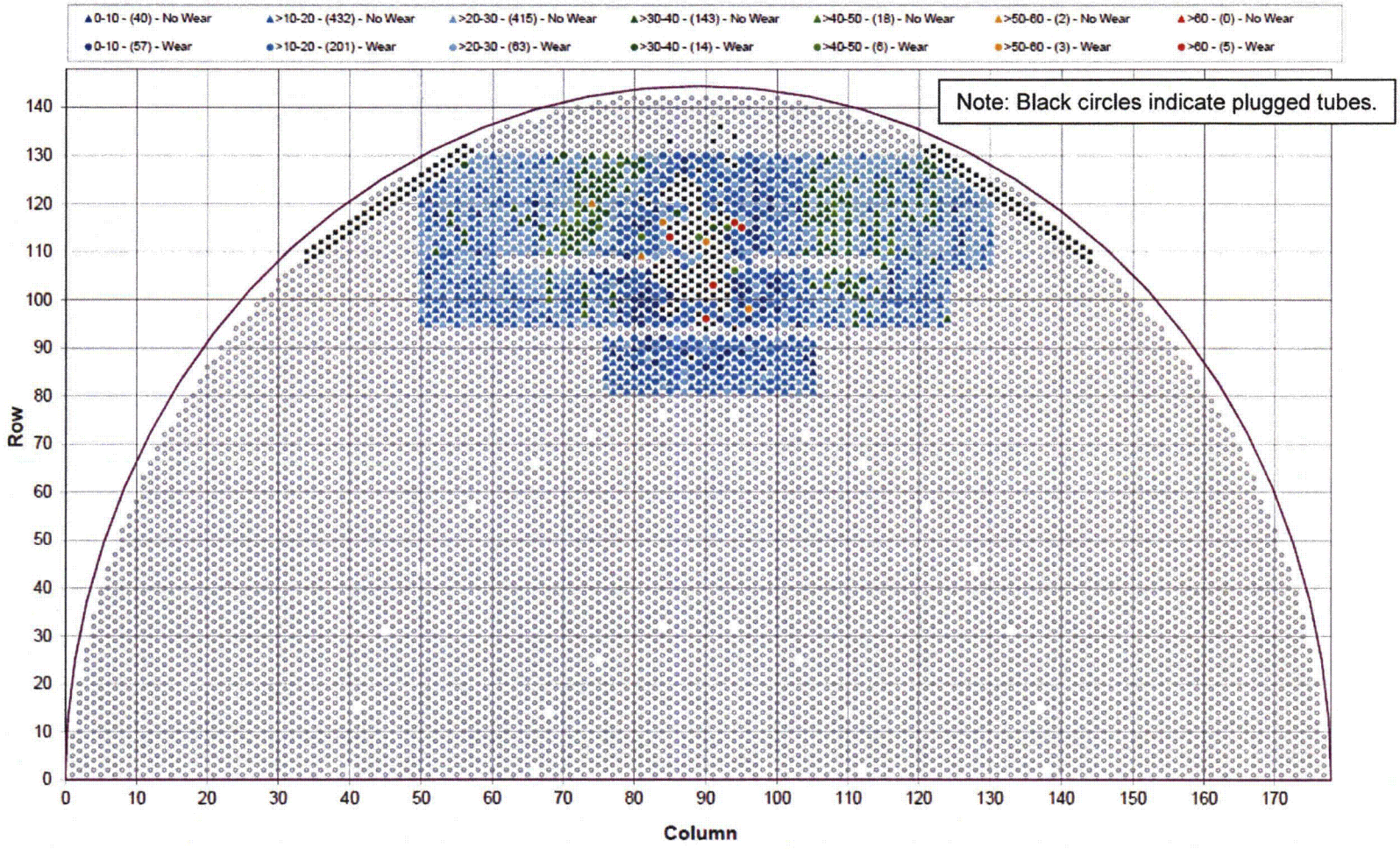

Figure 6-29: Tubesheet Map of ECT Gap Measurements, Total Gap for All AVB Locations per Tube, Unit 2, SG E-088, ISI

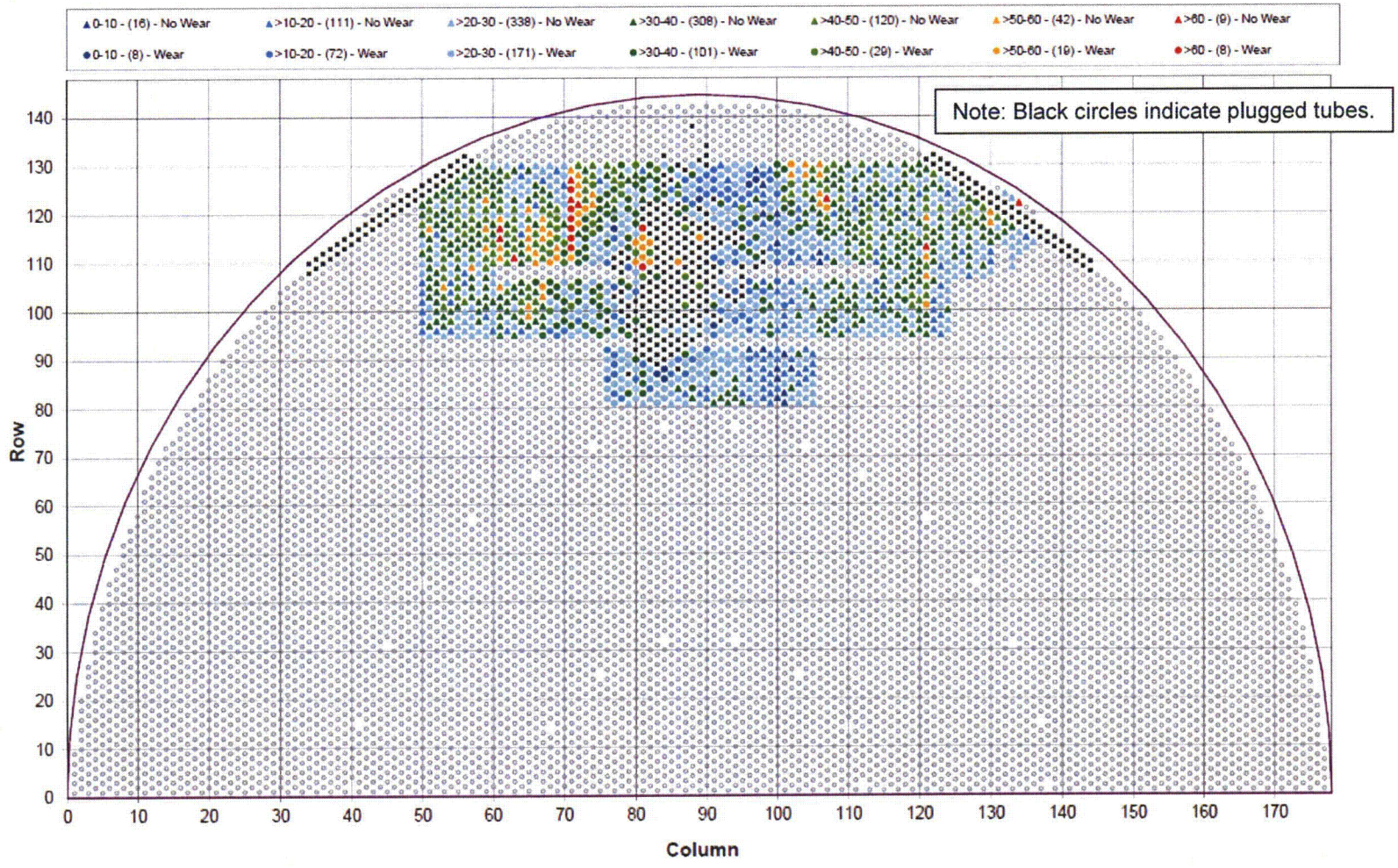

Figure 6-30: Tubesheet Map of ECT Gap Measurements, Total Gap for All AVB Locations per Tube, Unit 2, SG E-089, ISI

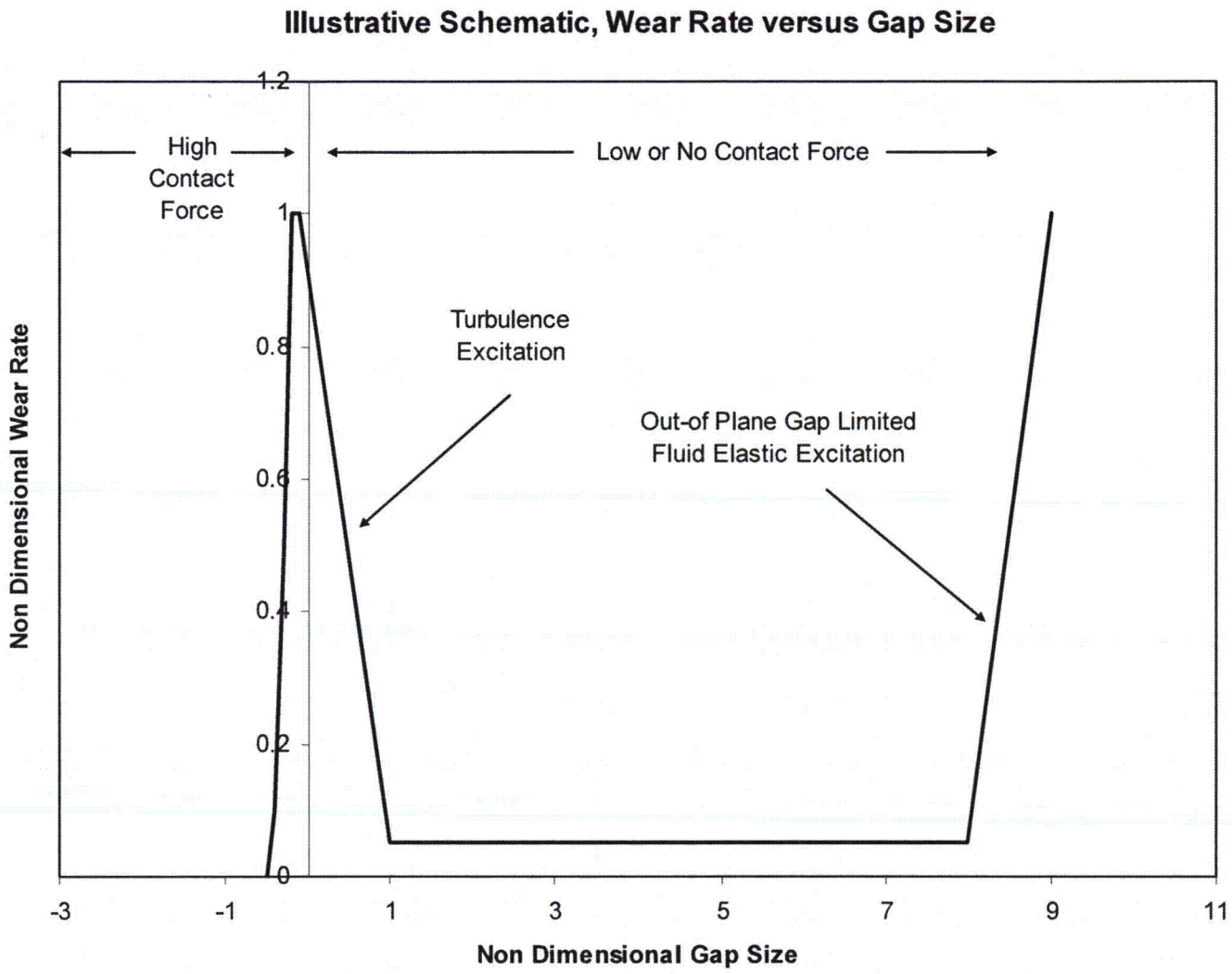

Figure 6-31: Illustrative Schematic of AVB Wear Rates, High Wear Rates are Possible for Very Small or Large Gaps

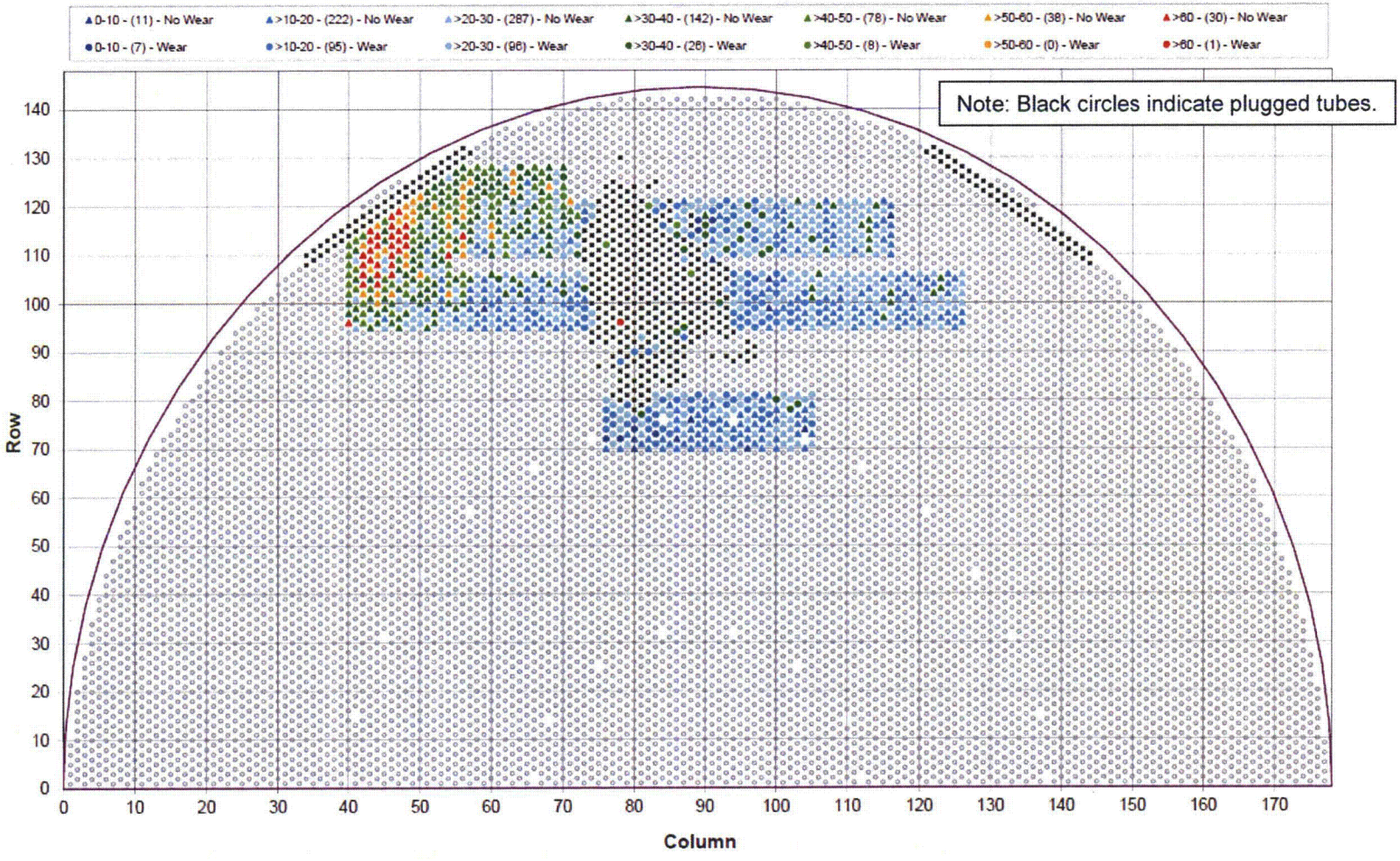

Figure 6-32: Tubesheet Map of ECT Gap Measurements, Total Gap for All AVB Locations per Tube, Unit 3, SG E-088, ISI

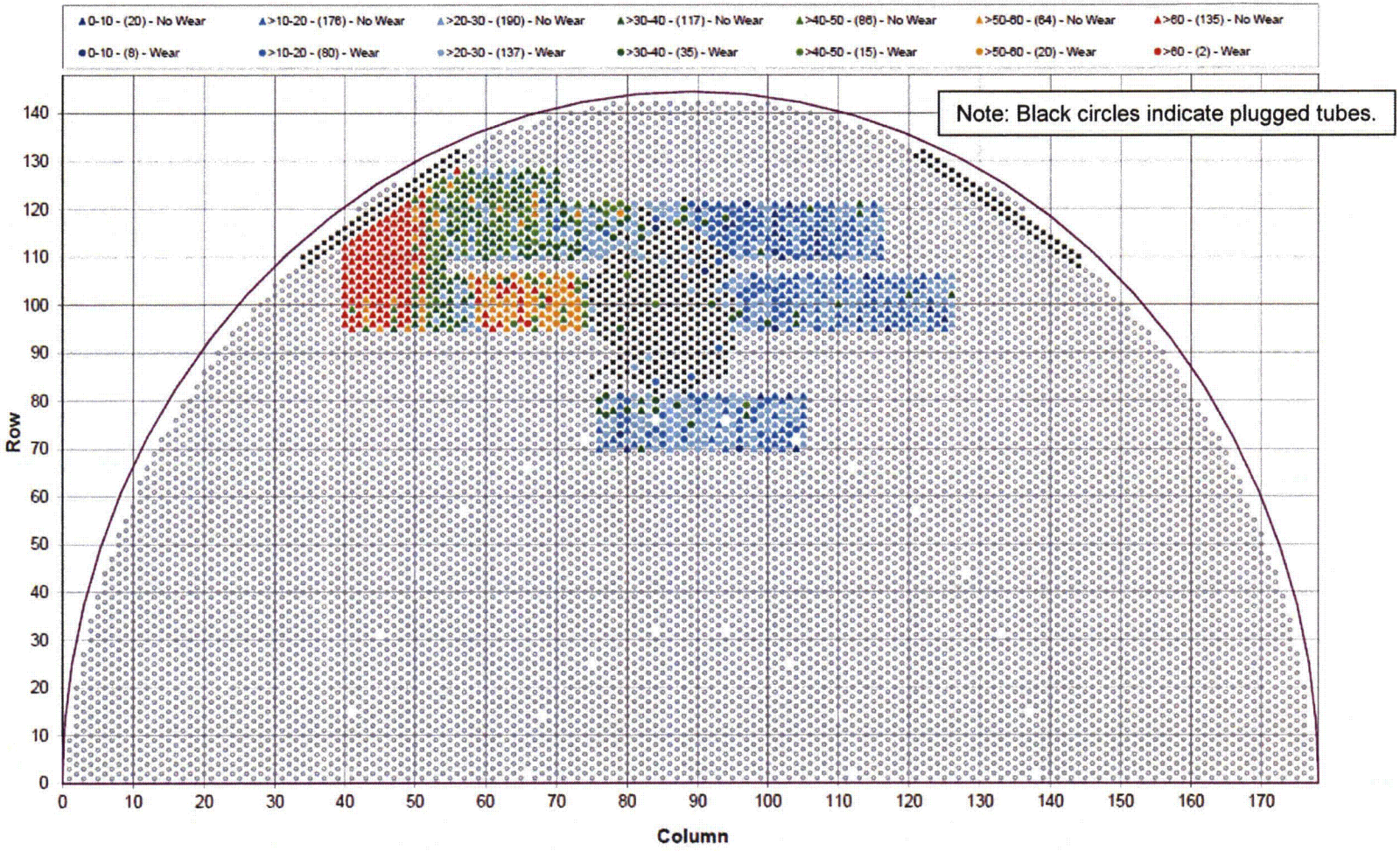

Figure 6-33: Tubesheet Map of ECT Gap Measurements, Total Gap for All AVB Locations per Tube, Unit 3, SG E-089, ISI

7.0 CRITERIA FOR EFFECTIVE VERSUS INEFFECTIVE SUPPORTS

There are no definitive criteria for effectiveness of steam generator tube supports, especially relative to the use of flat bar supports (AVBs) with large radius U-bends and in-plane fluid-elastic instability considerations. As noted in Section 4.0, extensive testing has been performed examining the in-plane support effectiveness of AVBs and large radius U-bends. The general conclusion is that AVBs with small clearances act as apparent nodal points for flow-induced tube response and have been shown by laboratory testing and operating experience to provide effective in-plane support. Westinghouse [21] has stated that no friction force is required for the in-plane effectiveness of AVB supports. In the context of turbulence induced wear the work of Pettigrew and Yetsir [24] suggests a contact force of [ ] as an effective support condition.

To arrive at a criteria for support effectiveness, three different expressions of force were investigated:

1. The contact force required if an equal force is applied at all 12 AVB locations.
2. Variable contact force at each AVB
3. The contact force required at one AVB if it is the only one that is resisting motion (upper bound contact force).

Each of these is explained in the paragraphs that follow.

7.1 Equal Contact Force at Each AVB

MHI has calculated the response of a large U-bend with AVB supports subjected to turbulence and fluid-elastic excitation forces. Various gap (clearances) conditions were included along with contact forces ranging from 1N to 10N (Appendix 10 of Reference [22]). An equal contact force was applied at all 12 AVB locations. The fluid-elastic excitation function was based on the work of Chen [25]. Given the uncertain nature of fluid-elastic excitation forces, a direct application of the selected excitation function to SONGS at 100% power is problematic. However the scale of the contact force that prevented in-plane vibration is highly useful. A contact force of 1N did not resist in-plane motion but a force of 10N was completely effective. Figure 7-1 is a schematic of movement amplitude versus time for a U-bend becoming fluid elastically unstable. At the instability point the energy added to the U-bend from the fluid just starts to exceed the energy dissipated in movement. From this point onward the energy and thus amplitude of U-bend motion increases continuosly over time. The initial forces needed to resist in-plane motion are very low. After instability develops even large friction forces at AVB locations are easily overcome.

7.2 Variable Contact Force at Each AVB

Since support effectiveness is possible with small clearances and no contact/friction forces, expressing support effectiveness in terms of contact forces is an oversimplification of complex support/U-bend interactions. This step is taken as a matter of calculation convenience to evaluate support effectiveness. It is recognized that this purely mechanical analogue is not difficult to overstate. One step in this direction is to consider contact forces which vary from one AVB location to another rather than being equal at each location. Ideally one would wish to consider turbulence and fluid-elastic excitation forces for a very broad range of support conditions and forces. Unfortunately, considering fluid-elastic excitation forces for more than a few cases is intractable. Even if only turbulence forces are considered, the number of possible cases is staggering. Considering only 5 levels of force taken 12 at a time (for 12 AVBs) where the order matters and repeats are possible leads to 244,140,625 cases.

Even after applying engineering judgment and being highly selective this would be a daunting exercise. This is particularly true since it would have marginal utility. Ultimately, the reasonableness of the chosen support effectiveness criteria is how well it corresponds to the observed stability behavior of Units 2 and 3 when combined with contact force and stability ratio calculations to develop probability of instability projections. Another, more practical, tack has been taken; that of examining an upper bound contact force for support effectiveness when no contact forces exist at any other supports.

7.3 Single AVB Effective (Upper Bound Contact Force)

MHI has analyzed the case of a U-bend with a contact force at a single AVB location with the U-bend subjected to turbulence excitation only [26]. The contact force at one AVB needed to resist tube motion was obtained, assuming no contact forces at any other AVB location. This force depends on the AVB location, the power level and the location of the U-bend in the tube bundle. It is considered as the upper bound requirement for support effectiveness when no other contact forces are present on the U-bend. From the analysis of contact forces as described in Section 6.0 this is a very low frequency occurrence. Figure 7-2 contains a plot of upper bound contact force for support effectiveness versus AVB number and power level. These upper bound contact forces vary slightly from one position to another in the bundle. Only the average values are shown. Turbulence excitation produces a spectrum of forces on U-bends. The calculated upper bound contact force prevents motion for 97.7% of this spectrum.

7.4 Chosen Approach for the OA

Figure 7-3 is a schematic of a large U-bend with AVB locations denoted. The contact force needed for support effectiveness at one location may depend on the contact forces at other locations. Note that this is judgment from the purely mechanical analogue viewpoint, which is admittedly simplistic and in some ways conservative since a support can be effective with no contact force. Proceeding with this logic, the contact force for support effectiveness is expressed in a probabilistic fashion. A median contact force is selected (see below) for support effectiveness while the upper bound contact force for support effectiveness is taken from the MHI calculations. From the cumulative distribution of contact forces for each AVB on each tube the probability that the median force will not be met is determined. If the median force is required the support will be ineffective. The same procedure is applied to determine the upper bound probability of support ineffectiveness using the upper bound contact force.

The probability of support ineffectiveness is then estimated as [

] The end result is illustrated in Figure 7-4. This is an example distribution of the probability that a given AVB on a given tube will be ineffective. [

]

In Monte Carlo simulations, the probability of support ineffectiveness [

]

[

] For all of the complexity of the above discussions it turns out that that same answer for probability of instability is obtained using either the 3N-log normal distribution approach or a single contact force threshold for effectiveness of 3N. Even though the upper and lower tails of the log normal distributions are not symmetric and have a bias toward the upper tail, the end result is controlled by the median value.

7.5 Summary – Criteria for Support Effectiveness

In summary, a single contact threshold of [ ] was chosen for AVB support effectiveness. This threshold was chosen for two reasons: [

]

The [ ] threshold is applied [

] All AVBs where the contact force exceeds [ ] are considered effective. Those that fall below 3N are considered ineffective. The total number of consecutive ineffective AVBs determines whether the tube is considered stable or unstable. This process is explained in more detail in Section 8.0.

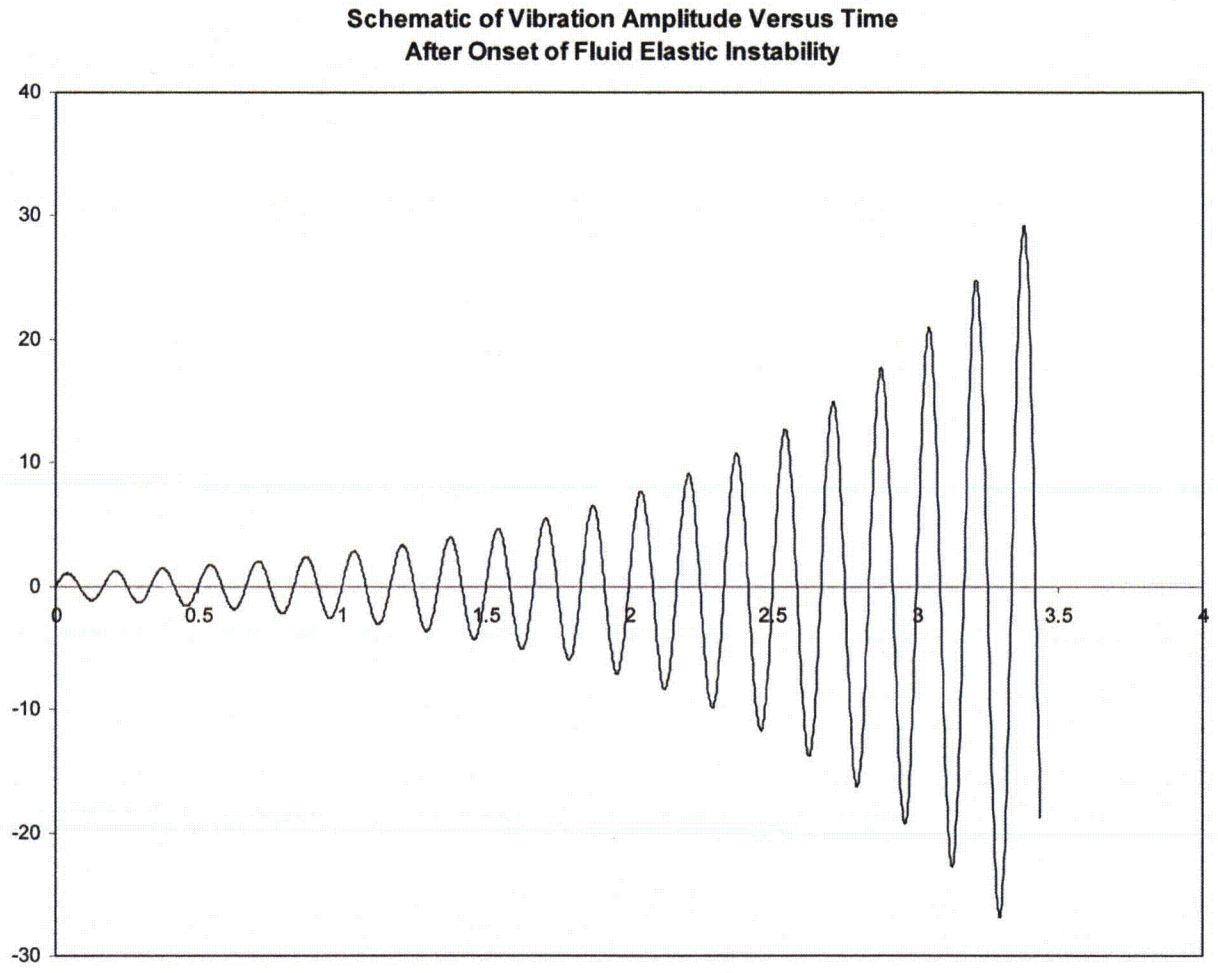

Figure 7-1: Schematic Illustration of a the Amplitude of Motion as a U-bend Becomes Unstable

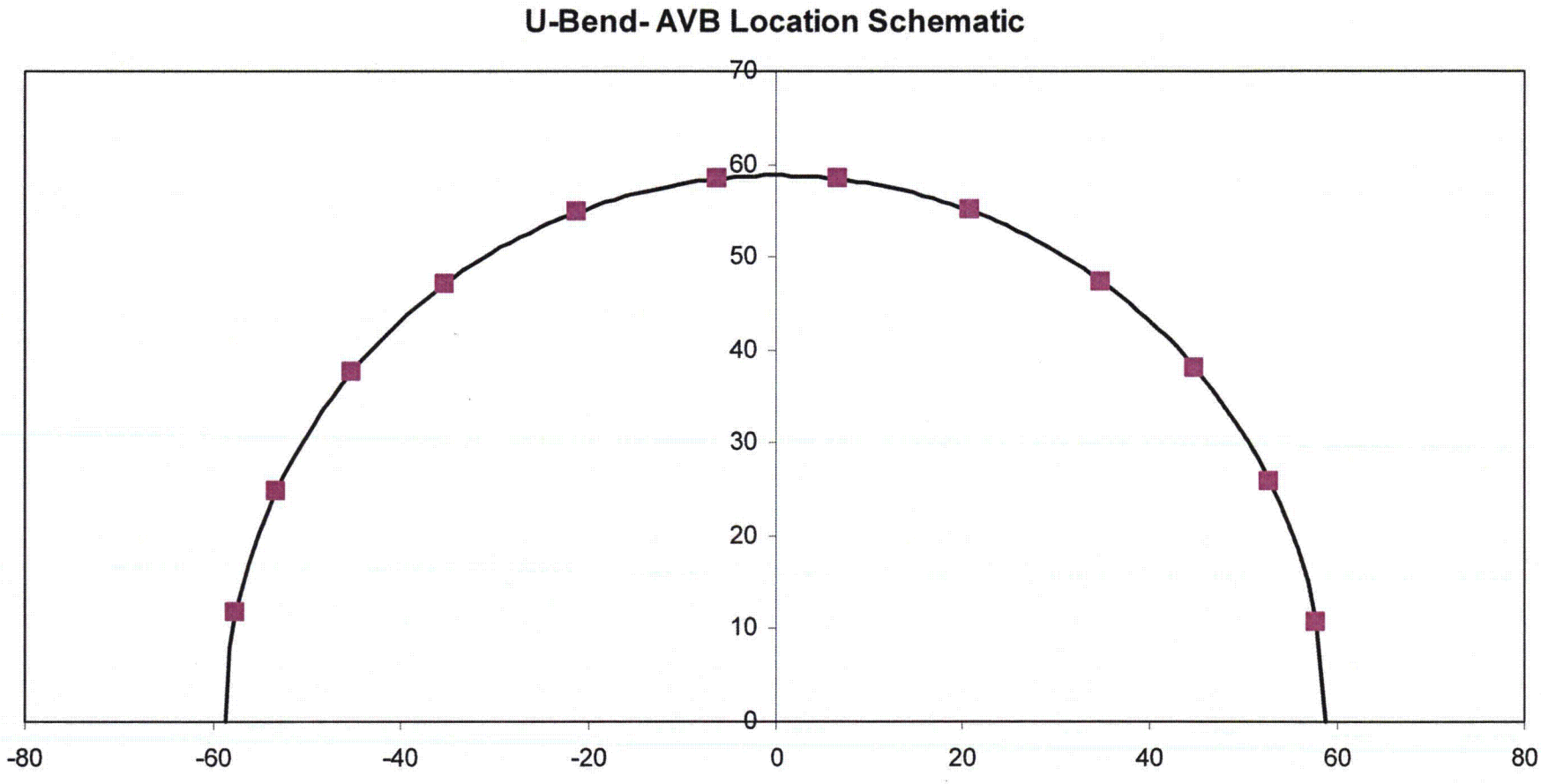

Figure 7-3: Schematic of a U-bend with AVB Locations Shown

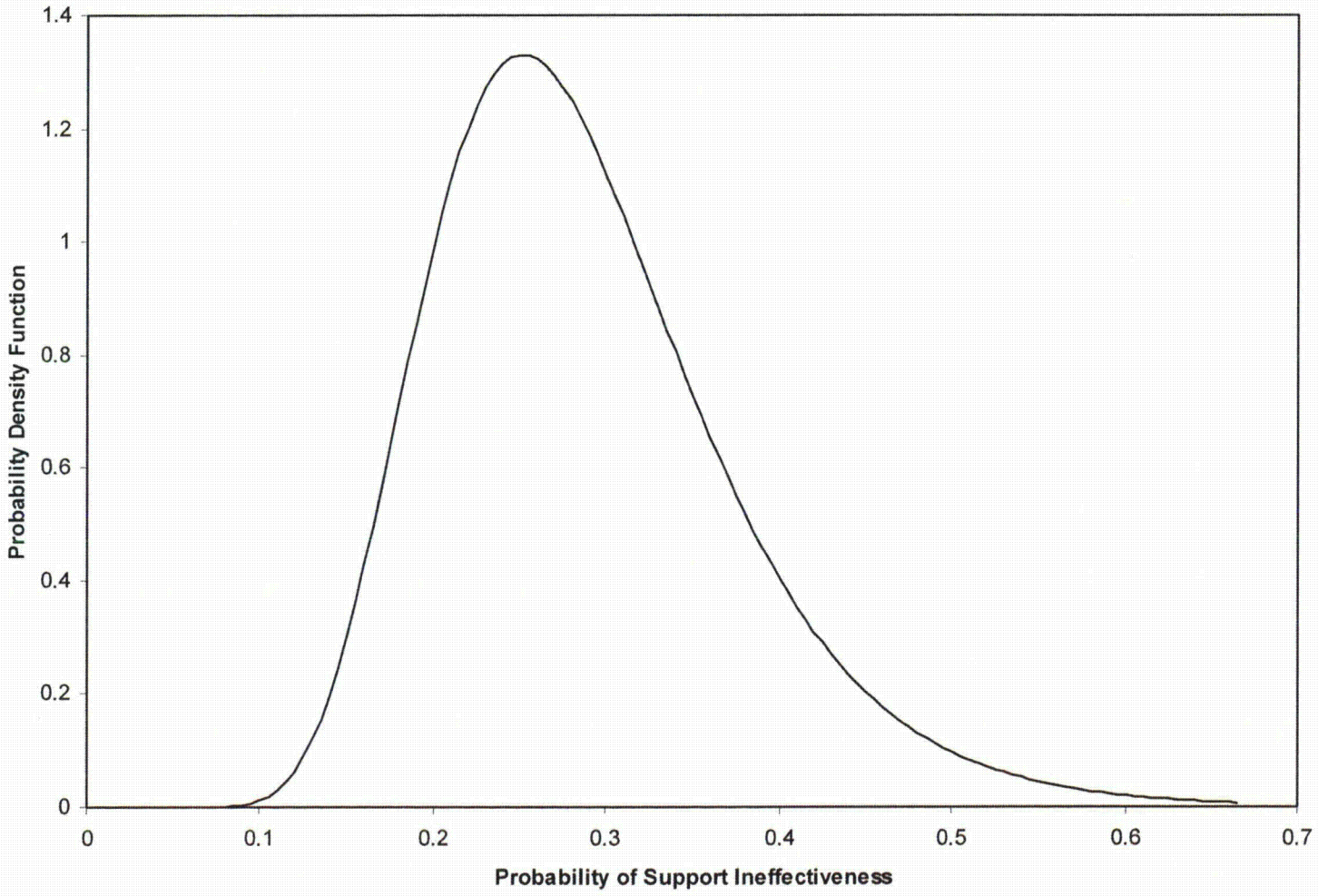

Figure 7-4: Illustrative Example of a Log Normal Distribution of the Probability of Support Ineffectiveness

8.0 PROBABILITY OF INSTABILITY RESULTS

The material presented in Section 5.0 on stability ratios demonstrated that all tubes are stable (SR < 1) at 70% power with a probability of 0.95 at 50% confidence without any effective in-plane supports. No TTW will develop and thus the operational assessment goal of meeting structural and leakage integrity requirements with 0.95 probability at 50% confidence is met. Probability of instability calculations are used only to demonstrate margin. The desired margin is a projected maximum stability ratio of 0.75 with 0.95 probability at 50% confidence over the next inspection interval of 5 months. Some effective in-plane supports are needed to maintain a stability ratio of 0.75. In the most limiting case, 4 effective supports are required. This requirement applies to approximately 120 U-bends. See Figure 5-10. Note that all U-bends are considered in probability calculations, including plugged tubes with split stabilizers inserted.

Wear at AVB locations will degrade in-plane support effectiveness over time. The essentially stable behavior of Unit 2, with only two tubes arguably unstable at 100% power at EOC 16, shows that no more than 5 supports were ineffective (Figure 5-6). Immediately after restart at 70% power, stability ratios less than 0.75 are expected. The question of interest is the length of operating time it takes for wear at AVBs to degrade support effectiveness to the point where the probability of a maximum stability ratio of 0.75 is greater than 0.05. The following paragraphs describe the procedure for calculating the probability of instability.

As noted earlier, calculations of the probability of instability is straightforward in principle. The development of in-plane fluid-elastic instability of U-bends depends on four factors. These are:

- Location in the bundle
- Operating power level
- Number of consecutive ineffective supports
- Operating time

These factors affect stability ratios. Support effectiveness in-plane is defined in terms of contact forces at AVB locations. The number of consecutive ineffective supports can change over time as AVB wear reduces contact forces. Descriptions of stability ratios, contact forces at AVB locations and criteria for determining support effectiveness are provided in previous sections. This is the information required to compute the likelihood of encountering in-plane fluid-elastic instability at a given power level as a function of operating time.

The probability of instability is computed using a Monte Carlo approach. One Monte Carlo trial of all tubes in a steam generator is constructed in the following manner:

[ ]

[

]

7. Whether or not the steam generator contains any unstable U-bend in one Monte Carlo trial of the steam generator is recorded.

8. Typically 10,000 Monte Carlo trials of a steam generator are performed. In this case the probability of instability is simply the number of trials where the steam generator contained one or more unstable tubes divided by 10,000.

Several independent programs use mathematically equivalent algorithms to compute the probability of instability. In this case, probability calculations were performed using [ ] [27]. Independent checks of test cases were performed to verify the methodology using an independent [ ]

Figure 8-1 illustrates the first step in constructing one Monte Carlo trial for a full bundle. The cumulative distribution, CDF, of contact forces for a given AVB location at a given position in the bundle is examined. If a single contact force for support effectiveness is used, for example [ ], the value of the CDF curve at [ ] provides the probability that the support will be ineffective. This is true because the value of the CDF curve at [ ] is the fraction of the total population of contact forces that are equal to or less than 3N. In this case, the support is considered effective if the contact force is any value greater than [ ]. The value of the CDF curve at [ ] is termed the probability threshold for support ineffectiveness. Support effectiveness for a given AVB on a given tube is determined by selecting a random number from a uniform distribution from 0 to 1. If this value is above the probability threshold for support ineffectiveness the support is effective. If it is equal to or below the threshold, the support is ineffective.

The above is an example of a single parameter criterion for support effectiveness. [

]

The first step is the crucial step in the Monte Carlo trial. It is repeated for all AVB locations in a particular U-bend. [

]

[

]

Before proceeding to probability of instability results for Units 2 and 3, it is worthwhile to examine the actual stability behavior of the two units. There are only 4 data points to consider. With all the caveats attending an extremely small sample size, it is a necessary exercise. Both steam generators in Unit 3 exhibited an advanced state of unstable behavior after 11 months of operation. In contrast, only one steam generator in Unit 2 exhibited "incipient instability" after 22 months of operation. Two out of two observations of instability in Unit 3 at 11 months leads to a 50% confidence estimate of probability of instability of 0.71 (0.71*0.71 = 0.5). This would be a minimum expected value since TTW estimates place the onset of instability near the beginning of the operating interval. Thus a probability somewhere near 0.7 early in life is expected. For Unit 2, with one out of two observations of instability at 22 months the 50% confidence estimate of probability of instability is 0.29. This would place the occurrence of no instability in either steam generator as a 50/50 proposition ((1-0.29)*(1-0.29) = 0.5) and the chance of instability occurring in both steam generators at 22 months at a probability of 0.08 (0.29*0.29 = 0.08).

The other point regarding the observed stability behavior is the location in the tube bundle where instability first developed. This is taken to be near the maximum observed TTW depths. These observations regarding actual stability behavior provides a means of evaluating the reasonableness of probability of instability calculations. Calculated probabilities should be in reasonable agreement with observed behavior.

Figure 8-3 provides a summary of probability of instability calculations. Figure 8-3 requires careful reading of the notes and legends. It traces the probability of instability versus time for Units 2 and 3. All results are based on 95th percentile stability ratios. First consider results for the probability of instability versus time for 100% power and instability defined as a stability ratio of 1 or more. This serves as a check of results to be reported for a stability ratio of 0.75 which is the main item of interest, that is, demonstrating margin. [

]

Unit 2 has more substantial contact forces and is much more resistant to loss of support effectiveness due to wear at AVB locations. After 22 months, the calculated probability of instability is about 0.85. The intermediate point at 12 months is near 0.3. Both of these values are high and thus conservative. This is judged to be the effect of an underestimation of contact forces. [

]

Before proceeding to a drop in power from 100% to 70%, it is of interest to check the predicted most likely locations of first instability at 100% power. Projections are shown in Figure 8-4 for Unit 3 and in Figure 8-5 for Unit 2. The hotter (yellow and red) colors are the more likely locations of first instability. The U-bends plotted have the largest TTW depths. Overall, calculated locations where first instability will occur agree very well with observations. This re-enforces the reasonableness of the probability of instability calculations and supports the reliability of the probabilistic argument for margin in terms of maintaining a stability ratio less than 0.75.

As noted above, a drop to 70% power makes all U-bends stable, SR < 1, with no effective in-plane supports using the 95th percentile stability ratio calculations. Since no effective in-plane supports are required, wear at AVB locations over time is not an issue. Stability will be maintained indefinitely.

The desired margin for stability is a projected maximum stability ratio of 0.75 with 0.95 probability at 50% confidence over the next inspection interval of 5 months. The green line in Figure 8-3 shows that a maximum stability ratio of 0.75 will be maintained with 0.95 probability at 50% confidence for 8 months after restart at 70% power. Note that this is the same as stating the probability of instability for SR = 0.75 or greater is less than or equal to 0.05. That is, the green line on Figure 8-3 is below the red line, 0.05 probability, for 8 months. This is a conservative demonstration of margin. The probability of instability at 100% power for SR ≥ 1 is conservatively high. This means support effectiveness is better than calculated at both 100% power and even then more so at 70% power. Recall the demonstrated stability at 100% power at EOC 16 necessitated that there were no more than 4 consecutive ineffective supports in the worst case region. Hence stability immediately upon restart as 70% power even for stability in terms of SR ≤ 0.75 is required. The calculated probability of instability at SR ≥ 0.75 immediately upon restart is 0.012; it is not zero because for an SR threshold of 0.75 there is a population of tubes that require between 1 and 3 effective AVBs to be stable, and the random gap distributions input to the Monte Carlo trials produce this condition for the susceptible population of tubes a small percentage of the time. [

]

With no effective in-plane supports the stability ratio of the two tubes with TTW, R111 C81 and R113 C81 in SG 2-89, is 0.88 at 70% power (Attachment 5 of [20]). It is an open question as to how many supports were effective at 100% power. It is highly likely that there are not 9 consecutive ineffective supports on these tubes under the moderate conditions of 70% power. Substantial margins are demonstrated at 70% power as the probability of maintaining a maximum stability ratio of 0.75 is greater than 0.95 for 8 months with conservative calculations. Other items of conservatism in the analysis are projected wear depth growth rates at AVB locations based on a constant rate of volume loss at levels observed at 100% power and the use of a support effectiveness criteria at 70% power that is effectively the same as at 100% power. In this later context, it is noted that use of the single parameter criteria for support ineffectiveness at [ ] provides essentially the same probability of instability as use of the log normal distribution of probability of support ineffectiveness with a [ ] median value and an upper tail based on the upper bound contact force for support ineffectiveness.

One final item is needed for completeness, although the answer is obvious based on the results for a stability ratio threshold of 0.75. Long term stability at 70% power was argued in Section 5.0 even for a 99th percentile stability ratio calculation. With the 99th percentile stability ratios and stability based on SR ≥ 1, the probability of instability for 12 months after restart is 0.0001. Long term stability will be maintained and large margins are conservatively demonstrated.

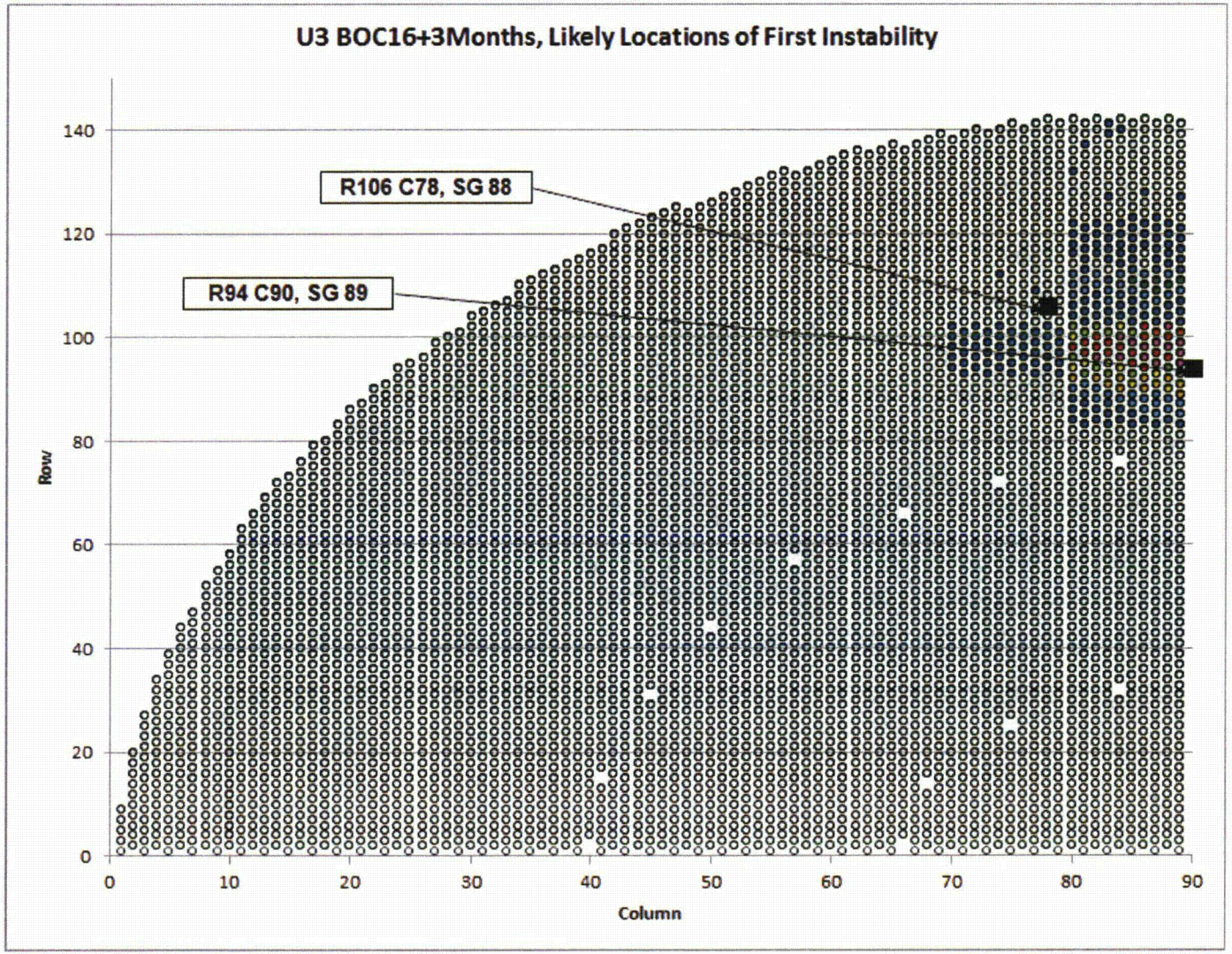

Figure 8-4: Map of Calculated Frequency of Occurrence of In-plane Instability, Unit 3

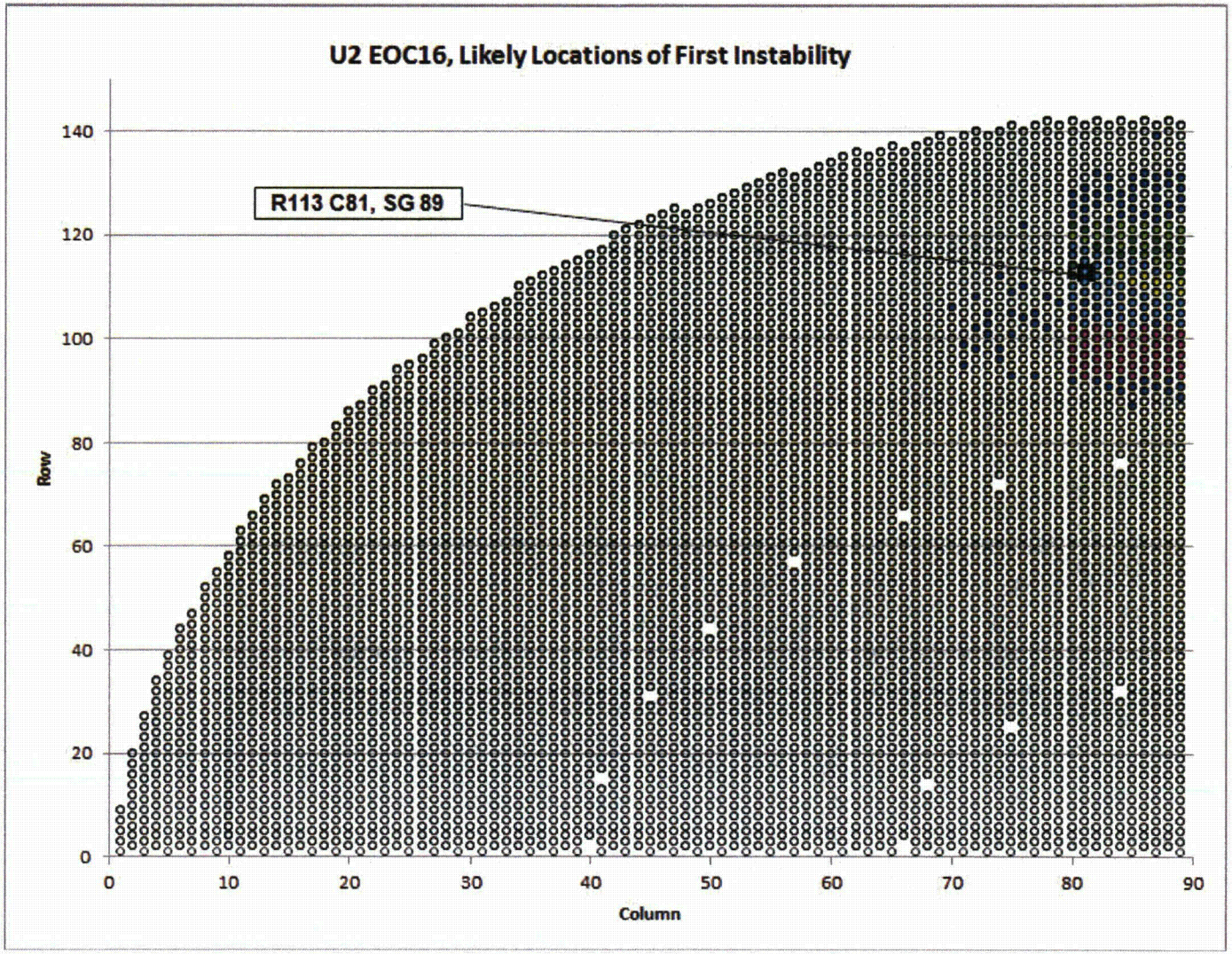

Figure 8-5: Map of Calculated Frequency of Occurrence of In-plane Instability, Unit 2

9.0 DEFENSE-IN-DEPTH

Defense in depth measures relative to TTW in Unit 2 add to the assurance that structural and leakage integrity requirements will be maintained throughout the next inspection interval. These measures go beyond the technical case for restart of Unit 2 at 70% power. A decrease in power to the 70% level returns the steam generators back inside the operational envelop of demonstrated successful performance and assures stability without dependence on any effective in-plane supports. Thus structural and leakage integrity of steam generator tubing is demonstrated. Also, substantial margins have been shown. Still, conservatism demands that the question of the consequences of developing in-plane fluid-elastic instability be addressed. Defense in depth measures are in place to mitigate these consequences if needed in extremis.

Tubes with a high risk of developing FEI, based on AVB wear patterns similar to those of unstable tubes in Unit 3, have been plugged. Wire cable stabilizers have been inserted. Figure 9-1 and Figure 9-2 show tubesheet maps, for Unit 2 SG E-088 and SG E-089 respectively, of tubes preventively plugged for increased susceptibility to in-plane FEI. If FEI occurs, the location will most likely be in the high risk region. Then FEI must progress through a buffer zone of plugged tubes to reach pressurized, in service tubes. From probability calculations this process of instability zone expansion took about 7 months to develop in Unit 3. Only at this point is an in-service pressurized tube driven to instability with consequent development of TTW. Only when instability develops for an in-service tube does structural and leakage integrity begin to be challenged. The preventive plugging patterns shown in Figure 9-1 and Figure 9-2 are based solely on AVB wear patterns in each given tube not a buffer zone concept based on possible instability zone expansion. Therefore there are gaps in the buffer zone. Consequently the time for possible instability zone expansion in Unit 2 at 70% power is reduced to half of the 7 month estimate from Unit 3. It is estimated at 3.5 months.

The function of the wire cable stabilizers is to prevent tube severance in plugged tubes should instability and instability zone expansions develop. Stabilizers provide additional damping for large amplitudes of motion of U-bends and this will mitigate TTW growth rates to some degree. After instability, deep wear scars can develop over time at the 48° U-bend positions on the hot leg and cold leg as well as at the top tube support plate. [ ] Stabilizers will prevent the generation of large loose parts if instability and instability zone expansion occurs.

With the assumption of instability and the subsequent instability zone expansion, eventually an in-service pressurized tube will be driven to instability. TTW will occur over time to an extent challenging structural and leakage integrity. For SONGS Unit 2, the SIPC is that the worst case projected wear will not lead to a tube burst at 3 times the normal operating differential pressure, 3ΔP. [ ] The actual physical wear depth associated with meeting the SIPC is approximately [ ]. For information purposes, the wear depth leading to failure at SLB conditions is [ ] and a tube burst at NOPD requires degradation that is [ ]. These values are based on very long, uniformly deep wear scars such as is expected from TTW.

Now the question of interest is "After TTW begins how long does it take to reach an unacceptable level of wear depth?". After 11 months of operation of Unit 3 the TTW depths of 3 tubes, based on ECT results, exceeded 75% TW. Estimates of wear depth growth rate for the tube with the worst case depth, R106 C78 in Unit 3, SG 3-88 were developed using three different approaches:

- Simple estimates
- Dynamic (time domain) modeling of U-bend impact with spring loaded contact areas under turbulence and fluid-elastic excitation.
- Dynamic (time domain) finite element analysis of one U-bend impacting a neighboring U-bend employing a parametric study of forcing function amplitude, conventional damping, and Coulomb (friction) damping during U-bend to U-bend contact.

Results are summarized below. More details are provided in Appendix A for the simple estimates and FEA dynamic analysis of one U-bend impacting its neighboring U-bend. Dynamic modeling of a U-bend impacting spring loaded contact areas is described in Appendix 10 of Reference [20]. All of these analyses assume that the TTW coefficient is the same as determined in wear tests of Alloy 690 wear couples in a secondary side environment under tests conditions (including SONGS SGs) appropriate for turbulence induced wear at AVB locations. It is an open question as to whether or not these wear coefficients are directly applicable to the higher loads and much larger single event sliding distances that are present with tube-to-tube impacts.

Dynamic modeling of a U-bend impacting spring loaded contact areas indicated that work rates and thus volumetric loss rates are consistent with the development of the worst case wear depth in approximately 11 months. This would be consistent with instability beginning in Unit 3 shortly after start-up. Simple estimates of wear rates with consideration of uncertainties in impact forces and wear coefficients set the range of worst case TTW occurring between 2.5 and 11 months. Sophisticated parametric dynamic FEA analysis of one U-bend impacting another show that contact forces and contact lengths vary from one impact event to another and vary even during an impact event. Contact forces were shown to be highly dependent on how tightly a neighbor tube is held in place by its own AVBs as it is impacted by an unstable tube. Further, evaluation of elongated wear scars at AVB locations reveals that the worst case tube, Unit 3 SG E-088 R106 C78, had a substantial amplitude of motion during instability to the point where two outboard neighbors (higher row same column) and two inboard neighbors had to be involved in impact events due to the motion of tube R106 C78. This multiple tube event was not included in any wear estimate. Given these uncertainties the estimated range of wear time for the worst case flaw remains between 2.5 and 11 months after an in-service pressurized tube becomes unstable.

The defense in depth argument then is a combination of time for instability zone expansion (3.5 months) and wear time of an in-service pressurized tube (2.5 months) driven to instability at the boundary of the expansion zone. Under the assumption that instability at 70% power begins immediately upon restart, a highly improbable circumstance, the minimum estimate for time to violate structural and leakage integrity requirements in an unplugged tube is 6 months. This is longer than the planned operating time of 5 months. This is not unreasonable given the extremely conservative assumption of instability occurring immediately upon restart at 70% power.

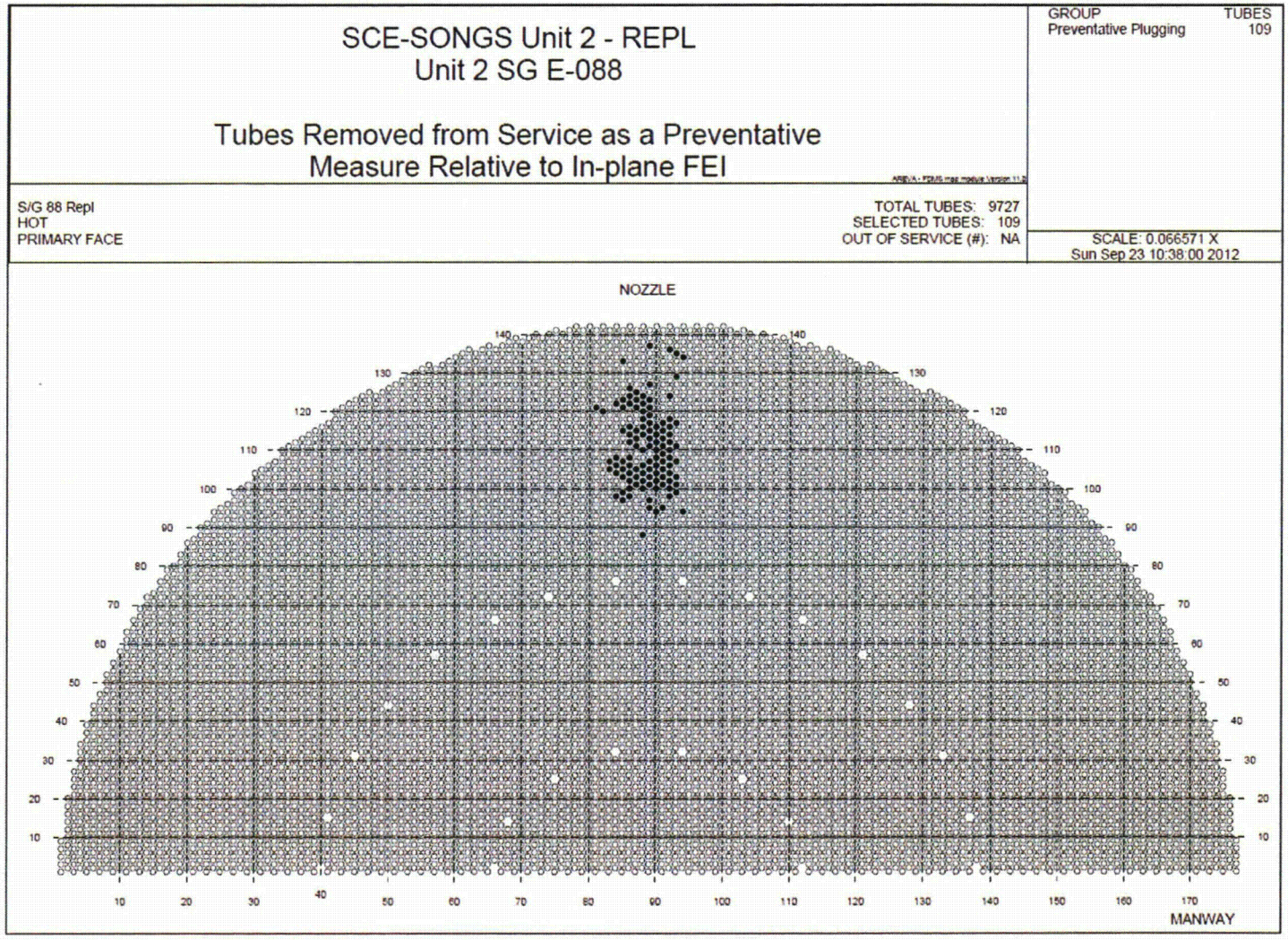

Figure 9-1: Tubes Removed from Service as a Preventative Measure Relative to In-plane FEI, Unit 2 SG 2-88

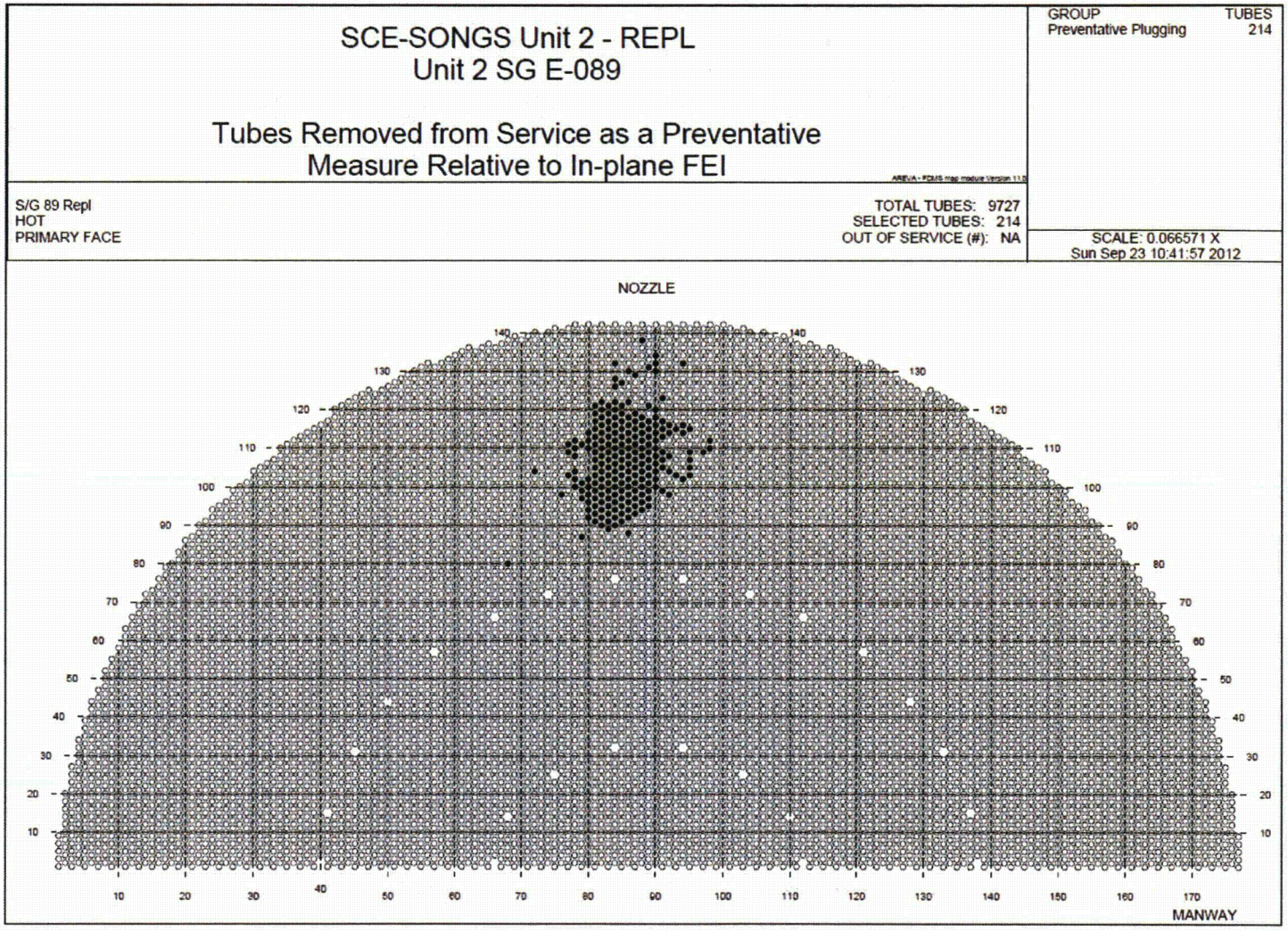

Figure 9-2: Tubes Removed from Service as a Preventative Measure Relative to In-plane FEI, Unit 2 SG 2-89

10.0 CONCLUSIONS

In accordance with the SONGS technical specifications and EPRI Steam Generator Integrity Assessment Guidelines [2], an operational assessment (OA) was performed to ensure that steam generator (SG) tubing will meet established performance criteria for structural and leakage integrity during the operating period prior to the next planned inspection. A conservative approach to prevent the occurrence of TTW ensures that tube integrity requirements will be met with the required probability of 0.95 at 50% confidence. A 70% operating power level returns the Unit 2 steam generators to within the operational envelope of demonstrated successful operation of U-tube nuclear steam generators relative to in-plane fluid-elastic stability. Operation at 70% power assures in-plane stability (SR<1) without dependence on any effective in-plane supports for U-bends. Without the development of in-plane instability no TTW will occur and thus structural and leakage integrity requirements are met.

Since stability at 70% power does not depend on any effective in-plane supports, detailed probabilistic calculations are only relevant to the demonstration of margin and conservatism. A maximum stability ratio of 0.75 will be maintained for 8 months at 70% power with a probability of 0.95 at 50% confidence. A conservative probabilistic analysis demonstrates substantial margin for the planned 5 month operating interval. Additionally, defense in depth measures in terms of preventive tube plugging with wire cable stabilizers in plugged tubes, provides for maintenance of tube integrity under the extreme assumption that instability at 70% power begins immediately upon restart. The minimum estimate for time to violate structural and leakage integrity requirements in an unplugged tube is 6 months based on instability zone expansion from higher risk plugged tubes out to an unplugged tube and then wear of the unplugged tube.

11.0 REFERENCES

1. SONGS Steam Generator Program, S023-SG-1.

2. EPRI Report 1019038, "Steam Generator Management Program: Steam Generator Integrity Assessment Guidelines: Revision 3", November 2009.

3. SONGS Technical Specifications Sections 5.5.2.11, "Steam Generator (SG) Program," Amendment 220.

4. SONGS Technical Specifications Section 3.4.13, "RCS Operational Leakage," Amendment 204.

5. NEI 97-06, "SG Program Guidelines", Rev. 3, January 2011.

6. AREVA Document 51-9182833-002, "SONGS 2C17 Outage – Steam Generator Operational Assessment" (SONGS Document 1814-AU651-M0144 Rev. 1).

7. AREVA NP Document 51-9176667-001, "SONGS 2C17 & 3C17 Steam Generator Degradation Assessment."

8. SONGS Drawing SO23-617-1-D116 Rev. 2, "San Onofre Nuclear Generating Station Unit 2 & 3 Replacement Steam Generators – Design Drawing – Tube Bundle 1/3" (MHI Drawing L5-04FU051 Rev. 1).

9. SONGS Drawing SO23-617-1-D507 Rev. 5, "San Onofre Nuclear Generating Station Unit 2 & 3 Replacement Steam Generators – Design Drawing – Anti-Vibration Bar Assembly 1/9" (MHI Drawing L5-04FU111 Rev. 2).

10. SONGS Drawing SO23-617-1-D542 Rev. 9, "San Onofre Nuclear Generating Station Unit 2 & 3 Replacement Steam Generators – Design Drawing – Anti-Vibration Bar Assembly 7/9" (MHI Drawing L5-04FU117 Rev. 9).

11. Root Cause Evaluation, San Onofre Nuclear Generating Station, Condition Report: 201836127, "Unit 3 Steam Generator Tube Leak and Tube-to-Tube Wear", Revision 0, 5/7/2012.

12. AREVA NP Document 51-9180143-001, "SONGS Unit 3 February 2012 Leaker Outage – Steam Generator Condition Monitoring Report" (SONGS Document 1814-AU651-M0143 Rev. 1).

13. AREVA NP Document 51-9181604-000, "SONGS Unit 2 Cycle-17 and 2012 Return to Service Technical Summary Steam Generator Eddy Current Inspection."

14. AREVA NP Document 51-9188725-000, "SONGS U2C17 and U3F16B AVB Gap and Tube-to-Tube Proximity Measurement Program" (SONGS Document 1814-AU651-M0151 Rev. 0).

15. Au-Yang, M. K., "Flow Induced Vibration in Power and Process Plant Components", ASME Press, New York, 2001.

16. Weaver, D.S. and Schneider, W., "The effect of Flat Bar Supports on the Crossflow Induced Response of Heat Exchanger U-Tubes," *Journal of Engineering for Power*, Vol. 105, October 1983, pp. 775-781.

17. Janzen, V.P., Hagberg, E. G., Pettigrew, M. J., and Taylor, C. E., "Fluidelastic Instability and Work-Rate Measurements of Steam-Generator U-Tubes in Air-Water Cross-Flow," *Journal of Pressure Vessel Technology*, Vol. 127, February 2005, pp. 84-91.

18. SONGS Document 90200, Rev. 0. Average and Maximum Thermal-Hydraulic Parameter Comparisons between Songs RSGs and Similar Plants.

19. Heat Exchanger Design Handbook, 1st Edition, Kuppan, CRC Press, 2000.

20. SONGS Document SO23-617-1-M1523 Rev. 5, "Replacement Steam Generators, Evaluation of Stability Ratio for Return to Service" (MHI Document L5-04GA567 Rev. 6).

21. SONGS Document 1814-AA086-M0189 Rev. 2, Westinghouse Report LTR-SGDA-12-36 Rev. 0, "Flow-Induced Vibration and Tube Wear Analysis of the San Onofre Nuclear Generating Station Unit 2 Replacement Steam Generators Supporting Restart."

22. SONGS Document SO23-617-1-M1520 Rev. 6, "Tube Wear of Unit-3 RSG – Technical Evaluation Report" (MHI Document L5-04GA564 Rev. 8).

23. AREVA NP Document 51-9182368-002, "SONGS 2C17 Steam Generator Condition Monitoring Report."

24. Pettigrew, M. J. and Yetisir, M., "A Simple Approach to Assess Fretting-Wear Damage," 4th CNS International Steam Generator Conference, Toronto, Ontario, Canada, May 5-8, 2002.

25. Chen, S. S., "Instability Mechanisms and Stability Criteria for a Group of Circular Cylinders Subjected to Cross-Flow, Part 2: Numerical Results and Discussions, Journal of Vibration, Acoustics, Stress and Reliably in Design, April, 1983, Vol. 105, pp 253-260.

26. SONGS Document SO23-617-1-M1532 Rev. 2, "Analytical Evaluations for Operational Assessment (MHI Document L5-04GA585 Rev. 2).

27. AREVA NP Document 32-9187024-000, "SONGS Steam Generator Probability of Fluid Elastic Instability Calculation."

References 1, 3, 4, 8, 9, 10, 11, 18, 20, 21, 22, 24, and 27 are available from Southern California Edison (SCE) and are approved for use as required by AREVA NP procedure 0402-01. See signature page for the Project Manager's approval signature.